Volcanic record of continental thinning in Baffin Bay margins: Insights from Svartenhuk Halvø Peninsula basalts, West Greenland

Arnaud Agranier, René C. Maury, Laurent Geoffroy, François Chauvet, Bernard Le Gall, Adriano R. Viana

Volcanic record of continental thinning in Baffin Bay margins: insights from Svartenhuk Halvø Peninsula basalts, West Greenland

Arnaud Agranier[a*], René C. Maury[a], Laurent Geoffroy[a], François Chauvet[ab], Bernard Le Gall[a], Adriano R. Viana[c]

[a] *Univ Brest, CNRS, IUEM, UMR 6538 Laboratoire Géosciences Océan, Rue Dumont d'Urville, 29280 Plouzané, France*

[b] *UMR 6538 / UBO / SEDISOR*

[c] *Petrobras, Petróleo Brasileiro S.A., Rio de Janeiro, 1301E Brazil; E&P/UN-RIO/ATEX/ABIG-PL*

* Corresponding author: Tel.: +33 2 98 49 87 07, fax: +33 2 98 49 87 60. E-mail address: arnaud.agranier@univ-brest.fr

Keywords

Plume-related basalts
Enriched mantle sources
Partial melting
West Greenland Volcanic Province
North Atlantic Igneous Province
Volcanic passive margins

8088 words, 52773 characters

Abstract

We report major, trace elements and Pb, Hf, Nd and Sr isotopes in 61-54 Ma old basalts from Svartenhuk Halvø Peninsula (Greenland). This area corresponds to the northernmost exposure of the West Greenland volcanic province, of which the emplacement marks the continental thinning and breakup process leading to the opening

of Baffin Bay during the Eocene. Its wedge structure displays typical characteristics of inner seaward-dipping-reflectors (SDR) with an exposed volcanic sequence thicker than 7 km. Our results cover the entire volcanic sequence starting with an earliest V1 unit reflecting rather low degree partial melts (transitional basalts), which are geochemically imprinted by continental crust contamination. This unit is followed by much thicker and mainly tholeiitic V2 and V3 basaltic lava piles, and ends with a rather thin V4 unit, consisting of alkali basalts and associated trachytes. Pressures and temperatures of melt extraction were estimated based on major element concentrations and rare earth elements patterns. Our results suggest that melts were extracted from the garnet-spinel transition zone at greater depths for the initial V1 and the final V4 lavas (alkali to transitional basaltic compositions) than for the main V2 and V3 mostly tholeiitic lava piles (at 2 ± 0.5 GPa and 1350 ± 100°C). Isotope signatures suggest that mantle sources of the melts were controlled by the mixing of ambient upper mantle and Icelandic plume-type materials. The proportion of ambient upper mantle involved in the lava source appears to increase together with melting rates and the upward propagation of melting zone during V3 emplacement, suggesting that melting in this area progessed as follows: 1. Initiation of partial melting (low degrees) of deep-seated Icelandic plume-type material (V1 and V2); 2. Upward propagation of the melting area within the shallower mixed upper mantle (V3); 3. Progressive decrease of "ambient upper mantle" involvement, deepening of magma extraction and decrease of partial melting associated with the emplacement of V4 lavas. We show that these changes are consistent with the tectonic stages of continental thinning that preceded the Eocene breakup in Baffin Bay.

1. Introduction

Volcanic passive margins (VPM) characterize continental breakup associated with the emplacement of large igneous provinces (White and McKenzie, 1989; Coffin and Eldholm, 1994). In detail, initial mantle melting is thought to start prior to significant lithosphere extension (Courtillot et al., 1999), leading to the eruption of voluminous flood basalts. Then, focusing of mantle melting combined with lithosphere extension and consecutive syn-magmatic break-up leads to the formation of volcanic passive margins (Geoffroy et al., 2015). The corresponding volcanic sequences, although emplaced subaerially, are usually found as immerged seaward-dipping reflectors (SDR) sequences beneath post-rift sediments, a common occurrence throughout the North Atlantic Igneous Province (NAIP; Saunders et al., 1997). Such sequences, linked to the

opening of the Baffin Bay oceanic basin, are exceptionally well-exposed along the West Greenland coast, where they are of Paleocene-Eocene age and up to 5-7 km thick (Larsen and Pulvertaft, 2000; Larsen and Pedersen, 2009; Larsen et al., 2015; Chauvet et al., accepted). Petrologic and geochemical studies of these volcanic successions as well as those of similar sequences exposed in the East Greenland margin raise several important (and still debated) petrogenetic and tectono-magmatic questions, e.g. (1) do the considerable volumes of erupted picrites indicate abnormally high temperatures of partial melting of plume-related materials (Francis, 1985; Larsen and Pedersen, 2000, 2009; Hole and Millett, 2016); (2) does the heterogeneity of the mantle sources of Paleocene-Eocene mafic magmas foreshadow that of the present-day Icelandic hotspot (Holm et al., 1993; Peate and Stecher, 2003; Barker et al., 2006); and finally (3) does the temporal evolution of melting rates and depths record the successive stages of continental extension and rupture in the East (Larsen and Saunders, 1998; Abdelmalak et al., 2012, 2018) and West Greenland (Tegner et al., 1998; Barker et al., 2006) margins as well as in other parts of the NAIP (Kerr, 1994; Geoffroy, 2005; Meyer et al., 2007; Saunders et al., 2007)?

Svartenhuk Halvø Peninsula represents the northernmost exposure of the West Greenland Volcanic Province. The Svartenhuk wedge typically displays the structural and stratigraphic characteristics of inner-SDR wedges observed on deep seismic reflection profiles from VPM worldwide (e.g. Planke et al. 2000; Stica et al., 2014; Geoffroy et al., 2015). The thickness of the exposed volcanic sequence may reach up to 7 km and at least one third of it is made of picrites (Larsen and Pulvertaft, 2000). The aims of the present study are (1) to analyze magmatic processes such as mantle source heterogeneity, depths and rates of partial melting, and crustal contamination that occurred during the c. 10 m.y. of its emplacement (i.e. from 62.5-61 Ma to 54-53 Ma; Larsen et al., 2015; Chauvet et al., accepted), and (2) to discuss their temporal evolution during the successive stages of the continental stretching and thinning margin system related to the opening of the Baffin Bay oceanic basin.

2. Geological setting

2.1. The Labrador-Baffin oceanic domain and West Greenland Volcanic Province

The Labrador-Baffin axis is part of a wider Phanerozoic divergent system including the NE-Atlantic area between Eurasia and Greenland (Fig. 1). A continental and diachronous rift system developed between Greenland and Canada during the Cretaceous. This a-magmatic extension led to continental breakup with mantle exhumation in the southern Labrador Sea. A now extinct oceanic spreading axis in the Labrador Sea led to the drifting apart of Greenland from North America since the Late Cretaceous (Roest and Srivastava, 1989) or Paleocene (Chalmers and Laursen, 1995) and ceased to operate during the Oligocene (~ magnetochron C13, Roest and Srivastava, 1989). The SW-NE-trending left-lateral Ungava transform-fault system (UFS) connected the Labrador Sea to Baffin Bay farther North (Fig. 1).

In the northern Labrador Sea, the oldest undisputed oceanic magnetic anomaly has a mid-Paleocene age (Chalmers and Laursen, 1995), i.e. C27n (62.2 – 62.5 Ma, according to Ogg, 2012). During the Paleocene, the spreading directions were oriented ~N060E, i.e. sub-orthogonal to earlier rifted structures on the conjugate margins. Both the oceanic fracture zones and magnetic anomalies in the Labrador Sea indicate that a major shift in kinematics occurred during the Early Eocene, between C25 and C24, when spreading directions rotated from N060E to N010E (Roest and Strivastava, 1989; Geoffroy et al., 2001; Fig. 1).

In Baffin Bay, the age of the earliest accretion is still debated since no obvious linear magnetic anomalies can be identified on its floor, although there is a consensus for the cessation of spreading during the Oligocene (Roest and Strivastava, 1989; Oakey and Chalmers, 2012). Two major N-S-trending fracture zones in the central part of the Baffin Bay (Fig. 1) suggest that oceanic spreading may have been coeval with the ~N-S reorientation of the kinematic trend in the Labrador Sea during Eocene (Chalmers and Pulvertaft, 2001; Geoffroy et al., 2001; Suckro et al., 2012; Funck et al., 2012). Other authors (Oakey and Chalmers, 2012; Suckro et al., 2012; Hosseinpour et al., 2013) consider that earlier oceanic-type crust of mid-Paleocene age could exist within Baffin Bay. However, none of these studies took into account the age of continental stretching and thinning recorded along the Baffin Bay continental passive margins.

The conjugate passive margins in Baffin Bay (Fig. 1) are clearly of volcanic type in the South of the basin (Geoffroy et al., 2001; Skaarup et al., 2006; Block et al., 2012). The inner part of the SE-Baffin volcanic passive margin (VPM) is largely exposed from latitudes 69°N to 72°N in the Disko-Svartenhuk area (Fig. 1). An inner-SDR (Planke et al., 2000) developed orthogonally to the regional stretching direction during the

135 Paleogene (Geoffroy et al., 2001; Abdelmalak et al., 2012) and is fully exposed at
136 Svartenhuk where its total thickness reaches up to 7 km. Recently published Ar-Ar ages
137 (Larsen et al., 2015; Chauvet et al., accepted) that range from 62.5-61 Ma to 54-53 Ma
138 for Svartenhuk basalts provide new constraints for the tectono-magmatic evolution of
139 the Baffin Bay margin system.
140
141 *2.2. The Svartenhuk Halvø Peninsula*
142 The tectonics of the Svartenhuk SDR has already been investigated (Larsen and
143 Pulvertaft, 2000; Geoffroy et al., 2001; Abdelmalak et al., 2012). Until recently, the age
144 of the regional strain remained a matter of debate due to the lack of age determinations
145 on lavas in this area (see discussion in Larsen and Pulvertaft, 2000). However, new sets
146 of $^{40}Ar/^{39}Ar$ ages recently published by Larsen et al. (2015) and Chauvet et al.
147 (accepted) provide new constraints on the timing of melting processes at the scale of the
148 NAIP. In Svartenhuk Peninsula, the thickness of the exposed volcanic sequence may
149 reach up to 7 km (Larsen and Pulvertaft, 2000). Its dense fault network results from a
150 seaward-migrating strain (Geoffroy et al., 2001). The Arfertuarssuk Fault represents the
151 exposed master fault bounding and controlling the development of the Svartenhuk
152 wedge (Fig. 2).
153 In the present study and in the companion paper by Chauvet et al. (accepted)
154 dealing with the same sample set, the volcanic formations making up the SDR wedge in
155 Svartenhuk Halvø have been subdivided into four successive sequences (labeled V1 to
156 V4 upwards; Fig. 2) (Fig. 2). The boundaries between these sequences are consistent
157 with the geological and petrographic distinctions of Larsen (1983) and Larsen and
158 Grocott (1992).
159 Coeval volcanics crop out on Disko Island, Nuussuaq Peninsula and Ubekendt
160 Ejland Island, where they form a plurikilometric pile of ultramafic to mafic Paleogene
161 lavas crosscut by sheeted intrusions (e.g. Pedersen et al., 2002). The stratigraphy and
162 age of the W-Greenland basalts were defined in these areas as follows (Storey et al.,
163 1998 and references therein). The Vaigat Fm. consists of a lower sequence dominated
164 by hyaloclastites and pillow lavas overlain by picrites and Mg-rich subaerial basalts.
165 The earliest subaqueous volcanics unconformably overlie the remnants of an Early
166 Cretaceous to Paleogene paleobasin (Fig. 2). The overlying Maligât Fm. is dominated
167 by feldspar-phyric and aphyric basalts associated with a sharp change in lava chemistry
168 (Larsen and Pedersen, 2009). Larsen and Pulvertaft (2000) suggested that the lava

stratigraphy established in the Disko-Nuussuaq area could be applied to the Svartenhuk area. As such, the V1 and V2 formations correlate with the southern Vaigat Formation, while the "Svartenhuk Fm." (V3 in Fig. 2) would be equivalent to the Maligât Fm. (Fig. 3). In Svartenhuk Halvø, a 1-2 km thick succession of transitional to alkaline basalts (V4 unit) lies above the V3 unit. A stratiform sill-like trachytic body marks the boundary between the V3 and V4 units. Larsen and Grocott (1992) considered these basalts and trachyte as the uppermost part of the Svartenhuk Fm. According to Larsen et al. (2015), this succession belongs to a newly introduced Naqerloq Fm. (Fig. 2), dominated by transitional light rare Earth element (LREE) enriched basalts.

From observations on the Disko and Nuussuaq areas, two main volcanic pulses have been identified and further correlated by radiometric dating and paleomagnetic data (Storey et al., 1998; Riisager and Abrahamsen, 1999; Riisager et al., 2003). The earliest pulse was mid-Paleocene in age and spans chrons 27n and 26r (62.5-59.2 Ma after Ogg, 2012). The second pulse occurred during the early Eocene at C24r (54-57 Ma), i.e., after a hiatus of 2 m.y. or more. An Early Eocene age was obtained from the basaltic succession of the Kanísut Mb. (Storey et al., 1998), that crops out exclusively West of the Itilli fault, and which is seaward tilted at about 15° (Fig. 2, Riisager et al., 2003). These basalts lie unconformably above the Vaigat-Maligat basalts, which are in turn deeply down-faulted westward (Larsen et al., 2015). It is noteworthy that early Eocene ages were also obtained for dykes crosscutting the Paleocene-related series in Disko and Nuussuaq (Storey et al., 1998) and also in the Svartenhuk Peninsula (Geoffroy et al., 2001). Larsen et al. (2015) proposed that the Paleocene magmatic pulse in West Greenland spans not only C27n-C26r but also up to chron C25r (59-57.7 Ma), based on four $^{40}Ar/^{39}Ar$ ages ranging from 60.3 ± 1.4 Ma to 58.0 ± 0.6 Ma on Svartenhuk Fm. basalts from the northern part of the Svartenhuk peninsula. This implies that the Svartenhuk Fm. was mostly contemporaneous with the Maligât Fm. but that its upper part was younger. These authors also outlined that the transitional to alkaline basaltic successions exposed along the Arfertuarssuk Fault in Svartenhuk Halvø (V4 unit) and on the western parts of the Ubekendt Ejland, Nuussuaq peninsula and Hareøen are all early Eocene in age (Naqerloq and Erqa Fms). Chauvet et al. (accepted) point out that both in W-Nuussuaq and Svartenhuk the Eocene lavas are part of the syn-extension inner SDR, i.e. that continental crust thinning and stretching still occurred during the Eocene (fig. 2).

203 *2.3. Svartenhuk volcanic facies*

204 We investigated and sampled 45 sites mostly located along the coastal cross-
205 section of the Svartenhuk volcanic margin (Fig. 1). Hyaloclastic sub-aquatic breccias
206 and associated pillowed lavas formed in a lacustrine environment (Escher and
207 Pulvertaft, 1995) are characteristic of the lower member of the Vaigat Fm (V1 unit,
208 sampling sites 40 and 38). They are up to 200 m thick and dip 20-30° westwards. These
209 dips are mostly of tectonic origin but may also be due to dipping prograding foresets
210 (Jerram, 2002), which have been identified for instance in the Naajaat syn-volcanic
211 lake, Nuussuaq Basin (Pedersen et al., 1998). Svartenhuk hyaloclastic breccias consist
212 of basaltic glassy clasts and pillow fragments, usually of centimeter- to decimeter-size,
213 set in a matrix of yellowish glass particles altered to clays and palagonite. Locally,
214 preserved pillow piles form cliffs up to 10-15 m high which delineate small high points
215 on the shoreline. Individual basaltic pillows, 10 cm to 1 m large, display typical glassy
216 margins and radial fractures together with flow features consistent with their
217 emplacement over moderate slopes. Attempts to recover geochemically fresh glassy
218 basaltic rims were unsuccessful, but the cores of large pillows proved to be rather well
219 preserved from post-magmatic alteration.

220 Lava flows from V2, V3 and V4 units were exclusively emplaced in subaerial
221 environments as suggested by lack of pillow lavas and hyaloclastites and common
222 occurrence of pahoehoe surface features. Their most common facies, especially in V3
223 and V4 units, is that of individual tabular flows, 1 to 10 m thick. They generally show a
224 basal scoriaceous autoclastic breccia, which overlies a reddish thermal metamorphic
225 sole. These breccias are, in turn, overlain by a massive basaltic part often displaying
226 rough columnar-jointing patterns, and less frequently sheet flow patterns. The rather
227 common occurrence, in these massive levels, of subvertical vesicle pipes, sometimes
228 feeding horizontal vesicle sheets (Caroff et al., 2000), suggests that the Svartenhuk
229 Peninsula basaltic magmas were water-rich at the time of their emplacement. Tuff
230 horizons usually less than 50 cm thick are occasionally interbedded between these
231 tabular flows, and probably correspond to subaerial ash and/or lapilli fall deposits.
232 Intercalated reworked (volcanic-sedimentary) deposits are much less common than in
233 Disko and Nuussuaq (Larsen and Pedersen, 2000). They correspond to basaltic pebble
234 conglomerates of probable laharic origin, filling local topographic channels. Their
235 maximal thickness is less than 10 m (sites 44 and 45), and they are sometimes overlain
236 by layered clay horizons less than 1 m thick.

Vaigat Fm picrites (V2 unit) and less commonly Vaigat and Svartenhuk Fms tholeiitic basalts (V2 and V3) display a more specific emplacement facies, i.e. a compound-braided flow facies (Jerram, 2002). The corresponding lava piles, up to 30 m thick (site 39), have a typical grayish color also characteristic of Disko and Nuussuaq picrites, (Larsen and Pedersen (2009), and are usually deeply altered and converted into assemblages of post-magmatic minerals (mostly zeolites and carbonates). They consist of thin (usually less than 50 cm thick) anastomosed individual layers emplaced as sheets and lobes of pahoehoe lava breakouts. These individual lobes are elongated (up to several meters) and usually hollow; all the transitions are observed between meter-size lobes and typical lava tubes. Well preserved small pahoehoe ropy lava "tongues" often occur within the central cavity of these lobes or tubes, and provide good markers of flow emplacement patterns. In V2 and V3 units they point usually upwards due to the tectonic tilting of these sequences. Massive (and geochemically better preserved) porphyritic layers 50 cm to 2-3 m thick are common within the lobe/tube piles. They display intrusive relationships with respect to them (locally chilled margins) and are thought to result from inflation processes within the pahoehoe compound flow sequences (Jerram, 2002; Self et al., 1997). In the studied picritic lava sequences, both pahoehoe lobes/tubes and intrusive (inflation-related) sheets commonly contain large vesicles and vesicle pipes typical of water-rich magma emplacement features (Caroff et al., 2000). These facies are often ascribed to relatively low volume, low viscosity eruptions occurring during early stages of emplacement of continental flood basalts (Jerram, 2002).

Most dykes range in width from 10-20 cm to 2-3 m, and display characteristic jointing patterns perpendicular to their chilled margins (which are glassy to microlitic) and have coarser-grained, often porphyritic, vesicle-rich central parts. These dykes tend to form swarms associated with fracture zones, and composite (multiple) dykes are common. Sills are usually easily distinguished from lava flows by their larger and more regular columnar jointing patterns. The thickest ones (> 10 m) display evidence for gravitational settling of olivine phenocrysts, which accumulate above their lower chilled margin.

3. Sampling and analytical methods

3.1. Sampling strategy

Sampling was conducted in 45 sites mostly located along the coastal cross-section of the volcanic margin (Table 1 and Fig. 2), from the basal lacustrine hyaloclastites and pillow basalts of the Vaigat Fm (labelled V1 in the geochemical discussion below; sites 40 and 38) towards successively: the subaerial picritic and basaltic flows of the main Vaigat Fm (labelled V2; sites 37, 39, 41, 42, 20, 43, 45, 44, 5, 3, 6, 7, 1, 27, 25, 28); then those of the overlying Svartenhuk Fm (labelled V3; sites 4, 2, 36, 35, 8, 31, 32, 11, 10, 34, 12, 9, 33); and finally the trachytic intrusion (site 29) and the subaerial alkali basaltic lava flows from the top of the Svartenhuk Fm, recently attributed to the Naqerloq Fm by Larsen et al. (2015) (site 30, labelled V4 below). Additional samplings were done for V2 (sites 19, 22, 23, 16, 14, 15, 13), V3 (site 26) and V4 (site 21). Major, trace element and isotopic measurements were only carried out on samples from lava flows, dykes and sills which were relatively fresh based on their macroscopic and microscopic features, and from which zeolite- and carbonate-bearing vesicles were removed by handpicking. The corresponding analytical database includes 5 samples from V1, 53 from V2, 28 from V3 and 5 from V4 lava flows, together with 47 intrusive (sills, dikes) samples (Tables 1, 2, 3 and 4). Most of the pillow fragments collected from V1 are altered (Loss on Ignition higher than 1.9 wt%), and a number of compound-braided basaltic flows (pahoehoe lobes and lava tube piles, see below), especially from V2, are too rich in secondary minerals (zeolites and carbonates) to have retained their primary magmatic features. Such samples were primarily collected to investigate these post-magmatic mineral associations found as vesicle fillings and vein/fracture deposits (57 samples from V2 and V3).

3.2. Analytical methods

All samples were subsequently crushed in stainless steal and agate mortars. Major element concentrations were obtained using an ICP-AES Jobin Yvon Ultima 2 at the University of Brest, after a HF-HNO_3 digestion, boric acid neutralization and dilution in nitric acid, as described in Cotten et al. (1995). Trace element concentrations were measured with a Thermo® Element2 HR-ICP-MS in Brest. 15 mg of samples were repeatedly (twice) dissolved at 120°C in 2 mL Teflon Savilex® beakers using in 1mL HF + 0.5 mL $HClO_4$. After total evaporation, samples were diluted 10000 times using 0.5N HNO_3 and analyzed using both medium and low resolution on the Thermo® Element2 as discribed by Mougel et al. (2014). All samples were externally calibrated using international standards BCR2, BHVO2 and BIR-1 (Li and Lee, 2006). These

standards demonstrated external reproducibilities better than 5–10% depending on the element and concentration as documented in Supplementary Table 1. Pb, Hf, Sr and Nd isotope compositions were obtained on single fractions (0.5-1 g of samples) leached for one hour at 100°C in 6mL of 6N HCl, and subsequently dissolved in 3mL HF + 1mL HNO_3 following the protocol described by Mougel et al. (2014). Hf, Nd and Pb were purified following the protocol of Blichert-Toft et al. (2005) (fluoride centrifugation, and column chromatography). Sr was separated from the Nd fraction using Eichrom Sr-specific resin following the protocol by Moynier et al. (2010), adapted from Fietzke and Eisenhauer (2006). Pb, Hf and Nd isotopes were analysed using a Thermo® Neptune MC-ICP-MS at Ifremer-Brest. Sr isotopes were obtained using a Thermo Triton TIMS at the University of Brest. 2σ internal errors for Hf and Nd are reported in Table 4 and never exceed the last significant digit (1E-5) in each analysis. External reproducibility of Pb isotopes is estimated based on the repeated measurements since 2008 of a mixed standard solution and never exceeded 60 ppm for $^{206}Pb/^{204}Pb$, 150 ppm for $^{207}Pb/^{204}Pb$ and 300 ppm for $^{208}Pb/^{204}Pb$. Measured values were compared with repeatedly analyzed international standards NBS981 (Todt et al., 1996), JMC475 (Blichert-Toft et al., 1997) and La Jolla48 (Tanaka et al., 2000) shown in Supplementary Table 2. Duplicated Sr, Nd, Hf, Pb isotope analyses of one of our samples (S39E1) are shown in Supplementary Table 3.

4. Petrographic and geochemical results

4.1. Petrographic features and lava classification

Lava samples were classified according to their position in the Total Alkali-Silica plot (TAS; Le Bas et al., 1986; Fig 3a). With the exception of a trachytic intrusion from V4 (site 29), all of them plot within or near the fields of picrobasalts and basalts (SiO_2 = 43-53 wt%, K_2O+Na_2O=0.1-5 wt%). A large majority of them are silica-saturated or -oversaturated, and plot below the alkaline-subalkaline boundary of Macdonald and Katsura (1964). Therefore, these samples, which include all the massive or pillowed flows of units V1, V2 and V3, the sills and about half the population of dykes can be termed as tholeiitic or transitional picrites and basalts. Alkali basalts plotting above this boundary include the V4 basaltic flows (site 30) and the other half of the analyzed dykes. Some V3 basalts plot near or slightly above Macdonald and Katsura's (1964)

boundary (Fig. 3a) and can be considered as transitional, as well as V1 basalts which plot definitively below this limit but display strong enrichments in highly incompatible elements (see below).

Pillowed tholeiitic basalts from V1 unit display groundmass textures ranging from glassy (devitrified) rims to microlitic cores. They are subaphyric, with 4-8 modal% phenocrysts and microphenocrysts of olivine (mostly altered to smectite and chlorite) and fresh plagioclase ranging in size from 0.1 to 0.5 mm. Their groundmass is variably altered into clays and palagonite-type mineral aggregates. Zeolites and carbonates are found as vesicle- and vein-filling materials.

Picrites and picritic basalts (picrobasalts in Fig. 3a) are much more common in subaerial Vaigat Fm flows (V2) than in the overlying main unit of Svartenhuk Fm (V3). They are highly porphyritic, with up to 60 modal% centimeter- to millimeter-size olivine phenocrysts, containing occasional magnesiochromite inclusions, and subordinate (and smaller) plagioclase phenocrysts and microphenocrysts. The percentage of olivine phenocrysts and their size tend to decrease together with decreasing MgO contents of bulk rocks, while the relative abundance of plagioclase increases. Clinopyroxene microphenocrysts are uncommon in picrites, and this mineral follows plagioclase in the crystallization sequence of V2 and V3 lavas. The picritic basalts from these two units are rather similar in thin section. Their groundmass is usually intergranular or microlitic. Neither native iron, nor graphite has been identified in the studied picrites. This suggests a weaker contamination in these samples (originally selected for their primitive features) than that described for some more acidic samples from Disko and Nuussuaq (Larsen and Pedersen, 2009).

Tholeiitic basalts from V2 and V3 are the most common petrographic type encountered in the studied sequences. Their phenocryst contents are highly variable and decrease together with MgO contents of bulk rocks, from 25-20 modal% (porphyritic basalts) to less than 5 modal% (subaphyric basalts). Olivine is followed by calcic plagioclase, and then sometimes by minor amounts of augitic clinopyroxene in their crystallization sequence. Plagioclase phenocrysts dominate over olivine in the most evolved (silica-rich) samples, which are especially common in the Svartenhuk Fm main unit (V3). Clinopyroxene phenocrysts mostly occur in this V3 unit, and are uncommon in V2 basalts. The groundmass of tholeiitic basalts usually display microlitic to intergranular textures. Subdoleritic textures occur in sills and in the cores of thick flows and dykes.

372 Post-magmatic mineral associations are commonly found in V2 and V3 tholeiitic
373 picrites and basalts. They occur as vesicle- and vein-fillings, and include a variety of
374 zeolites, carbonates (calcite, Mg-calcite, aragonite, dolomite), and clays (smectites,
375 chlorites).
376 Alkali basalts from Naqerloq Fm. (V4) and from a number of dykes display
377 microlitic to intergranular groundmass textures. They contain about 10 to 15 modal%
378 phenocrysts, which are, by order of decreasing abundance, calcic plagioclase (up to 0.5
379 cm large), diopsidic clinopyroxene and magnesian olivine. They contain significantly
380 smaller amounts of post-magmatic minerals than V1, V2 and V3 lavas.
381 The fresh alkali trachyte collected at site 29 (V4 unit) is highly porphyritic, with
382 ~40 modal% centimeter-size sanidine phenocrysts, and lesser amounts of smaller
383 titanomagnetite, olivine and green clinopyroxene phenocrysts. Its groundmass, almost
384 exclusively made of alkali feldspar laths, displays a fluidal texture.
385
386 *4.2. Major element trends*
387 The Loss on Ignition (LOI) values (Table 2) range from 0.58 wt% to 10 wt%,
388 with an average of 2.8 wt%. These rather high values are accounted for by the common
389 occurrence of post-magmatic water-rich minerals (zeolites and clays) and of carbonates
390 in the studied lavas. The variations of SiO_2 and MgO in the studied basaltic flows (V1
391 to V4) are plotted against their Ni, CaO and alkali element contents. The higher MgO
392 contents of V2 lavas (Table 2) evidence the dominance of picrites (MgO> 12 wt%) and
393 Mg-rich basalts in the Vaigat subaerial flows. An upward increase of TiO_2 is also
394 observed in the stratigraphic pile: contents higher than 2 wt%, usually considered
395 typical of High-Ti basalts from Large Igneous Provinces (Pik et al., 1998; Shellnutt and
396 Jahn, 2011), are only observed in some V3 evolved tholeiitic and transitional basalts
397 and in V4 alkali basalts (Table 2). Conversely, all V1 and V2 basalts and a majority of
398 V3 tholeiites are typical Low-Ti basalts (TiO_2 < 2 wt%, Table 2). Similar features have
399 been reported by (Larsen and Pedersen, 2009) for the Disko and Nuussuaq areas, where
400 the lower Vaigat Fm is exclusively made of Low-Ti basalts while High-Ti lavas occur
401 within the overlying Maligât Fm (lateral equivalent of Svartenhuk Fm according to
402 Escher and Pulvertaft (1995).
403 Major element variations in the studied sequence are dominated (and largely
404 overprinted) by processes linked to accumulation or removal/fractionation of olivine
405 phenocrysts. Indeed, as shown in Figure 3B, addition or removal of magnesian olivine

406 are consistent with the covariation of CaO and MgO: olivine-rich picritic basalts are
407 CaO-poor while evolved basalts are CaO-rich. These variations are partly accounted for
408 by local gravitational settling effects involving olivine phenocrysts in thick lava flows
409 or sills. However, such shallow processes during and after emplacement are unlikely to
410 occur in thin pahoehoe units and meter-thick tabular flows which make up most of the
411 Vaigat and Svartenhuk Fms sequences. Therefore, fractional crystallization involving
412 olivine separation/accumulation must have occurred at depth, possibly within thick sills
413 or genuine underlying magma chambers. In addition, the least Mg-rich basalts, mostly
414 sampled from dykes, display a co-linear decrease of CaO and MgO (Fig. 3B), that is
415 consistent with concomitant removal/ fractionation of olivine plus augite and/or calcic
416 plagioclase. Such variations might result from differential motions of crystal-rich and
417 crystal-poor liquids during dyke emplacement ("Bagnold effect", e.g. Komar, 1972),
418 and thus cannot be taken as evidence for deep-seated fractional crystallization involving
419 olivine, augite and plagioclase.
420
421 *4.3. Trace element variations*
422 Compatible trace elements Ni, Co and Cr, which are hosted by olivine and
423 magnesiochromite, display positive correlations with MgO contents (Fig. 3B). Their
424 contents decrease from picrites to evolved basalts, and their behaviors are mainly
425 controlled by olivine removal/accumulation processes.
426 Incompatible element concentrations vary in a more complex fashion, as
427 illustrated by Rare Earth Element (REE) plots normalized to CI chondrite (Fig. 4). V1
428 transitional basalts display the most fractionated REE patterns and the highest contents
429 in Light REE (LREE; e.g. La, Ce), up to 80 times the primitive mantle (PM). V4 alkali
430 basalts also display fractionated REE patterns, although their LREE enrichment remains
431 lower than that of V1 lavas. V2 and V3 REE patterns are fan-shaped, and display
432 variable enrichments in LREE, those of picritic samples being the lowest. The REE
433 patterns of dykes are also fan-shaped, and they encompass the variability found within
434 lava flows (Fig. 4). Alkali basaltic dykes show fractionated patterns and LREE
435 enrichments similar to those observed for V4 alkali basaltic flows. A second family of
436 dykes (and the analyzed sills) has rather flat patterns which resemble those of picrites;
437 and a third dyke family shows moderately LREE enriched patterns similar to those of
438 V2 and V3 evolved tholeiitic basalts. Large Ion Lithophile Elements (LILE: Cs, Rb, Ba,
439 Sr) display somewhat erratic behaviors, with highly variable enrichments or depletions

generating positive or negative spikes in incompatible multi-element patterns normalized to the primitive mantle (Figure 4B). Given the high solubility of these elements into water, such variations can be considered as post-magmatic and attributed to alteration by surface waters and/or percolation of hydrothermal fluids through the studied lava piles. The elements less affected by post-magmatic processes (ie rare earth elements, high field strength elements…) define patterns similar to that of typical OIB (Fig. 5).

Highly incompatible elements (e.g. Th and La) versus MgO (not shown) in V2 and V3 lavas define a rough negative correlation (not shown) consistent with the "dilution" of incompatible elements in bulk rocks as a result of accumulation of incompatible element-poor olivine phenocrysts in picritic and Mg-rich lavas. Compared to V2 and V3, V4 alkali basalts and alkaline dykes display higher Th and La contents (Fig. 4) consistent with their more fractionated REE and multi-element patterns, as well as higher Nb/La ratios (Fig. 5). These features might indicate either lower degrees of partial melting, or a more incompatible element enriched source (with respect to V2 and V3 ones), or a combination of both. Finally, despite their transitional character, some V1 pillowed lavas (together with a few dykes) show the highest La, Th and Pb contents found in the studied lava sequence (Figs. 4 and 5), and consistent with their highly fractionated REE and multi-element patterns. Once again, these features could be attributed to a more enriched source, lower degrees of melting, or both.

4.4. Sr, Nd, Pb and Hf isotopes

Lead isotopes define two distinct trends (Figs. 6 and 7). ^{208}Pb /^{204}Pb range from 36.7 to 39, $^{207}Pb/^{204}Pb$ from 15 to 15.5 and $^{206}Pb/^{204}Pb$ from 16.13 to 19.26. A principal component analysis calculated on these Pb isotopes reveals the existence of only two significant principal components (the first one accounting for 94.2% of the total variability, principal component 2 for about 5.3%, and principal component 3 is insignificant). This result indicates that a mixture of three end-members is sufficient to explain the isotope variability in this area (Blichert-Toft et al., 2005). Hafnium isotopes are scattered as well, and feature both radiogenic and unradiogenic signatures ($^{176}Hf/^{177}Hf$ from 0.28247 to 0.2832; ε_{Hf}= -10.81 to +15.95). They also define a three end-members-pattern corresponding to two distinct mixing trends (Fig. 6). Nd isotopes correlate with Hf data ranging from $^{143}Nd/^{144}N$=0.51222 (ε_{Nd}=-8.15) to

$^{143}Nd/^{144}N=0.51309$ ($\varepsilon_{Nd}=8.9$). Even if most of the samples have "mantle-like" Sr isotopic compositions ($^{87}Sr/^{86}Sr < 0.704$), 16 of them display significantly more radiogenic Sr signatures (up to $^{87}Sr/^{86}Sr = 0.708$). Ten out of those 16 samples also have unradiogenic Pb ($^{206}Pb/^{204}Pb< 17$), and trace element patterns (low Nb, Ta and high Pb contents, Fig. 5) typical of continental crust contamination (Rudnick and Fountain, 1995; Rudnick and Gao, 2003). These samples include all of those collected from the basal unit V1.

The two mixing trends identified in Sr, Pb and Hf isotope spaces, are also visible on diagrams using isotopic and REE ratios (e.g., $^{206}Pb/^{204}Pb$, La/Sm, Sm/Yb and La/Yb, Fig. 8). They are also related to the stratigraphic position of the samples, i.e. their height within the lava pile. Indeed, all the samples from basal units V1 and V2 lie within the same trend (Figs. 6 and 7) connecting a component "Sk1" (with low $^{207}Pb/^{204}Pb$ and "intermediate" $^{208}Pb/^{204}Pb$) to a moderately high $^{208}Pb/^{204}Pb$ and $^{206}Pb/^{20}4Pb$ component "Sk2". Complementarily, all samples from units V3 and V4, together with those from sills and dykes, plot along a trend connecting "Sk2" to a component "Sk3" (with high $^{208}Pb/^{204}Pb$, $^{207}Pb/^{204}Pb$ and $^{206}Pb/^{204}Pb$).

5. Discussion

5.1. Trace element and isotopic evidence for a minor role of crustal contamination

The highly incompatible elements Nb and Ta display positive or negative peaks in multi-element patterns (Fig. 4B) which are unlikely of post-magmatic origin considering the insoluble character of these High Field Strength Elements (HFSE). Nb/La ratios show a tentative negative correlation with SiO_2, whereas Pb contents are positively correlated with silica for V1 and V2 lavas (Fig. 5). These features likely reflect crustal contamination effects in these two lowermost units, since silica-rich continental crust is selectively depleted in Nb and Ta and enriched in Pb with respect to elements of similar incompatibility, e.g. La (Tang et al, 2019 and references therein)..

Component Sk1 is clearly distinct from either "typical" mantle-reservoirs (Hart et al., 1992), or any North Atlantic volcanic rocks. Its radiogenic Sr, unradiogenic Hf and Nd, as well as the low Nb, Ta, and high Pb contents (Fig. 5) of lavas plotting close to it (Figs. 6 and 7) suggest that the origin of this component is related to continental crust contamination of mantle-derived melts by materials similar in composition to

Greenland basement late Archean orthogneisses and granodiorites analyzed by Larsen and Pedersen (2009). The fact that these contamination effects are limited to the oldest units V1 and V2 is consistent with the hypothesis of an uprise of the younger melts (constituting units V3 and V4) through a plumbing system coated with earlier basaltic lavas (e.g. Arndt and Christensen, 1992) or exhausted of fertile material by previous melting events (e.g. Meade et al, 2014).

5.2. Partial melting conditions

Si and Mg contents can be used as proxies in order to estimate pressure and temperature of melt extraction in the mantle (Lee et al., 2009). Only a limited number of samples are "primitive enough" (i.e. experienced only olivine fractionation), to adequately estimate their pristine major element concentrations by simple olivine addition (Albarède, 1992; Lee et al., 2009). Moreover, some of them, with MgO contents >15 wt%, need to be afterwards corrected for olivine accumulation (back to equilibrium with their olivine phenocrysts Mg#~0.83, Supplementary Table 4) and olivine fractionation (back to equilibrium with olivine of mantle-like composition Mg#~0.89). Thermobarometric estimates thus obtained on ten samples from units V2 and V3 suggest temperatures and pressures of ~1350±100 °C and 2.5±0.5 GPa, respectively. These results, although consistent with those recently reported by Hole and Natland (2019), need to be considered with caution, given the number of approximations in the thermobarometric approach, as well as uncertainties concerning the precise geological setting at that time (crustal thickness). The estimated temperature range suggests that the mantle beneath Svartenhuk was not very hot compared with other published evaluations for the NAIP (e.g. 1480-1550 °C, Hole and Millett, 2016; see also Herzberg et al. 2007 and references therein). Our estimated P-T conditions overlap the spinel/garnet transition zone in the mantle (2.2 GPa at 1300 °C, O'Neill, 1981; Robinson and Wood, 1998), and it is therefore probable that Svartenhuk Fm. lavas were extracted from melting columns involving both garnet- and spinel-bearing peridotites, as often proposed for NAIP magmas (Kerr, 1994; Kerr et al, 1999; Saunders et al., 2007; Hole and Millett, 2016).

Even if the "fan-shaped" rare earth elements (REE) patterns observed on figure 4 are partly the result of different rates of partial melting, LREE/HREE fractionation can also be accounted for by the presence of residual garnet in the source (e.g. Frey et al. 1978, Thirlwall et al.,1994). In figure 8 plots, Pb isotopes, La/Sm and Sm/Yb ratios are

compared with the average slope of REE spectra quantified by La/Yb ratios. The upper diagram ($^{206}Pb/^{204}Pb$ vs La/Yb) reflects the effects of crustal contamination (units V1 and V2) on geochemical compositions (see section 5.1). The middle diagram documents the concomitant effects of crustal contamination and degrees of partial melting on LREE/intermediate REE relative abundances. The lower plot provides insights concerning the amount of garnet-bearing peridotites involved in the melting column. Altogether, these three diagrams suggest that:

i/ Lavas derived from rather high degrees of partial melting all belong to units V2 and V3. Basalts from units V1 and V4 were generated by smaller degrees of mantle melting (as suggested by their alkali to transitional signatures in Figs. 4 and 5). Precise amounts of melting are difficult to assert considering the uncertainties concerning the initial composition(s) of mantle source(s). Nevertheless, models of garnet- (shown in red) and spinel-bearing (shown in green) batch lherzolite melting (see Gurenko and Chaussidon, 1995 for details on initial compositions, McKenzy and O'nion, 1991 for partition coefficients; and Thirlwall et al.1993 for mineral proportions in the melting) show that V1 and V4 lavas would are derived from melting degrees lower than 5%, and most V2 and V3 lavas from clearly higher ones (Fig. 8).

ii/ On average, basalts from units V2 and V3 feature Sm/Yb ratios 50% lower than those of samples from units V1 and V4. This stronger fractionation between intermediate and heavy REE in V1 and V4 suggests a larger involvement of garnet peridotites (and therefore greater melting depths) at the beginning and the end of the magmatic history than during the emplacement of the main V2-V3 volcanic sequences. These results are in agreement with previous petrogenetic studies of West Greenland picritic and Mg-rich basalts demonstrating that their main sequences derived predominantly from spinel-bearing peridotites (Gill et al., 1991; Ryabchikov et al., 1998; Larsen and Pedersen, 2000, 2009).

Therefore, we propose that small degrees of melting leading to V1 lavas were initiated at depths greater than 75 km below a relatively thick lithosphere. Subsequently, these melts propagated upwards into the spinel peridotite zone in connection with lithospheric thinning. The melting rates increased consistently during this process, forming V2 and V3 lavas. Finally, the melting zone deepened again, and melting rates decreased, thereby generating V4 alkali basalts.

5.3. Mantle source heterogeneity and its temporal evolution

The isotope diversity reported in this study covers a range similar to that previously reported for the neighboring Disko Island (Larsen and Pedersen, 2009) and the only differences concern the extent of crustal contamination (Fig. 5). The least contaminated samples (identified on Figs. 5 and 8) also largely overlap with samples from Iceland and the adjacent ridges, as well as with those from East Greenland (figs. 6 and 7). The isotopic diversity within the Iceland plume has been widely discussed (Chauvel and Hémond, 2000; Thirlwall et al., 2004; Kokfelt et al., 2006; Maclennan, 2008; Kitawaga et al., 2008) and is denoted in figure 7 by both depleted (D, Kitawaga et al., 2008; ID-1 and ID-2, Thirlwall et al., 2004), and enriched (E-1and E-2, Kitawaga et al., 2008; IE-1 and IE-2, Thirlwall et al., 2004) Icelandic internal components (Fig. 7). In figures 6 and 7, Hf, Sr and Pb compositions of component "Sk2" are very similar to those of OIB and E-MORB related to the Iceland hotspot, and more especially to a mixture of the Icelandic inner components "D" (for depleted) and "E-1" (for Enriched 1) of Kitawaga et al. (2008) or "ID1" – "ID2" (for Iceland Depleted 1 and 2) and "IE1" (for Iceland enriched 1) of Thirlwall et al. (2004).

Alternatively, Sk3 seems to correspond to the Iceland E-2 enriched component of Kitagawa et al. (2008) (or "IE-1" of Thirlwall et al., 2004) that point toward the common component C (Hanan and Graham, 1996) in all isotope spaces. This enriched component has been proposed to be intrinsic to the Icelandic hotspot (Hanan and Schilling, 1997; Kitawaga et al., 2008; Thirlwall et al., 2004; Peate et al., 2010). The presence of distinct Icelandic isotopic components has also been described in Eastern Greenland (Barker et al., 2006). Nevertheless, in that region, the different signatures appear in separate areas (Milne, Rømer and Skræterne), located hundreds of kilometers away from each other. In the present study, we report distinct signatures on samples all coming from a restricted segment (<40 km along the coast) and covering a time span shorter than 8 m.y. Such diversity can therefore hardly be imagined as the result of the tapping of distinct parts of an Iceland type mantle plume. Instead, we suggest that the Sk3 signature in our dataset corresponds to a trend toward the C component of Hanan and Graham (1996). This component has been recognized as being widely disseminated within the upper mantle feeding the Arctic segments of the mid-Atlantic ridges and is therefore believed to correspond to an ubiquitous ingredient of the North Atlantic upper mantle (Blichert-Toft et al., 2005).

Nb, Zr and Y concentrations also suggest consistency between uncontaminated Svartenhuk samples and Iceland plume geochemical signatures. Indeed, Fitton et al. (1997) used the comparison of Nb/Y and Zr/Y in order to decipher whether the magmatic sources of basalts are more likely related to the Iceland plume or to the neighboring MORB mantle. They proposed a ΔNb index =1.72 + log(Nb/Y) - 1.92log(Zr/Y); where ΔNb is negative in MORB samples, but positive in Iceland plume-derived material. Even if this approach has been criticized as possibly biased by differences in pressures of melting (Hanan et al., 2000; Stracke et al., 2003), it is worth noting that most samples from this study feature positive ΔNb values. Indeed, in Figure 9, only some samples from units V2 and V3 display negative ΔNb (Fig. 9), suggesting that the contribution of Icelandic material in lava sources was lower during these intermediate stages than during the emplacement of the earliest and latest V1 and V4 units. Moreover, a plume imprint on geochemical signatures of Svartenhuk lavas is also consistent with the extremely primitive helium isotopic compositions recently published by Péron et al. (2018) for olivines from our V3 samples S33E7 and S35E7 (R/Ra=31.0 and 34.9, respectively), similar to those previously reported for samples from Disko Island and Baffin Island (Graham et al., 1998; Jackson et al., 2010).

Altogether, these features suggest that the Sk2-Sk3 trend (common to both V3 and V4 units) could be accounted for by a mixture of Icelandic-type material (Sk2) and a mixed ambient upper mantle reservoir (Sk3). The respective proportions of these two components appear to evolve through time, since only samples coming from unit V3 carry isotope signatures suggesting the involvement of significant amounts of C-like material, whereas the uppermost V4 lavas seem to tap preferentially Iceland hotspot material. Furthermore, even if geochemical signatures of V1 and V2 are partly controlled by crustal contamination, they also point solely toward the Iceland-like signature. This sequence of magmatic events is summarized in figures 10 (petrogenetic constraints) and 11 (speculative tectonic interpretation). During the emplacements of basal units V1 and V2 (61 to 59.5 Ma old, Chauvet et al., accepted), initially low, but temporally increasing degrees of melting of enriched Icelandic plume material (displaying Sk2 isotopic signatures) generated basaltic melts at depths starting beneath 75 km, and these magmas were contaminated during their ascent through the continental crust. During V3 emplacement (59.5-57.7 Ma), the melting process affected a wider range of lithologies in the spinel stability field and propagated to neighboring

(shallower) materials from the upper mantle (involving material displaying component Sk3 isotope signatures), with little or undetectable crustal contamination. Finally, during V4 emplacement, i.e. between 57.7 and 53.3 Ma (Chauvet et al., accepted), the melting zone deepened again and was once more mostly restricted to the enriched mantle material (Figs. 10 and 11).

5.4. Baffin Bay breakup and tectonic controls of mantle melting

This sequence of events as reported by combining geochemical and tectonic data can be interpreted as the progressive initiation of decompression melting of an upwelling mantle below a progressively thinning lithosphere in a continental extension setting (Fig. 11). The thinning observed between the emplacement of V1 and V2-V3 lavas likely results from a combination of the tectonic stretching of the upper part of the lithosphere and of the thermal erosion of its base by convecting hot mantle (Fig. 11). Such a combination has been proposed as an explanation of the magmatic history of Mull and Skye islands (Kerr, 1994; Kerr et al., 1999; Saunders et al., 1997). In these islands, as well as in Giant's Causeway basalts (Barrat and Nesbitt, 1996), temporally increasing melting rates and decreasing melting pressures similar to those described in Svartenhuk are observed, despite rather different tectonic contexts characterized by lower extension rates (Meyer et al., 2007). A temporal decrease of lithospheric thickness seems the most likely factor controlling such changes in NAIP basaltic magma compositions (Ellam, 1992; Kerr, 1994).

The decreasing involvement of the ambient mantle (component Sk3) contribution from V3 to V4 (Fig. 10), and the concomitant deepening and decrease of partial melting rates (back to alkali basaltic compositions) in this most proximal part of the volcanic margin, may be (at least partly) attributed to the gradual westward shift of extension with time (Geoffroy et al., 2015; Chauvet et al., accepted). Indeed, the innermost Svartenhuk margin progressively became passive although extension still continued (as attested by syn-tectonic control of V4 emplacement), albeit at lower rates (Chauvet et al, accepted). It is also possible that the accumulation beneath the lithosphere of refractory mantle residues left after melt extraction blocked the ascent of hot and fertile mantle sources and resulted in deeper, lower-degree melting as previously suggested for East Greenland flood basalts (Fram and Lesher, 1993, 1997).

6. **Conclusions**

Geochemical data obtained on 93 samples of basaltic to trachytic rocks from the Svartenhuk peninsula allow us to document the c. 7 m.y. long volcanic activity accompanying the continental thinning process that preceded the Eocene opening of Baffin Bay, the chronological and tectonic aspects of which are discussed in a companion paper (Chauvet et al., accepted). The sequence of magmatic events started with (i) the deep (>75 km) low degree partial melting of an Iceland plume-like source, followed by (ii) shallower and higher degrees of melting of a mixture of Iceland hotspot and "ambient upper mantle" materials, and finally ended with (iii) lower degrees of melting of a deeper source dominated again by Icelandic-type signatures. The first melting event could have been triggered by the adiabatic ascent of the Iceland plume below a ~75-km-thick lithosphere, inherited from the previous Mesozoic extension. The OIB-type signature of V1 lavas is clear despite the crustal contamination processes that they experienced during their ascent. The following melting events (V2 to V3 lavas) occurred at decreasing pressures and were coeval with syn-magmatic extension in the upper crust (Chauvet et al., accepted) and therefore a subsequent reduction in lithosphere thickness (Figs. 10 and 11). Thus, V2-V3 melts were a direct consequence of the convective upwelling of Icelandic OIB-type mantle in the necked sub-lithospheric area (Boutiller and Keen, 1999), associated with lithospheric thinning resulting from a combination of tectonic stretching and thermal erosion of the Svartenhuk lithosphere. The later decrease in magmatic activity (emplacement of V4 lavas) was concomitant with a progressive focusing of syn-magmatic strain towards the central axis of the proto-Baffin Bay during the Eocene. This shift in extension was likely accompanied by a progressive cooling (and thus, thickening) of the proximal W-Greenland lithosphere over a still convecting asthenosphere. The combined decrease in melting rates and the return to enriched source materials suggest a further deepening of the melting zone, possibly linked to the accumulation beneath the lithosphere of refractory mantle residues.

Acknowledgments

This study is part of the Petrobras-UBO Volcabasin program. The field work was carried out during a five-week expedition in the summer of 2012 and benefited from the logistic support of the research vessel Porsild from the Arctic Station in Godhavn (Greenland) and the French polar yacht Vagabond. Philippe Nonnotte's help was especially appreciated before and during the fieldwork in Greenland. We also thank the

Vagabond family, who provided pleasant and efficient assistance, both at sea and in the field. AA and RCM thank Claire Bassoullet, Philippe Nonnotte, Céline Liorzou and Bleuenn Gueguen for their help during the analytical work. AA thanks David Graham and Barry Hanan for insightful discussions. We are grateful to Elishevah Van Kooten for her careful reading. The manuscript was considerably improved following the suggestions of Editor A.C. Kerr and the thorough reviews of Drs. R. Gooday and N. Arndt.

References

Abdelmalak, M.M, Geoffroy, L., Angelier, J., Bonin, B., Callot, J.P., Gelard, J.P., Aubourg, C., 2012. Stress fields acting during lithosphere breakup above a melting mantle: A case example in West Greenland. Tectonophysics 581, 132-143.

Abdelmalak, M.M, Planke, S., Polteau, S., Hartz, E.H., Faleide, J.I., Tegner, C., Jerram, D.A., Millett, J.M., Myklebust, R., 2018. Breakup volcanism and plate tectonics in the NW Atlantic. Tectonophysics in press, doi.org/10.1016/j.tecto.2018.08.002

Agranier, A., Blichert-Toft, J., Graham, D., Debaille, V., Schiano, P., Albarede, F., 2005. The spectra of isotopic heterogeneities along the mid-Atlantic Ridge. Earth Planet. Sci. Lett. 238, 96–109.

Albarède, F., 1992. How deep do common basaltic magmas form and differenciate. J. Geophys. Res.-Solid Earth 97, 10997–11009.

Arndt, N., Christensen, U., 1992. The role of lithospheric mantle in continental flood volcanism - thermal and geochemical constraints. J. Geophys. Res.-Solid Earth 97, 10967–10981.

Barrat, J.A., Nesbitt, R.W., 1996. Geochemistry of the tertiary volcanism of Northern Ireland. Chem. Geol. 129, 1-2, 15-38.

Barrat, J. A., Yamaguchi, A., Greenwood, R. C., Bohn, M., Cotten, J., Benoit, M., Franchi, I.A., 2007. The Stannern trend eucrites: Contamination of main group eucritic magmas by crustal partial melts. Geochim. Cosmochim. Acta, 71, 16, 4108-4124

Barker, A. K., Baker, J. A., Peate, D., W., 2006. Interaction of the rifting East Greenland margin with a zoned ancestral Iceland plume. Geology 34, 481–484.

Blichert-Toft, J., Agranier, A., Andres, M., Kingsley, R., Schilling, J., Albarède, F., 2005. Geochemical segmentation of the Mid-Atlantic Ridge north of Iceland and ridge-hot spot interaction in the North Atlantic. Geochem. Geophys. Geosystems 6. https://doi.org/10.1029/2004GC000788

Blichert-Toft, J., Chauvel, C., Albarede, F., 1997. Separation of Hf and Lu for high-precision isotope analysis of rock samples by magnetic sector multiple collector ICP-MS. Contrib. Mineral. Petrol. 127, 248–260.

Block, M., Damm, V., Ehrhardt, A., Berglar, K., Schnabel, M., Altenbernd, T., 2012. Characteristics of the West Greenland Margin in the Southern Baffin Bay. 74th EAGE Conference & Exhibition, Abstract, 10.3997/2214 4609.20148225.

Boutiller, R.R., Keen, C.E., 1999. Small-scale convection and divergent plate boundaries. J. Geophys. Res.-Solid Earth 104, B4, 7389–7403.

753 Breddam, K., 2002. Kistufell: Primitive melt from the Iceland mantle plume. Journal
754 of Petrology 43, 2, 345–373.
755 Callot, J.-P., 2002. Origine, structure et developpement des marges volcaniques:
756 l'exemple du Groenland. Univerité Paris 6, Ecole Normale Supérieure.
757 Caroff, M., Maury, R.C., Cotten, J., Clément, J.P., 2000. Segregation structures in
758 vapor-differentiated basaltic flows. Bull. Volcanol. 62, 171–187.
759 Chalmers, J.A. and Laursen, K.H., 1995. Labrador Sea – the extent of continental and
760 oceanic-crust and the timing of the onset of sea-florr spreading. Marine
761 Petroleum Geology 12, 2, 205-217.
762 Chalmers, J.A. and Puvertaft, T.C.R., 2001. Development of the continental margins
763 of the Labrador Sea: a review. Geol. Soc. Special Pub. 187, 77-105.
764 Chauvel, C., Hemond, C., 2000. Melting of a complete section of recycled oceanic
765 crust: Trace element and Pb isotopic evidence from Iceland. Geochem.
766 Geophys. Geosystems 1, 1001. https://doi.org/10.1029/1999GC000002
767 Chauvet, F., Geoffroy, L., Guillou, H., Maury, R.C., Le Gall, B., Agranier, A.,
768 Aviana, A., accepted. Eocene continental breakup in Baffin Bay.
769 Tectonophysics
770 Coffin, M.F., Eldholm, O., 1994. Large Igneous provinces – crustal structure,
771 dimensions, and external consequences. Reviews Geophysics 32, 1-36.
772 Cotten, J., Le Dez, A., Bau, M., Caroff, M., Maury, R., Dulski, P., Fourcade, S.,
773 Bohn, M., Brousse, R., 1995. Origin of anomalous rare-Earth element and
774 Yttrium enrichments in subaerially exposed basalts, evidence from French
775 Polynesia. Chem. Geol. 119, 115–138.
776 Courtillot, V., Jaupart, C., Manighetti, I., Tapponnier, P., Besse, J., 1999. On causal
777 links between flood basalts and continental breakup. Earth Planet. Sci. Lett.
778 166, 3-4, 177-195.
779 Eggins, S.M., Woodhead, J.D., Kinsley, L.P.J., Mortimer, G.E., Sylvester, P.,
780 McCulloch, M.T., Hergt, J.M., Handler, M.R., 1997. A simple method for the
781 precise determination of >=40 trace elements in geological samples by ICPMS
782 using enriched isotope internal standardisation. Chem. Geol. 134, 4, 311-326.
783 Ellam, R.M., 1992. Lithospheric thickness as a control on basalt geochemistry.
784 Geology, 20, 2, 153-156.
785 Escher, J.C., Pulvertaft, T.C.R., 1995. Geological map of Greenland, 1:2 500 000.
786 Geol. Surv. Greenl.
787 Fietzke, J., Eisenhauer, A., 2006. Determination of temperature-dependent stable
788 strontium isotope (Sr-88/Sr-86) fractionation via bracketing standard MC-ICP-
789 MS. Geochem. Geophys. Geosystems 7, Q08009.
790 https://doi.org/10.1029/2006GC001243
791 Fitton, J.G., Saunders, A.D., Norry, M.J., Hardason, B.S., Taylor, R.N., 1997.
792 Thermal and chemical structure of the Iceland plume. Earth Planet. Sci. Lett.
793 153, 3-4, 197–208.
794 Francis, D.,1985. The Baffin-Bay lavas and the value of picrites as analogs of primary
795 magmas. Contrib. Mineral. Petrol., 89, 2-3, 144-154.
796 Fram, M.S., Lesher, C.E., 1993. Geochemical constraints on mantle melting during
797 creation of the North-Atlantic basin. Nature 363, 6431, 712-715.
798 Fram, M.S., Lesher, C.E., 1997. Generation and polybaric differentiation of East
799 Greenland early tertiary flood basalts. Journal of Petrology 38, 2, 231-275.
800 Frey, F.A., Green, D.H., Roy, S.D., 1978. Integrated models of basalt petrogenesis: a
801 study of quartz tholeiites to olivine melilites from south eastern Australia

utilizing geochemical and experimental petrological data. Journal of Petrology 19, 463-513.
Funck, T., Gohl, K., Damm, V., Heyde, I., 2012. Tectonic evolution of southern Baffin Bay and Davis Strait: Results from a seismic refraction transect between Canada and Greenland. J. Geophys. Res. 117, B04107.
Geoffroy, L., 2005. Volcanic passive margins. C. R. Geoscience 337, 1395–1408.
Geoffroy L., Burov, E.B., Werner, P., 2015. Volcanic passive margins: another way to break up continents. Scientific Reports 5, 14828, DOI: 10.1038/srep14828.
Geoffroy, L., Callot, J.P., Scaillet, S., Skuce, A.S., Gélard, J.-P., Ravilly, M., Angelier, J., Bonin, B., Cayet, C., Perrot-Galmiche, K., Lepvrier, C., 2001. Southeast Baffin volcanic margin and the North American–Greenland plate separation. Tectonics 20, 566–584.
Gill, R.C.O., Pedersen, A.K., Larsen, J.G., 1991. Tertiary picrites in West Greenland: Melting at the periphery of a plume?, in: Magmatism and the Causes of Continental Break-Up. Programme and Abstracts. p. 13.
Gurenko, A.A., Chaussidon, M., 1995. Enriched and depleted primitive melts included in olivine from Icelandic tholeiites – origin by continuous melting of a single Mantle column. Geochim. Cosmochim. Acta 59, 14, 2905-2917.
Graham, D.W., Larsen, L.M., Hanan, B.B., Storey, M., Pedersen, A.K., Lupton, J.E., 1998. Helium isotope composition of the early Iceland mantle plume inferred from the Tertiary picrites of West Greenland. Earth Planet. Sci. Lett. 160, 241-255.
Hanan, B.B., Blichert-Toft, J., Kingsley, R., Schilling, J.G., 2000. Depleted Iceland mantle plume geochemical signature: artifact of multicomponent mixing? Geochem. Geophys. Geosystems 1, 1003, http://doi:10.1029/1999GC000009.
Hanan, B.B., Graham, D.W., 1996. Lead and helium isotope evidence from oceanic basalts for a common deep source of mantle plumes. Science 272, 991–995.
Hanan, B.B., Schilling, J.G., 1997. The dynamic evolution of the Iceland mantle plume: the lead isotope perspective. Earth Planet. Sci. Lett. 151, 43–60.
Hart, S., Hauri, E., Oschmann, L., Whitehead, J., 1992. Mantle plumes and entrainment - isotopic evidence. Science 256, 517–520.
Herzberg, C., Asimow, P.D., Arndt, N., Niu, Y.L., Lesher, C.M., Fitton, J.G., Cheadle, M.J., Saunders, A.D., 2007. Temperatures in ambient mantle and plumes: Constraints from basalts, picrites, and komatiites. Geochem. Geophys. Geosystems 8, Q02006. https://doi.org/10.1029/2006GC001390
Hole, M.J., Millett, J.M., 2016. Controls of Mantle Potential Temperature and Lithospheric Thickness on Magmatism in the North Atlantic Igneous Province. Journal of Petrology 57, 2, 417-436.
Hole, M.J., Natland, J.H., 2019. Magmatism in the North Atlantic Igneous Province; mantle temperatures, rifting and geodynamics. Earth-Science Reviews, in press, https://doi.org/10.1016/j.earscirev.2019.02.011
Holm, P.M., Gill, R.C.O , Pedersen, A.K., Larsen, J.G., Hald, N., Nielsen, T.F.D., Thirlwall, M.F., 1993. The Tertiary picrites of West Greenland – contribution from Icelandic and other sources. Earth Planet. Sci. Lett. 115, 1-4, 227-244.
Hosseinpour, M., Müller, R.D., Williams, S.E., Whittaker J.M., 2013. Full-fit reconstruction of the Labrador Sea and Baffin Bay. J. Geophys. Res. -Solid Earth 4, 461–479.
Jackson, M.G., Carlson, R.W., Kurtz, M.D., Kempton, P.D., Francis, D., Blusztajn, J., 2010. Evidence for survival of the oldest terrestrial mantle reservoir. Nature 466, 853-856, doi:1.138/nature09287.

Jerram, D.A., 2002. Volcanology and facies architecture of flood basalts. Geological Society of America Special Papers 362, 119-132 .
Kerr, A.C. 1994, Lithospheric thinning during the evolution of continental large igneous provinces – a case study from the North-Atlantic **T**ertiary province. Geology 22, 11, 1027-1030.
Kerr, A.C., Kent, R.W., Thomson, B.A., Seedhouse, J.K., Donaldson, C.H., 1999. Geochemical evolution of the Tertiary Mull volcano, Western Scotland. Journal of Petrology 40, 6, 873-908.
Kitawaga, H., Kobayashi, K., Makishiama, A., Nakamura, E., 2008. Multiple pulses of the mantle plume: evidence from tertiary Icelandic lavas. Journal of Petrology 49, 7, 1365–1396.
Kokfelt, T.F., Hoernle, K., Hauff, F., Fiebig, J., Werner, R., Garbe-Schonberg, D., 2006. Combined trace element and Pb, Nd, Sr, O isotope evidence for recycled oceanic crust (upper and lower) in the Iceland mantle plume. Journal of Petrology 47, 9, 1705–1749.
Kokfelt, T.F., Hoernle, K., Lundstrom, C., Hauff, F., Van den Bogaard, C., 2009. Time-scales for magmatic differentiation at the Snaefellsjokull central volcano, western Iceland: Constraints from U-Th-Pa-Ra disequilibria in post-glacial lavas. Geochim. Cosmochim. Acta 73, 4, 1120–1144.
Komar, P.D. 1972. Mechanical interactions of phenocrysts and flow differentiation of igneous dikes and sills. Geol. Soc. Am. Bull. 83, 973-988
Kuritani, T., Yokohama, T., Kitawaga, H., Kobayashi, K., Nakamura, E., 2011. Geochemical evolution of historical lavas from Askja Volcano, Iceland: Implications for mechanisms and timescales of magmatic differentiation. Geochim. Cosmochim. Acta 75, 2, 570–587.
Larsen, J.G., 1983. Geologisk kort over Grønland, 1:100 000, Igdlorssuit, 71 V.1 Syd. København: Grønlands Geologiske Undersøgelse (English legend).
Larsen, J.G., Grocott, J., 1992. Geologisk kort over Grønland, 1:100 000, Svartenhuk, 71 V.1 Nord. København: Grønlands Geologiske Undersøgelse (English legend).
Larsen, L.M., Pedersen, A.K., 2000. Processes in high-Mg, high-T magmas: Evidence from olivine, chromite and glass in palaeogene picrites from West Greenland. Journal of Petrology 41, 1071–1098.
Larsen, L.M., Pedersen, A.K., 2009. Petrology of the Paleocene Picrites and Flood Basalts on Disko and Nuussuaq, West Greenland. Journal of Petrology 50, 1667–1711.
Larsen L.M., Pedersen, A.K., Tegner, C., Duncan, R.A., Hald, N., Larsen, J.G., 2015. Age of Tertiary volcanic rocks on the West Greenland continental margin: volcanic evolution and event correlation to other parts of the North Atlantic Igneous Province. Geol. Mag. 153, 487-511.
Larsen, J.G., Pulvertaft, T.C.R. 2000. The structure of the Cretaceous-Palaeogene sedimentary-volcanic area of Svartenhuk Halvø, central West Greenland. Geology of Greenland Survey Bulletin, 188, 1-40.
Larsen, H.C., Saunders, A.D., 1998. Tectonism and volcanism at the southeast Greenland rifted margin: a record of plume impact and later continental rupture. Proc. Ocean Drill. Program Sci. Results 152, 503-533.
Le Bas, M., Le Maitre, R., Streckeisen, A., Zanettin, B., 1986. A chemical classification of volcanic rocks based on the total alkali silica diagram. Journal of Petrology 27, 745–750.

Le Breton, E., Cobbold, P.R., Dauteuil, O., Lewis, G., 2012. Variations in amount and direction of seafloor spreading along the northeast Atlantic Ocean and resulting deformation of the continental margin of northwest Europe. Tectonics 31, TC5006.

Lee, C.-T.A., Luffi, P., Plank, T., Dalton, H., Leeman, W.P., 2009. Constraints on the depths and temperatures of basaltic magma generation on Earth and other terrestrial planets using new thermobarometers for mafic magmas. Earth Planet. Sci. Lett. 279, 20–33.

Li, Z.X.A., Lee, C.-T.A., 2006. Geochemical investigation of serpentinized oceanic lithospheric mantle in the Feather River Ophiolite, California: Implications for the recycling rate of water by subduction. Chemical Geology 235, 161-185.

Macdonald, G.A., Katsura, T., 1964. Chemical composition of Hawaii lavas. Journal of Petrology 5, 82-133.

Maclennan, J., 2008. Lead isotope variability in olivine-hosted melt inclusions from Iceland Geochim. Cosmochim. Acta 72 4159–4176.

McDonough, W.F., Sun, S.S., 1995. The composition of the Earth. Chem. Geol. 120, 223–253.

McKenzie, D., O'Nions, R.K., 1991. Partial melt distribution from inversion of Rare Earth Element concentrations. Journal of Petrology 32, 5, 1021-1091.

Meade, F.C., Troll, V.R., Ellam, R.M., Freda, C., Font, L., Donaldson, C.H., Klonowska, I., 2014. Bimodal magmatism produced by progressively inhibited crustal assimilation. Nat. Commun. 5, 4199, DOI: 10.1038/ncomms5199.

Meyer, R., Van Wijk, J., Gernigon, L., 2007. The North Atlantic Igneous Province: a review of models for its formation. Geol. Soc. Amer., Special Paper 430, 525-552.

Mougel, B., Agranier, A., Hemond, C., Gente, P., 2014. A highly unradiogenic lead isotopic signature revealed by volcanic rocks from the East Pacific Rise. Nat. Commun. 5, 4474. https://doi.org/10.1038/ncomms5474

Moynier, F., Agranier, A., Hezel, D.C., Bouvier, A., 2010. Sr stable isotope composition of Earth, the Moon, Mars, Vesta and meteorites. Earth Planet. Sci. Lett. 300, 359–366.

Oakey, G.N., Chalmers, J.A., 2012. A new model for the Paleogene motion of Greenland relative to North America: Plate reconstructions of the Davis Strait and Nares Strait regions between Canada and Greenland. J. Geoph. Res. Solid Earth 117, B10401.

Ogg, J.G., 2012. Geomagnetic Time Scale. In: Gradstein, F.M., Ogg, J.G., Schmitz, M., Ogg, G. (eds), The Geologic Time Scale 2012. Elsevier, Amsterdam, 85-113.

O'Neill, H.S.C., 1981. The transition between spinel lherzolite and garnet lherzolite, and its use as a geobarometer. Contrib. Mineral. Petrol. 77: 185–194.

Peate, D.W., Baker, J.A., Jakobsson, S.P., Waight, T.E., Kent, A.J.R., Grassineau, N.V., Skovgaard, A.C., 2009. Historic magmatism on the Reykjanes Peninsula, Iceland: a snap-shot of melt generation at a ridge segment. Contrib. Mineral. Petrol. 157, 3, 359–382.

Peate, D.W., Breddam, K., Baker, J.A., Kurtz, M., Barker, A.K., Prestvik, T., Grassineau, N., Skovgaard, A.C., 2010. Compositional characteristics and spatial distribution of enriched Icelandic mantle components. Journal of Petrology 51, 7, 1447–1475.

Peate, D.W., Stecher, O., 2003. Pb isotope evidence for contributions from different Iceland mantle components to Palaeogene East Greenland flood basalts. Lithos 67, 1-2, 39-52.

951 Pedersen, G.K., Larsen, L.M., Pedersen, A.K., Hjortkjaer, B.F., 1998. The syn-
952 volcanic Naajaat lake, Paleocene of West Greenland. Palaeogeogr.
953 Palaeoclimatol. Palaeoecol. 140, 271–287.
954 Pedersen, A.K., Larsen, L.M., Riisager, P., Dueholm, K.S., 2002. Rates of volcanic
955 deposition, facies changes and movements in a dynamic basin: the Nuussuaq
956 Basin, West Greenland, around the C27n-C26r transition. In: Jolley, D. W. and
957 Bell, B.R. (eds) The North Atlantic Igneous Province: Stratigraphy, Tectonic,
958 Volcanic and Magmatic Processes. Geological Society, London, Special
959 Publications 197, 157-181.
960 Péron, S., Moreira, M., Agranier, A., 2018. Origin of Light Noble Gases (He, Ne, and
961 Ar) on Earth: A Review. Geochem. Geophys. Geosystems 19, 4, 979-996,
962 http://DOI: 10.1002/2017GC007388.
963 Petersen, K.D., Schiffer, C., Nagel, T., 2018. LIP formation and protracted lower
964 mantle upwelling induced by rifting and delamination. Scientific Reports 8,
965 16578, DOI:10.1038/s41598–018–34194–0.
966 Pik, R., Deniel, C., Coulon, C., Yirgu, G., Hofmann, C., Dereje, A., 1998. The
967 Northwestern Ethiopian Plateau flood basalts : Classification and spatial
968 distribution of magma types. J. Volcanol. Geotherm. Res. 91–111.
969 Planke, S., Symonds, P.A., Avelstad, E., Skogseid, J., 2000. Seismic
970 volcanostratigraphy of large-volume basaltic extrusive complexes on rifted
971 margins. J. Geophys. Res. 105, 19333–19351.
972 Riisager, P., Abrahamsen, N., 1999. Magnetostratigraphy of Palaeocene basalts from
973 the Vaigat Formation of West Greenland. Geophysical Journal International
974 137, 774-782.
975 Riisager, J., Riisager, P., Pedersen, A.K., 2003. Paleomagnetism of large igneous
976 provinces:Case-study from West Greenland, North Atlantic igneous province,
977 Earth Planet. Sci. Lett. 214, 409–425.
978 Robinson, J.A.C., Wood, B.J., 1998. The depth of the spinel to garnet transition at the
979 peridotite solidus. Earth Planet. Sci. Lett. 164, 277–284.
980 Roest W. R., Srivastava, S.P., 1989. Sea-floor spreading in the labrador sea – a new
981 reconstruction. Geology 17, 11, 1000-1003.
982 Rudnick, R., Fountain, D., 1995. Nature and composition of the continental crust, a
983 lower crustal perspective. Rev. Geophys. 33, 267–309.
984 Rudnick, R., Gao, S., 2003. Composition of the continental crust, in: The Crust.
985 Elsevier, Oxford, pp. 1–64.
986 Ryabchikov, I., Brooks, C.K., Kogarko, L.N., Nielsen, T., Solovova, I.P., Turkov, V.,
987 1998. Tertiary picrites from Greenland: modelling sources and petrogenesis
988 from melt inclusioncompositions. Mineral. Mag. 62A, 3, 1306-1307
989 Saunders, A.D., Fitton, J.G., Kerr, A.C., Norry, M.J., Kent, R.W., 1997. The North
990 Atlantic igneous province. In: Mahoney, J.J., Coffin, M.F. (Eds.), Large Igneous
991 Provinces: Continental, Oceanic, and Planetary Flood Volcanism. AGU
992 Geophysical Monograph, Washington, 45–93.
993 Saunders A.D., Jones, S.M., Morgan, L.A., 2007. Regional uplift associated with
994 continental large igneous provinces: The roles of mantle plumes and the
995 lithosphere. Chem. Geol. 241, 3-4, 282-318.
996 Self, S., Thordarson, T., Keszthelyi, L., 1997. Emplacement of continental flood
997 basalt lava flows. In: Mahoney, J.J., Coffin, M.F. (Eds.), Large Igneous
998 Provinces: Continental, Oceanic, and Planetary Flood Volcanism. AGU
999 Geophysical Monograph, Washington, 381–410.

Shellnutt, J.G., Jahn, B.-M., 2011. Origin of Late Permian Emeishan basaltic rocks from the Panxi region (SW China): Implications for the Ti-classification and spatial-compositional distribution of the Emeishan flood basalts. J. Volcanol. Geotherm. Res. 199, 85–95.

Simon, K., Huismans, R.S., Beaumont, C., 2009. Dynamical modelling of lithospheric extension and small-scale convection: Implications for magmatism during the formation of volcanic rifted margins. Geophys. J. Int. 176, 1, 327–350.

Sims, K.W.W., Maclennan, J., Blichert-Toft, J., Mervine, E.M., Blusztajn, J., Gronvold, K., 2013. Short length scale mantle heterogeneity beneath Iceland probed by glacial modulation of melting. Earth Planet. Sci. Lett. 379, 146–157.

Skaarup, N., Jackson, H.R., Oakey, G., 2006. Margin segmentation of Baffin Bay/Davis Strait, eastern Canada, based on seismic reflection and potential field data. Marine Petroleum Geology 23, 127–144.

Stica, J.M., Zalan, P.V., Ferrari, A.L. , The evolution of rifting on the volcanic margin of the Pelotas Basin and the contextualization of the Parana-Etendeka LIP in the separation of Gondwana in the South Atlantic. Marine Petroleum Geology 50, 1-21.

Storey, M., Duncan, R.A., Pedersen, A.K., Larsen, L.M., Larsen, H.C., 1998. $^{40}Ar/^{39}Ar$ geochronology of the West Greenland Tertiary volcanic province. Earth and Planetary Science Letters 160, 569–586.

Stracke, A., Zindler, A., Salters, V.J.M., McKenzie, D., Blichert-Toft, J., Albarede, F., Gronvold, K., 2003. Theistareykir revisited. Geochem. Geophys. Geosystems 4, 8507. https://doi.org/10.1029/2001GC000201

Suckro, S.K., Gohl, K., Funck, T., Heyde, I., Ehrhardt, A., Schreckenberger, B., Gerlings, J., Damm, V., Jokat, W., 2012. The crustal structure of southern Baffin Bay: implications from a seismic refraction experiment. Geophys. J. International 190, 1, 37-58.

Tanaka, T., Togashi, S., Kamioka, H., Amakawa, H., Kagami, H., Hamamoto, T., Yuhara, M., Orihashi, Y., Yoneda, S., Shimizu, H., Kunimaru, T., Takahashi, K., Yanagi, T., Nakano, T., Fujimaki, H., Shinjo, R., Asahara, Y., Tanimizu, M., Dragusanu, C., 2000. JNdi-1: a neodymium isotopic reference in consistency with LaJolla neodymium. Chem. Geol. 168, 279–281.

Tang, M., Lee, C.T.A., Chen, K., Erdman, M., Costin, G., Jiang, H.H., 2019. Nb/Ta systematics in arc magma differentiation and the role of arclogites in continent formation. Nat. Commun., 10, 235, DOI: 10.1038/s41467-018-08198-3.

Tegner, C., Lesher, C.E., Larsen, L.M., Watt, W.S., 1998. Evidence from the rare-earth-element record of mantle melting for cooling of the tertiary Iceland plume. Nature 395, 6702, 591-594.

Thirlwall, M.F., Gee, M.A.M., Taylor, R.N., Murton, B.J., 2004. Mantle components in Iceland and adjacent ridges investigated using double-spike Pb isotope ratios. Geochim. Cosmochim. Acta 68, 361–386.

Thirlwall, M.F., Upton, B.G.J., Jenkins, C., 1993. Interaction between continental lithosphere and the Iceland Plume – Sr, Nd, Pb, isotope geochemistry of Tertiary basalts, NE Greenland. Journal of Petrology 35, 3, 839-879.

Todt, W., Cliff, R.A., Hansen, A., Hofmann, A., 1996. Evaluation of a ^{202}Pb-^{205}Pb double spike for high-precision isotope analysis. In: Earth Processes: Reading the Isotopic Code (Eds: A. Basu, S.R. Hart).Am.Geophys. Union Geophysical Monograph 95, 429–437.

1048 Torsvik, T.H., Van der Voo, R., Meert, J.G., Mosar, J., Walderhaug, H.J., 2001.
1049 Reconstructions of the continents around the North Atlantic at about the 60th
1050 parallel. Earth Planet. Sci. Lett. 187, 55–69.
1051 White, W., McKenzie, D., 1989. Magmatism at rift zones-the generation of volcanic
1052 continental margins and flood basalts. Journal of Geophys. Res.- Solid Earth 94,
1053 7685-7729.
1054 Willbold, M., Hegner, E., Stracke, A., Rocholl, A., 2009. Continental geochemical
1055 signatures in dacites from Iceland and implications for models of early
1056 Archaean crust formation. Earth Planet. Sci. Lett. 279, 1-2, 44–52.
1057 Wilson, S.A., 1997. The collection, preparation, and testing of USGS reference
1058 material BCR-2, Columbia River, Basalt: U.S. Geological Survey Open-File
1059 Report 98.
1060
1061
1062 **Figure captions**

1063 Figure 1: Simplified structural map of Greenland and Northern Atlantic Igneous
1064 Province, modified after Chauvet et al (accepted). The studied area (red square) is
1065 located on the western volcanic margin of Greenland.

1066

1067 Figure 2: The 45 sampling sites (numbers) located on the simplified geological map
1068 of Svartenhuk Peninsula (West Greenland), modified after Chauvet et al. (accepted).
1069 Locations of cross sections AA', BB' and CC' are shown on the map.

1070

1071 Figure 3: Major element compositions of samples from units V1 (purple triangles),
1072 V2 (beige circles), V3 (blue hexagons) and V4 (yellow triangles). A: Total alkali –
1073 Silica plot (Le Bas et al., 1986). The thick black line (Macdonald and Katsura, 1964)
1074 separates the fileds of subalkaline basaltic series (below) from alkali basaltic series
1075 (above).
1076 B: CaO *vs* SIO_2 and Ni *vs* SiO_2 plots. Compositions range from basaltic to trachytic
1077 (the latter in V4 unit only) following olivine and plagioclase + pyroxene fractionation
1078 trends. Dashed line identifies primitive Ni concentrations (higher than 400 ppm) and
1079 dotted line denotes samples with MgO=12 wt%, consistent with olivine phenocryst
1080 compositions (Mg#=0.83, supplementary table 1).

1081

1082 Figure 4: Multielement patterns of Svartenhuk samples. A: Rare earth element (REE)
1083 patterns normalized to CI Chondrite (McDonough and Sun, 1995) for samples from
1084 units V1 (pink), V2 (beige), V3 (blue) and V4 (yellow). Samples from V1 and V4
1085 have comparable REE patterns with significant light REE enrichments compared with

heavy REE, typical of alkali and transitional basaltic lavas. Samples from units V2 and V3 have more diverse signatures ranging from alkali to tholeiitic (LREE depleted) patterns. B: Multielement plot normalized to Primitive mantle (McDonough and Sun, 1995) compiling all samples (V1=purple lines, V2= beige lines, V3= blue lines, V4= yellow lines) and the median compositions of each group (V1= purple triangles, V2= beige circles, V3= blue hexagons, V4= yellow triangles).

Figure 5: Plot of SiO_2 vs Pb concentrations and Nb/La ratios. Continental crust contamination typically generates SiO_2 and Pb enrichments (Rudnick and Fountain, 1995) associated with Nb depletions (Tang et al, 2019 and references therein) illustrated here by low Nb/La ratios. Crustal contamination trends (black arrows) can be identified within samples from units V1 and V2 only.

Figure 6: Pb, Hf, Sr and Nd isotopic data. Samples from units V1 to V4 (see figure 3 for color codes) are plotted together with basalts from the North Atlantic ridge : blue crosses (Agranier et al., 2005; Blichert-Toft et al., 2005), Iceland : gray squares: (Breddam, 2002; Chauvel and Hémond, 2000; Hanan and Schilling, 1997; Hanan et al., 2000, Kitawaga et al., 2008; Kokfelt et al., 2009; Kuritani et al., 2011; Peate et al., 2010, 2009; Sims et al., 2013; Stracke et al., 2003; Thirlwall et al., 2004; Willbold et al., 2009) and East Greenland: orange crosses (Barker et al., 2006). Samples from this study plot between three end-members materialized by letters Sk1, Sk2 and Sk3. The Sk1-Sk2 trend can be accounted for by crustal contamination (Sk1 features radiogenic Sr, and unradiogenic Pb, Hf and Nd); while Sk2-Sk3 largely overlaps with mantle like signatures (Kitawaga et al. 2008) including North Mid-Atlantic Ridge and Iceland basalts. Its trend in all diagrams appears to point toward the common component C of Hanan and Graham (1996).

Figure 7: Pb isotopic data. Samples from this study are represented together with basalts from Iceland (gray squares, see figure 6 for references) and East Greenland (Barker et al., 2006) (orange crosses). The Iceland plume inner components: D, E-1 and E-2 (Kitawaga et al., 2008; Thirlwall et al., 2004) are also located in this diagram. Apart from continental crust trend (segment Sk1-Sk2), all samples plot within in a triangle delineated by D, E-1 and E-2.

1120 Figure 8: Plots of $^{206}Pb/^{204}Pb$, La/Sm, Sm/Yb against La/Yb. Pb isotopes (upper
1121 diagram) evidence crustal contamination for some V1 and V2 lavas and mantle-like
1122 compositions for most of the sample set. La/Sm as well as Sm/Yb provide insights
1123 about melting rates. On the Sm/Yb plot are reported for comparison the results of
1124 simple batch melting models considering garnet bearing (red line) and spinel bearing
1125 (green line) depleted lherzolite as proposed for Iceland by Gurenko and Chaussidon
1126 (1995), partition coefficients by McKenzie and O'Nions (1991) and mineral
1127 proportions by Thirlwall et al. (1993). Numbers from 0.02 to 0.1 denote F values. The
1128 higher Sm/Yb values observed for most of V1 and V4 lavas suggest a stronger
1129 involvement of garnet in their sources.
1130
1131 Figure 9: Plots of $^{206}Pb/^{204}Pb$, La/Sm and Sm/Yb against $\Delta Nb = 1.74+\log(Nb/Y)-1.92\log(Zr/Y)$ (Fitton et **al.,** 1997). ΔNb is considered as a bench marker of Iceland
1132 1.92log(Zr/Y) (Fitton et **al.,** 1997). ΔNb is considered as a bench marker of Iceland
1133 plume affinity. Only samples from units V2 and V3 display negative ΔNb, indicative
1134 of the contribution of "normal" upper mantle devoid of plume related enriched
1135 component. The thick black arrows illustrate the temporal evolution of Icelandic
1136 material contribution from V1 to V4.
1137
1138 Figure 10: Sketch summarizing the four main stages of Svartenhuk volcanism deduced
1139 from geochemical and petrologic constraints. Sk1, Sk2 and Sk3 represent the three
1140 geochemical reservoirs defined in figures 6 and 7. The tectonic evolution of the
1141 lithosphere (crustal thinning) is more precisely depicted in figure 11. During V1 stage,
1142 decompression melting affects Iceland plume-like material ascending through the
1143 asthenosphere below an already thinned lithosphere. During V2, the ongoing crustal
1144 thinning leads to an uprise of the isotherms and therefore to the upward propagation of
1145 partial melting and to its increase. During the emplacement of these two first units,
1146 geochemical signatures (benchmarked by Pb isotopes on the bottom diagram) can be
1147 accounted for by the simple binary mixture of components Sk1 and Sk2. During V3, the
1148 melting has propagated within Sk3 reservoir. Finally, during V4, the melting deepens
1149 again and is once more mostly restricted to reservoir Sk2. See text for details.
1150
1151 Figure 11: Tentative tectonic sketches depicting Svartenhuk magmatic evolution in
1152 relation with the evolution of South Baffin Bay during the Paleogene, at the times of
1153 V1, V2-V3 and V4 emplacements. Sk1, Sk2 and Sk3 refer to crustal and mantle

reservoirs discussed in the text and shown in figure 10. Convection geometry is purely conceptual, and based on small scale convection models (Petersen et al., 2018; Simon et al., 2009). In the V1 sketch (top left), the occurrence of Cretaceous sediments, shown in light green suggests that crustal thinning started during the Cretaceous. The melting zones are indicated with coloured dots. Red boxes show the location of our field and petrologic investigations. The shaded areas on the left of some diagrams underline the speculative character of these interpretations when extrapolated to areas located away from our study area.

Table 1: Sample locations. K/Ar and Ar/Ar ages are from Chauvet et al (accepted)

Table 2: Major element data (oxide wt%, total iron as Fe_2O_3, LOI: Loss On Ignition). Analytical methods are presented in the text.

Table 3: Trace element data (ppm). Analytical methods are presented in the text.

Table 4: Pb, Hf, Sr and Nd isotopic data. Analytical methods are presented in the text.

Supplementary Table 1: ICP-MS repeated trace element analyses for standards BHVO2, BCR-2 and BIR1.

Supplementary Table 2: MC-ICP-MS repeated Nd, Hf and Pb isotope analyses of standards JNDi-1, JMC475 and NIST981, respectively.

Supplementary Table 3: Replicated analyses of Pb, Hf, Nd and Sr isotopic compositions of sample S39E1.

Supplementary Table 4: Olivine compositions obtained on Cameca SX100 electron microprobe at Service Commun “Microsonde Ouest” (Plouzané), at 15 kV accelerating voltage with a probe current of 12 nA.

Figure 1

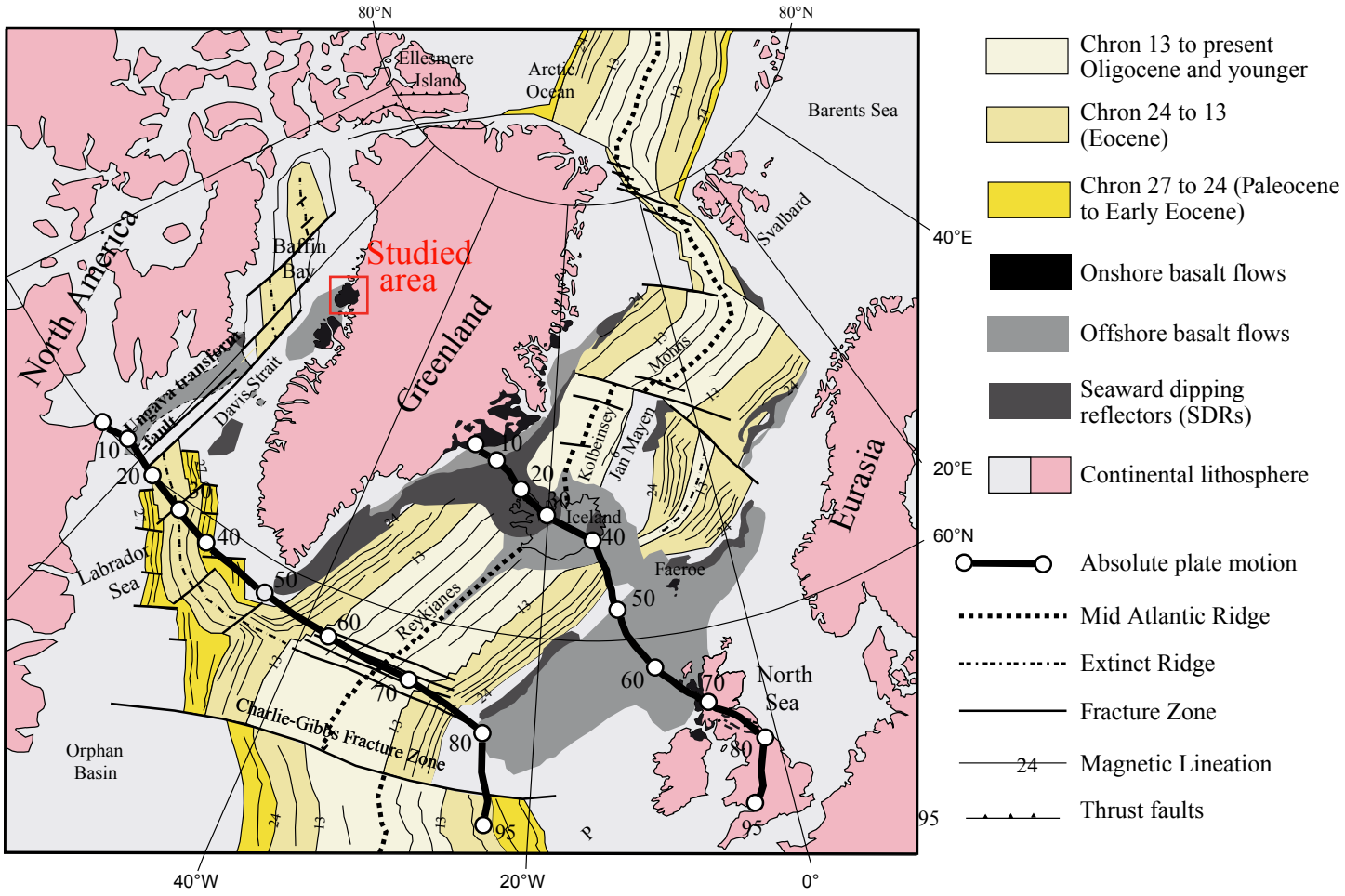
80°N
80°N
Ellesmere Island
Arctic Ocean
Barents Sea
Svalbard
40°E
North America
Baffin Bay
Studied area
Greenland
Davis Strait
Lingayva transform fault
Mohns
Kolbeinsey
Jan Mayen
Eurasia
20°E
Iceland
Faeroe
60°N
Labrador Sea
Reykjanes
North Sea
Charlie-Gibbs Fracture Zone
Orphan Basin
40°W
20°W
0°
Chron 13 to present Oligocene and younger
Chron 24 to 13 (Eocene)
Chron 27 to 24 (Paleocene to Early Eocene)
Onshore basalt flows
Offshore basalt flows
Seaward dipping reflectors (SDRs)
Continental lithosphere
Absolute plate motion
Mid Atlantic Ridge
Extinct Ridge
Fracture Zone
24
Magnetic Lineation
Thrust faults

Figure 2

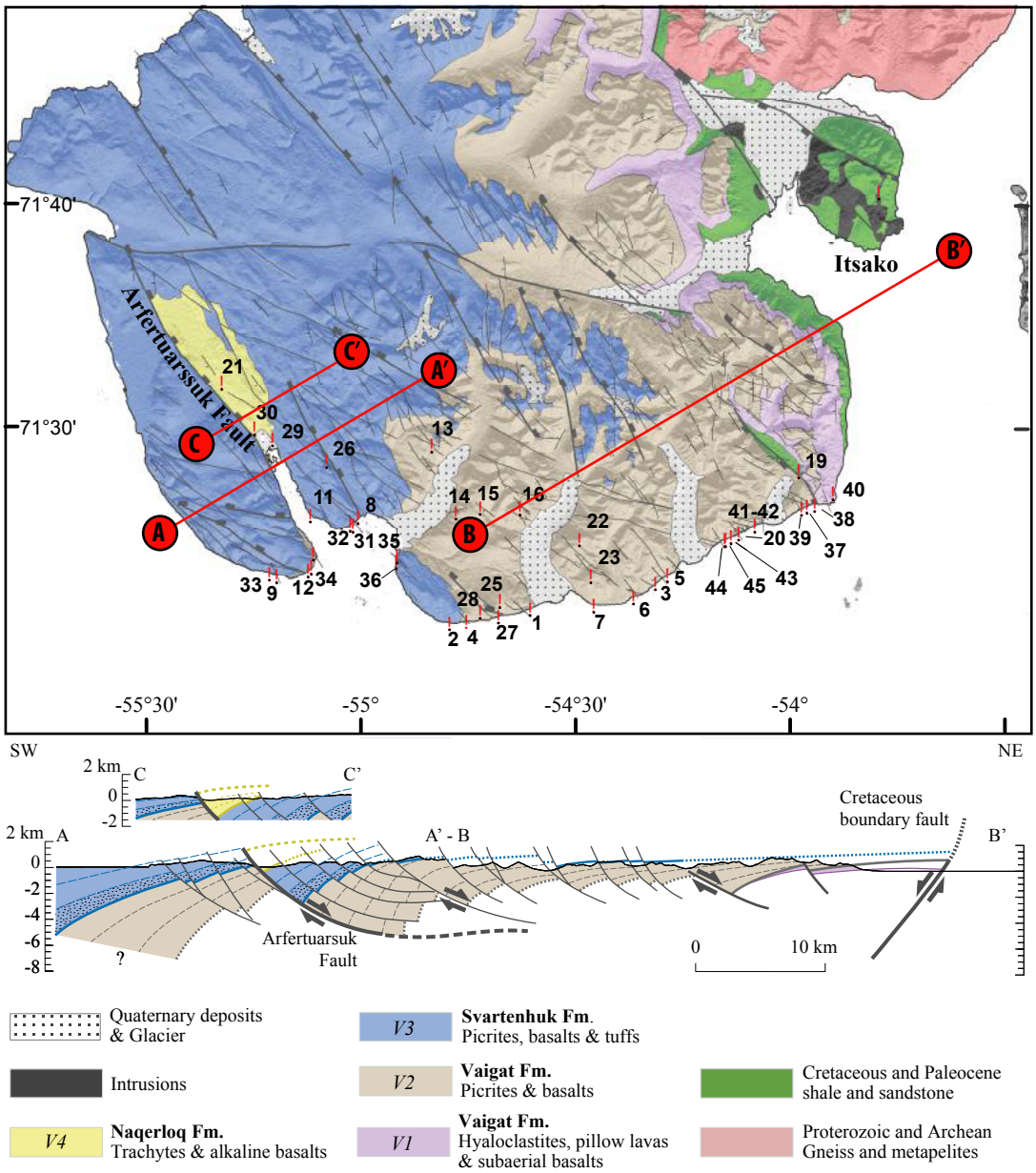
71°40'
71°30'
-55°30'
-55°
-54°30'
-54°
Itsako
Arfertuarssuk Fault
A
A'
B
B'
C
C'
21
30
29
26
13
11
8
14
15
16
19
40
41-42
38
22
32
31
35
20
39
37
23
33
9
12
34
36
25
5
44
45
43
28
3
6
2
4
27
1
7
SW
NE
2 km
0
-2
A
A' - B
B'
Cretaceous
boundary fault
-4
-6
-8
?
Arfertuarsuk
Fault
0
10 km
Quaternary deposits
& Glacier
Intrusions
V4
Naqerloq Fm.
Trachytes & alkaline basalts
V3
Svartenhuk Fm.
Picrites, basalts & tuffs
V2
Vaigat Fm.
Picrites & basalts
V1
Vaigat Fm.
Hyaloclastites, pillow lavas
& subaerial basalts
Cretaceous and Paleocene
shale and sandstone
Proterozoic and Archean
Gneiss and metapelites

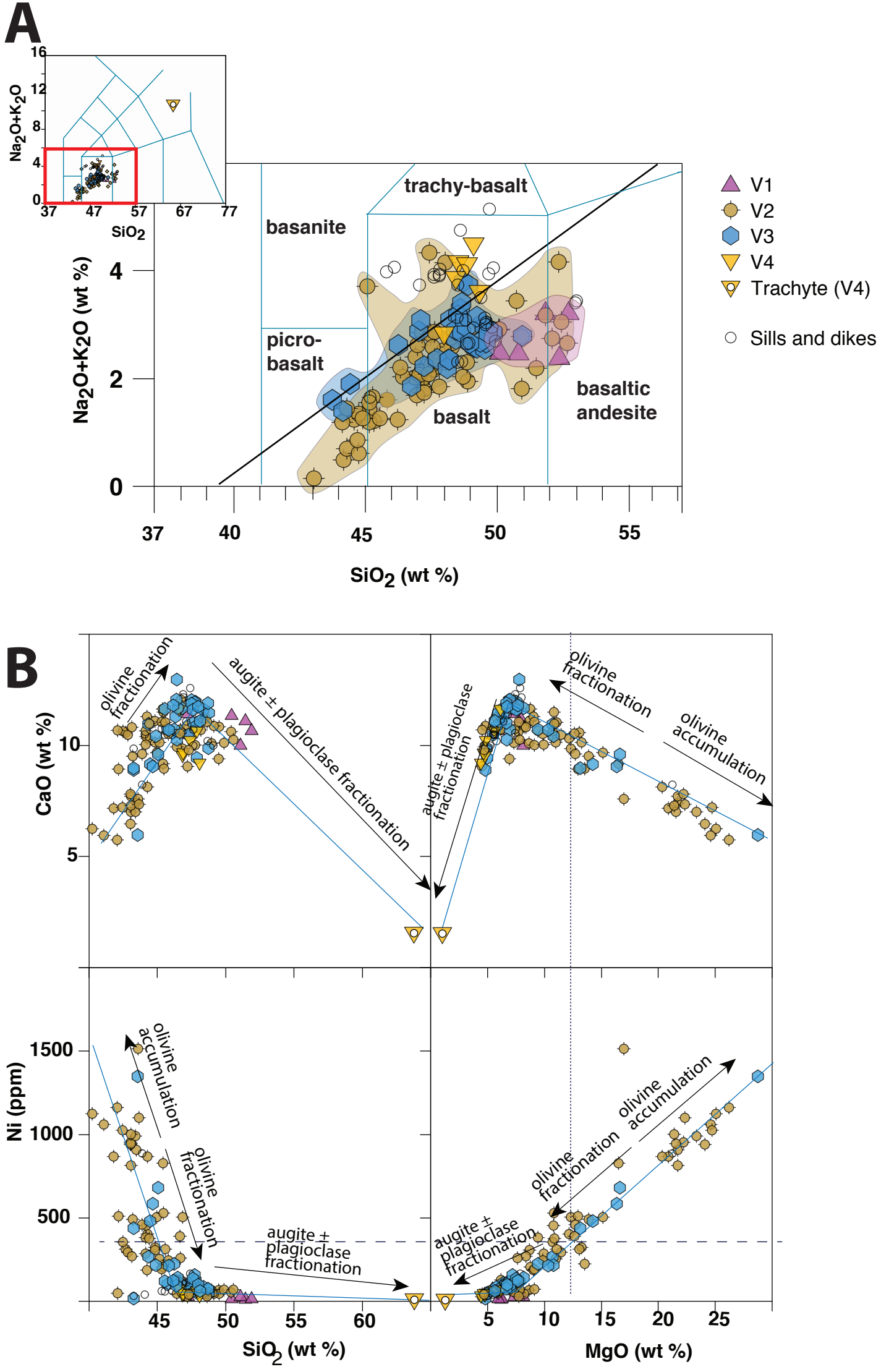
A
Na2O+K2O
SiO2
trachy-basalt
basanite
picro-basalt
basalt
basaltic andesite
Na2O+K2O (wt %)
SiO2 (wt %)
V1
V2
V3
V4
Trachyte (V4)
Sills and dikes
B
CaO (wt %)
olivine fractionation
augite ± plagioclase fractionation
olivine accumulation
Ni (ppm)
SiO2 (wt %)
MgO (wt %)

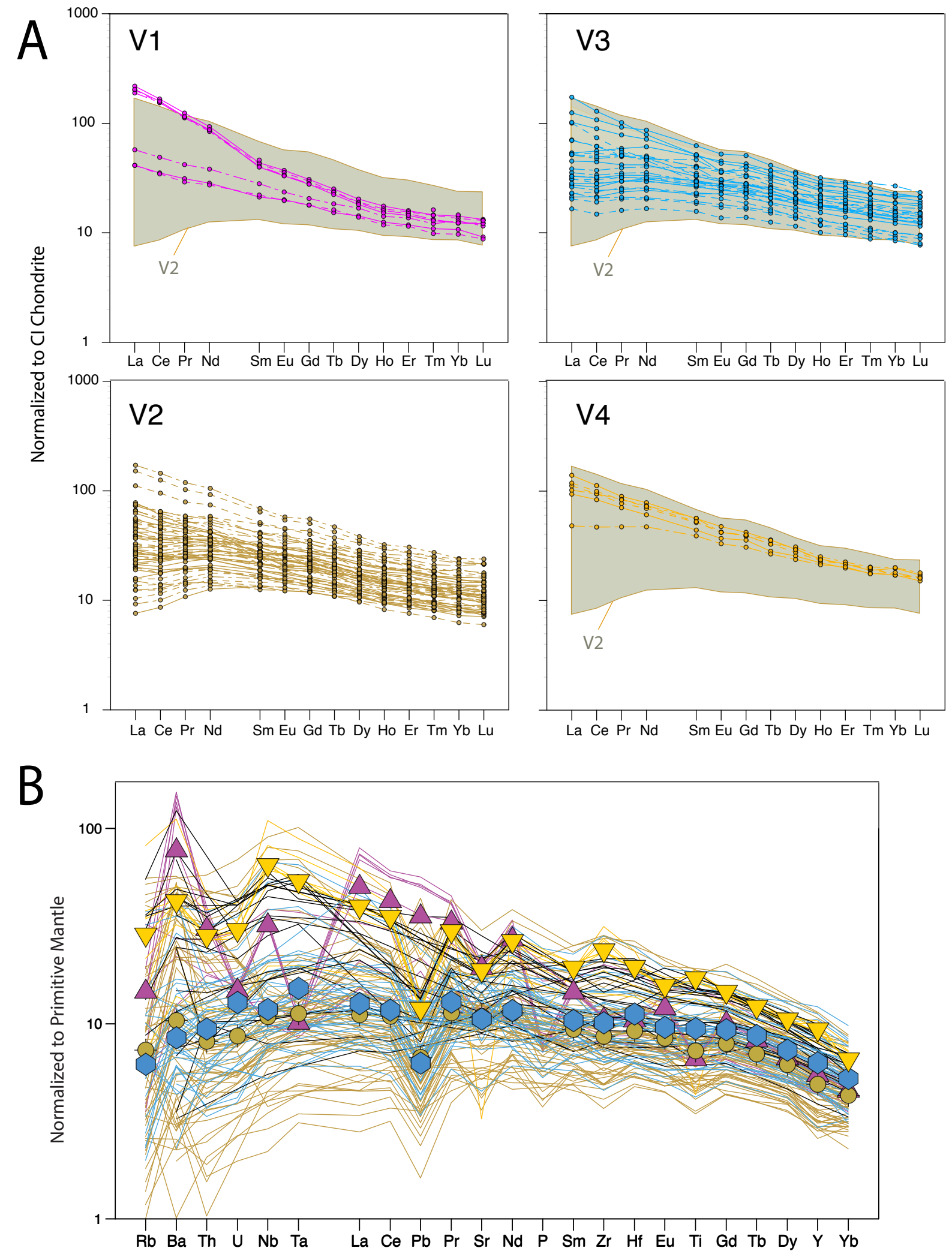
A
V1
V2
V3
V2
V2
V4
V2
Normalized to CI Chondrite
1000
100
10
1
La Ce Pr Nd Sm Eu Gd Tb Dy Ho Er Tm Yb Lu
B
Normalized to Primitive Mantle
100
10
1
Rb Ba Th U Nb Ta La Ce Pb Pr Sr Nd P Sm Zr Hf Eu Ti Gd Tb Dy Y Yb

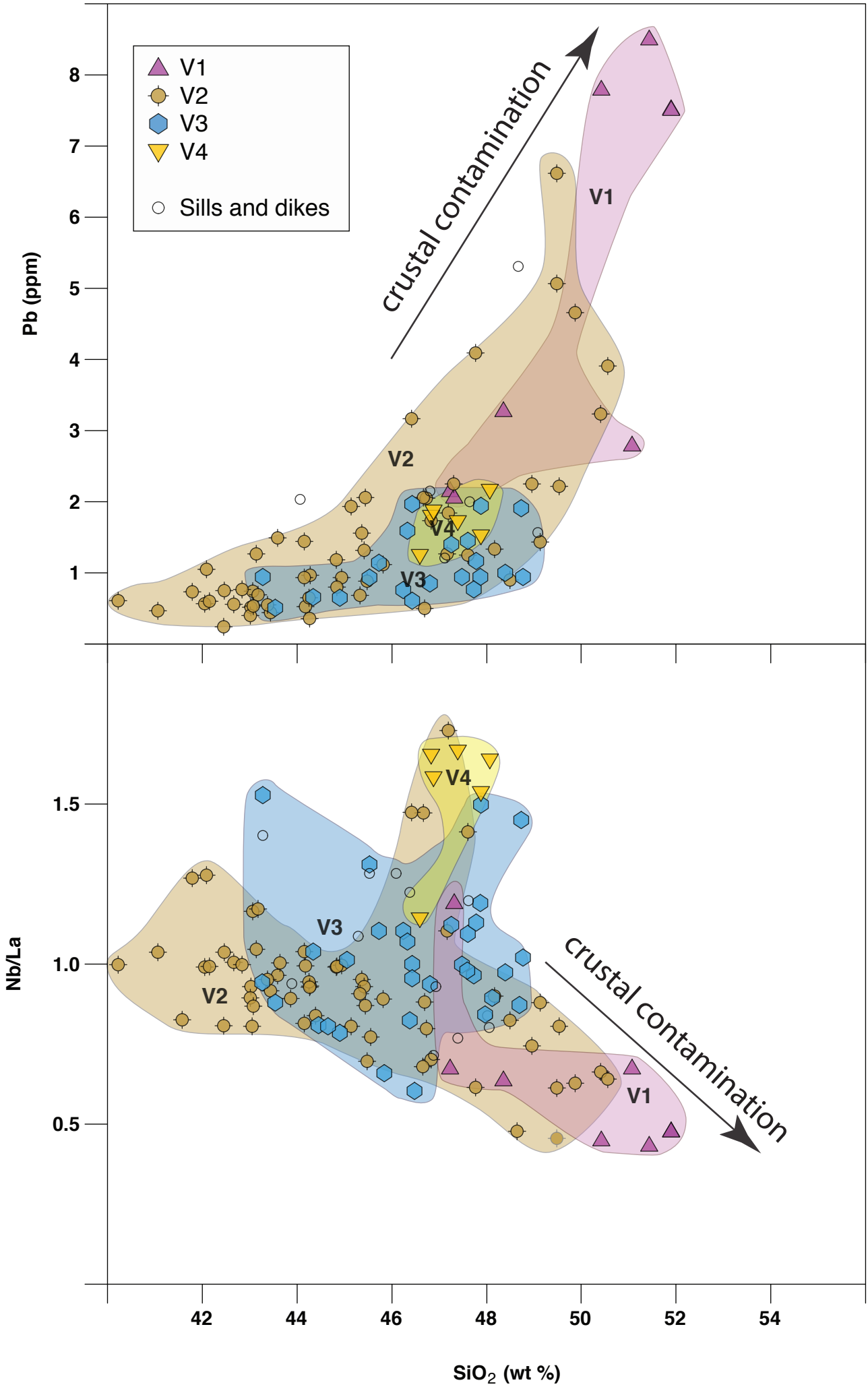
V1
V2
V3
V4
Sills and dikes
crustal contamination
V1
V2
V4
V3
Pb (ppm)
8
7
6
5
4
3
2
1
V4
V3
V2
V1
crustal contamination
Nb/La
1.5
1.0
0.5
42
44
46
48
50
52
54
SiO2 (wt %)

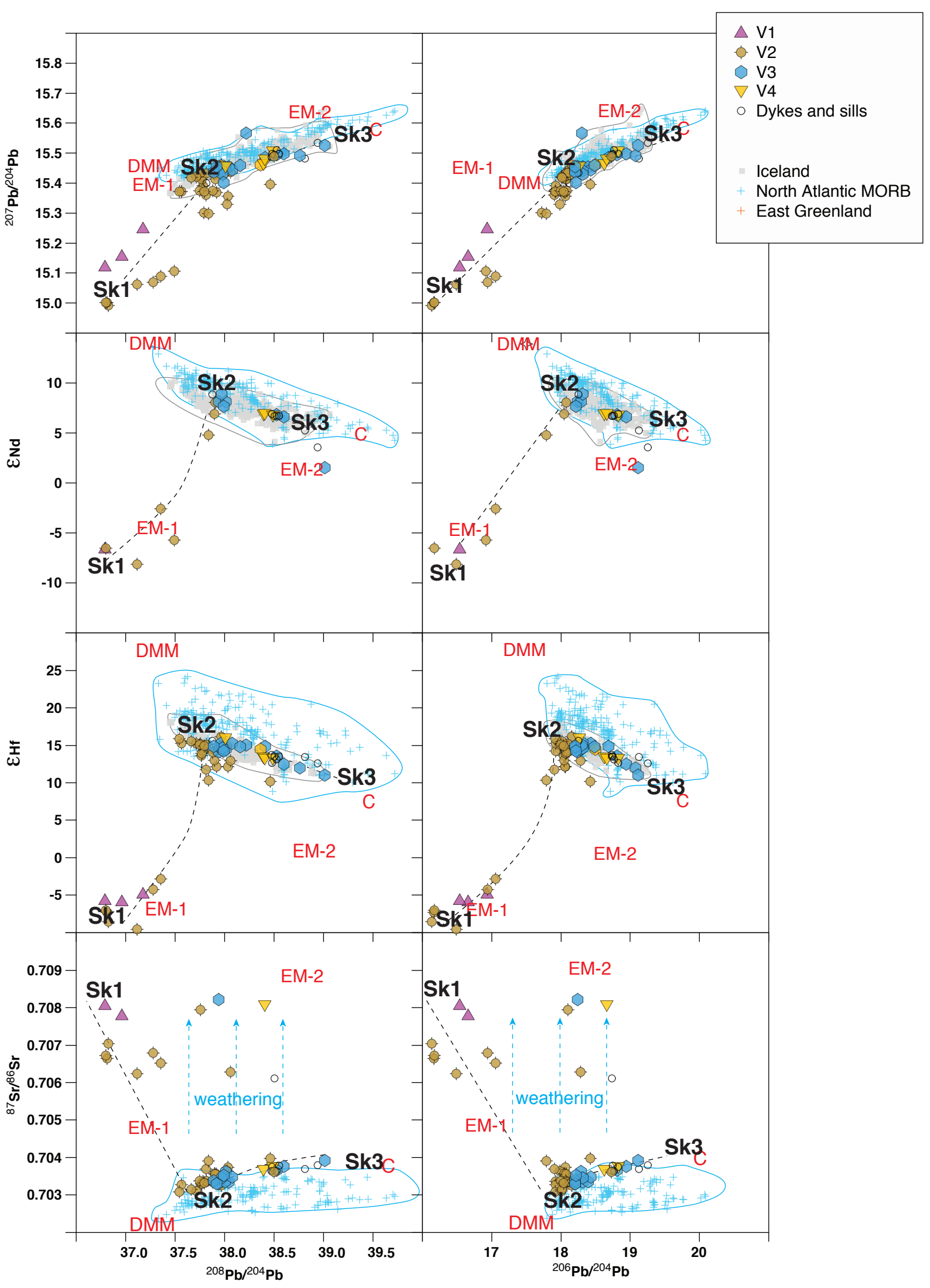
V1
V2
V3
V4
Dykes and sills
Iceland
North Atlantic MORB
East Greenland
$^{207}Pb/^{204}Pb$
$^{208}Pb/^{204}Pb$
$^{206}Pb/^{204}Pb$
εNd
εHf
$^{87}Sr/^{86}Sr$
DMM
EM-1
EM-2
C
Sk1
Sk2
Sk3
weathering

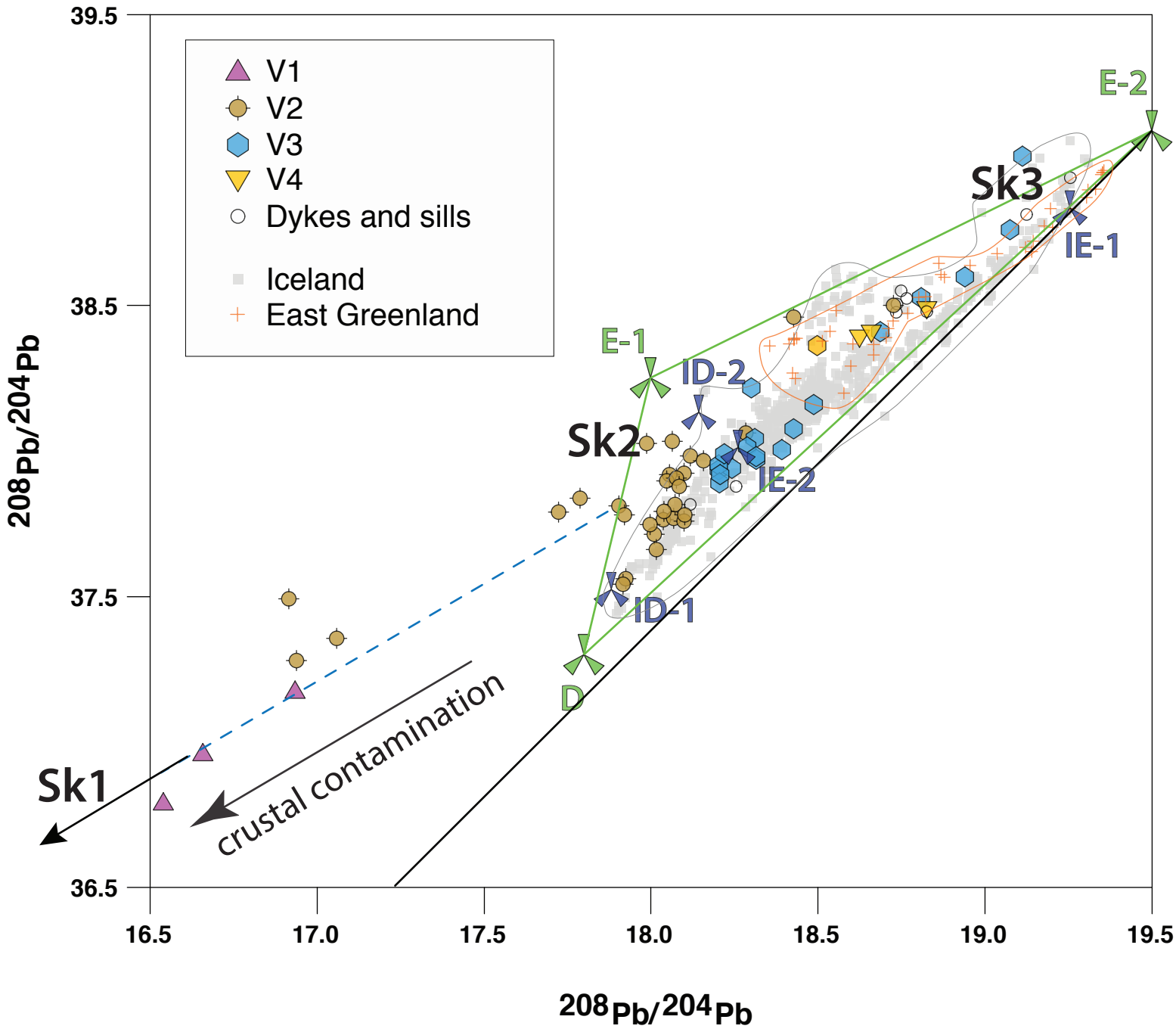
V1
V2
V3
V4
Dykes and sills
Iceland
East Greenland
E-2
Sk3
IE-1
E-1
ID-2
Sk2
IE-2
ID-1
D
Sk1
crustal contamination
39.5
38.5
37.5
36.5
16.5
17.0
17.5
18.0
18.5
19.0
19.5
208Pb/204Pb
208Pb/204Pb

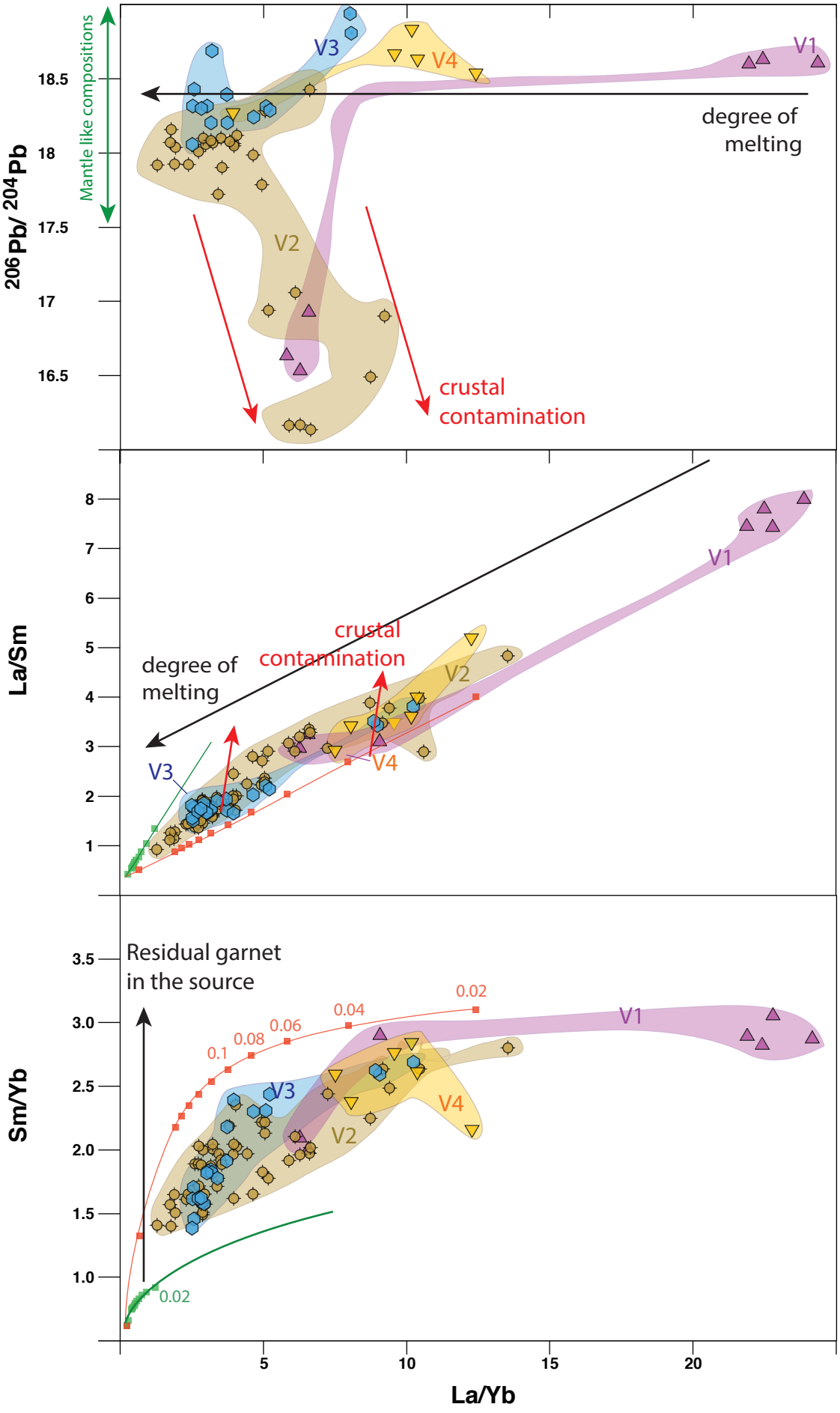
Mantle like compositions
$^{206}Pb/^{204}Pb$
18.5
18
17.5
17
16.5
V3
V4
V1
V2
degree of melting
crustal contamination
La/Sm
8
7
6
5
4
3
2
1
crustal contamination
degree of melting
V1
V2
V3
V4
Sm/Yb
3.5
3.0
2.5
2.0
1.5
1.0
Residual garnet in the source
0.02
0.04
0.06
0.08
0.1
0.02
V1
V3
V4
V2
5
10
15
20
La/Yb

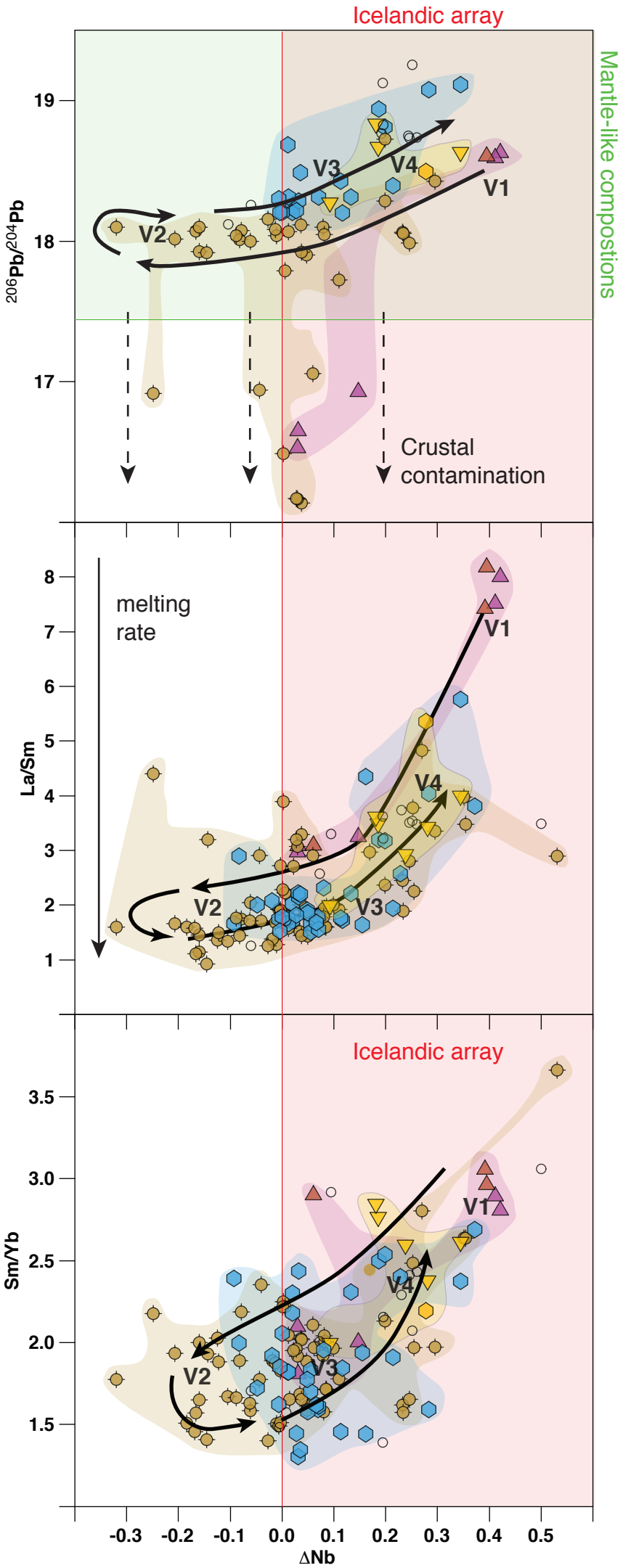
Icelandic array
Mantle-like compostions
$^{206}Pb/^{204}Pb$
19
18
17
V1
V2
V3
V4
Crustal
contamination
La/Sm
8
7
6
5
4
3
2
1
melting
rate
V1
V4
V2
V3
Icelandic array
Sm/Yb
3.5
3.0
2.5
2.0
1.5
V1
V4
V3
V2
-0.3
-0.2
-0.1
0.0
0.1
0.2
0.3
0.4
0.5
ΔNb

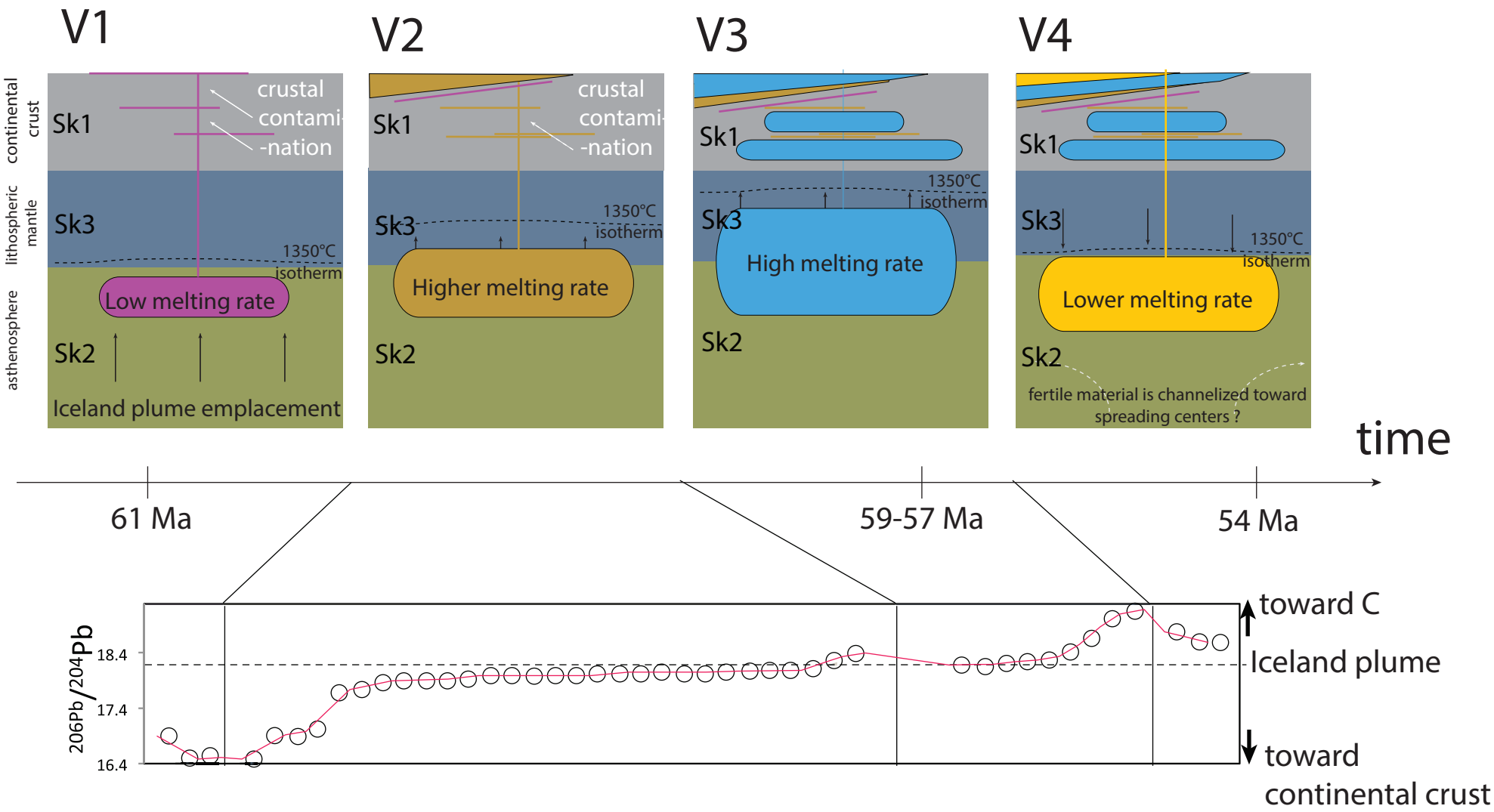
V1
V2
V3
V4
continental crust
lithospheric mantle
asthenosphere
Sk1
Sk3
Sk2
crustal contami-nation
1350°C isotherm
Low melting rate
Higher melting rate
High melting rate
Lower melting rate
Iceland plume emplacement
fertile material is channelized toward spreading centers ?
time
61 Ma
59-57 Ma
54 Ma
206Pb/204Pb
18.4
17.4
16.4
toward C
Iceland plume
toward continental crust

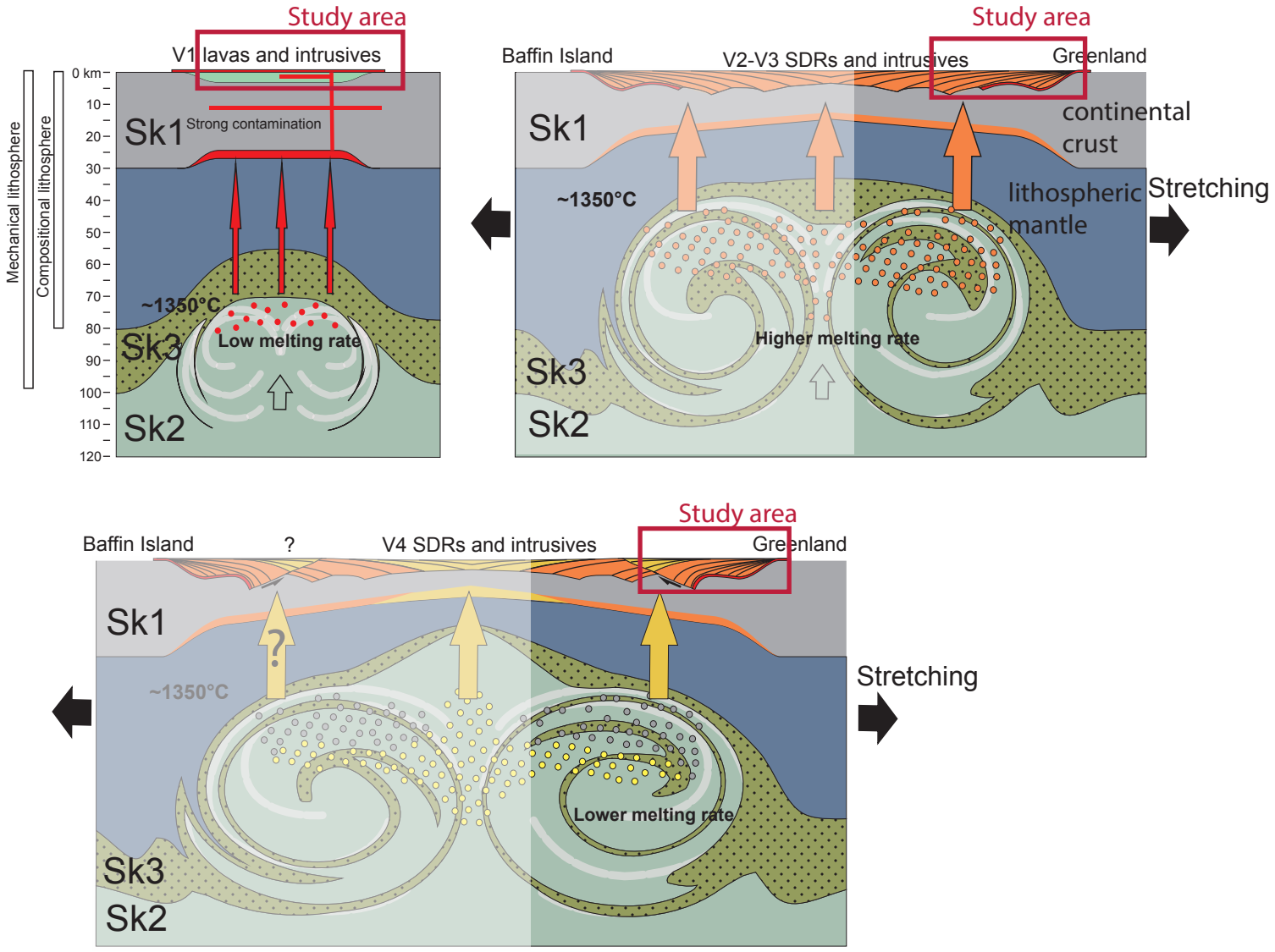
Study area
V1 lavas and intrusives
Mechanical lithosphere
Compositional lithosphere
0 km
10
20
30
40
50
60
70
80
90
100
110
120
Sk1
Strong contamination
~1350°C
Sk3
Low melting rate
Sk2
Study area
Baffin Island
V2-V3 SDRs and intrusives
Greenland
Sk1
continental crust
~1350°C
lithospheric mantle
Stretching
Higher melting rate
Sk3
Sk2
Study area
Baffin Island
?
V4 SDRs and intrusives
Greenland
Sk1
?
~1350°C
Stretching
Lower melting rate
Sk3
Sk2

Sample names	longitude	latitude	Fm	^{39}Ar-^{40}Ar age	K-Ar age (My)
	Lon	lat	Fm		
S19E1	-53.974	71.470	V1		
S19E2	-53.974	71.470	V1		
S38E2	-53.936	71.446	V1		
S38E8	-53.936	71.446	V1		
S40E1	-53.899	71.455	V1		59.11 ± 0.83
S40E2	-53.899	71.455	V1		
S40E4	-53.893	71.453	V1		
S40E5	-53.893	71.453	V1		
S40E6	-54.067	71.426	V1		60.38 ± 1.34
S1E1	-54.605	71.370	V2		
S1E2	-54.605	71.370	V2		
S1E3	-54.606	71.370	V2		
S1E4	-54.606	71.370	V2		
S1E5	54.604	71.368	V2		
S1E6	-54.607	71.369	V2		
S3E1	-54.300	71.386	V2		
S4E1	-54.679	71.363	V2		
S5E11	-54.282	71.395	V2		
S5E5	-54.288	71.394	V2		
S5E6	-54.287	71.394	V2		
S6E10	-54.359	71.374	V2		
S6E11	-54.367	71.378	V2		
S6E6	-54.364	71.378	V2		
S6E9	-54.366	71.378	V2		
S7E10	-54.458	71.371	V2		
S7E11	-54.457	71.371	V2		
S7E4	-54.461	71.372	V2		
S7E5	-54.461	71.372	V2		
S7E6	-54.456	71.370	V2		
S7E7	-54.459	71.371	V2		
S7E8	54.455	71.370	V2		
S7E9	-54.459	71.371	V2		
S15H4	54.719	71.438	V2		
S17H1	-54.218	71.835	V2		
S17H2	-54.224	71.834	V2		
S2014	-54.117	71.425	V2		
S20E10	-54.109	71.422	V2		
S20E15	-54.118	71.425	V2		
S20E17	-54.119	71.425	V2		
S20E7	-54.112	71.426	V2		
S22H3	-54.486	71.417	V2		
S27E10	-54.738	71.356	V2		
S27E12	-54.740	71.359	V2		
S27E13	-54.741	71.359	V2		
S27E15	-54.751	71.356	V2		
S27E17	-54.751	71.356	V2		
S27E18	-54.752	71.359	V2		
S27E20	54.752	71.356	V2		
S37E1	55.204	71.389	V2		
S38E10	-53.942	71.446	V2		
S38E67	-53.936	71.446	V2		
S39E1	-53.974	71.443	V2		
S41E1	-54.066	71.432	V2		
S41E3	-54.066	71.432	V2		
S42E1	-54.074	71.432	V2		
S42E2	-54.074	71.432	V2		
S42E4	-54.082	71.431	V2		
S42E5	-54.082	71.431	V2	61.08 ± 0.56	
S43E1	-54.133	71.423	V2		
S43E2	-54.134	71.423	V2		
S43E4	-54.136	71.423	V2		
S43E5	-54.136	71.423	V2		
S43E6	-54.139	71.422	V2		
S44E10	-54.163	71.419	V2		
S44E2	-54.154	71.420	V2		
S44E4	-54.156	71.420	V2		
S44E7	-54.157	71.420	V2		
S44E8	-54.159	71.420	V2		
S44E9	-54.160	71.419	V2		
S45E10	-54.151	71.420	V2		
S45E4	-54.150	71.421	V2		
S45E9	-54.151	71.420	V2		
S2E2	-54.791	71.358	V3		
S2E3	-54.792	71.358	V3		
S2E5	-54.793	71.358	V3		
S2E7	-54.791	71.355	V3		
S2E8	-54.791	71.355	V3		54.98 ± 1.16
S2E9	-54.796	71.358	V3		
S8E10	-55.006	71.438	V3		
S8E13	-55.013	71.437	V3		55.73 ± 2.49
S8E6	-55.004	71.438	V3		
S8E9	-55.003	71.436	V3		
S9E1	-55.201	71.393	V3		
S11E10	-55.102	71.436	V3		
S11E12	-55.104	71.437	V3		
S11E7	-55.110	71.435	V3		
S26H1	-55.086	71.479	V3		54.20 ± 2.88
S26H3	-55.088	71.479	V3		
S33E1	-55.206	71.393	V3		
S33E12	-55.219	71.394	V3		
S33E4	-55.206	71.393	V3		
S33E7	-55.208	71.393	V3		
S33E8	-55.210	71.393	V3		57.78 ± 1.88
S34E2	-55.118	71.401	V3		
S34E5	-55.117	71.403	V3		
S34E6	-55.120	71.399	V3		
S34E7	-55.120	71.399	V3		
S35E1	-54.920	71.408	V3		
S35E11	-54.916	71.410	V3		
S35E12	-54.916	71.410	V3		
S35E3	-54.919	71.408	V3		
S35E5	-54.918	71.409	V3	59.78 ± 0.41	59.15 ± 0.85
S35E7	-54.917	71.409	V3		
S35E8	-54.917	71.410	V3		
S36E1	-54.922	71.404	V3		
S36E4	-54.922	71.403	V3		
S36E5	-54.922	71.403	V3		
S21H1	-55.338	71.541	V4	55.20 ± 0.79	55.86 ± 1.25
S21H2	-55.340	71.541	V4		
S29E2	-55.218	71.495	V4		
S30E1	-55.249	71.502	V4	54.39 ± 0.60	59.07 ± 1.16
S30E2	-55.236	71.503	V4		
S30E3	-55.244	71.503	V4		57.96 ± 1.20
S30E4	-55.241	71.502	V4		58.73 ± 1.53
S11E9	-55.118	71.435	dike		
S13H1	-54.823	71.489	dike		
S13H5	-54.823	71.489	dike		
S14H1a	-54.773	71.438	dike		
S14H2	-54.773	71.438	dike		56.43 ± 1.06
S15H3	-54.719	71.438	dike		
S16H1	-54.635	71.441	dike		
S16H2	-54.635	71.441	dike		
S16H4	-54.635	71.441	dike		
S20E18	-54.108	71.422	dike		55.42 ± 1.91
S22H2	-54.491	71.423	sill		53.85 ± 2.84
S22H4	-54.486	71.417	dike	54.41 ± 0.99	
S23H1	-54.456	71.390	dike		
S23H4	-54.456	71.390	dike V3	58.98 ± 0.93	
S23H5	-54.456	71.390	dike		
S24H1	-53.783	71.679	Sill Itsako	55.31 ± 1.09	
S27E4	-54.752	71.356	dike		55.95 ± 0.88
S27E8	-54.738	71.356	dike		
S41E2	-54.060	71.426	dike		

Sample names	Fm.	wt. %	SiO_2	TiO_2	Al_2O_3	FeO*	MnO	MgO	CaO	Na_2O	K_2O	P_2O_5	LOI	total
S19E1	V1		44.8	1.38	11.9	11.4	0.2	13.2	10.1	1.57	0.15	0.15	4.27	100.5
S19E2	V1		48.4	1.31	14.1	9.6	0.16	8.0	11.2	2.05	0.31	0.15	4.27	100.5
S38E2	V1		47.2	1.29	14.8	9.5	0.19	7.4	11.5	2.1	0.26	0.15	3.65	99.0
S38E8	V1		51.1	1.29	14.5	9.9	0.16	8.2	10.0	2.13	0.21	0.15	2.03	100.7
S40E1	V1		51.4	1.32	14.6	9.4	0.17	6.2	11.1	2.56	0.59	0.17	1.37	100.0
S40E2	V1		50.4	1.33	14.9	9.4	0.21	6.3	11.4	2.63	0.51	0.17	1.94	100.3
S40E4	V1		51.9	1.37	14.9	9.5	0.16	6.0	10.7	2.73	0.61	0.16	1.07	100.1
S40E5	V1		47.3	3.1	13.7	12.7	0.2	5.4	10.5	2.83	1.06	0.36	0.91	99.5
S40E6	V1		52.5	1.33	15.2	9.5	0.17	6.2	10.6	2.72	0.68	0.16	1.29	101.3
S1E1	V2		43.9	1.45	11.6	10.7	0.16	12.7	9.6	1.93	0.15	0.17	1.1	94.6
S1E2	V2		41.6	0.91	8.1	10.8	0.17	23.4	7.2	0.75	0.05	0.12	5.65	99.9
S1E3	V2		43.1	1.01	9.4	11.1	0.17	21.6	7.0	1.15	0.05	0.12	3.87	99.7
S1E4	V2		45.6	1.44	13.2	10.8	0.18	11.1	11.0	2.09	0.17	0.16	1.12	98.0
S1E5	V2		46.7	1.82	15.6	10.3	0.19	7.3	12.1	2.3	0.37	0.22	2.63	100.7
S1E6	V2		44.4	1.44	12.9	10.8	0.2	10.9	11.0	1.86	0.08	0.16	5.52	100.4
S3E1	V2		47.3	4.11	12.6	15.1	0.25	4.7	9.8	2.91	1.18	0.54	-0.58	99.6
S4E1	V2		45.3	1.66	13.9	11.0	0.18	9.1	11.1	2.49	0.24	0.14	3.63	100.0
S5E11	V2		49.5	1.02	12.7	8.5	0.17	13.0	6.5	1.88	0.99	0.12	3.79	99.1
S5E5	V2		49.0	1.37	13.9	10.1	0.26	8.7	10.1	2.13	0.54	0.15	2.46	99.7
S5E6	V2		49.5	1.56	14.6	9.2	0.17	8.2	10.8	2.52	0.84	0.17	1.96	100.6
S6E10	V2		42.1	3.8	13.0	13.5	0.21	5.9	10.7	2.74	0.72	0.71	2.69	97.6
S6E11	V2		43.1	1.1	9.1	11.3	0.18	21.7	7.7	0.82	0.31	0.13	5.88	102.5
S6E6	V2		43.4	1.04	9.5	11.4	0.17	21.7	7.4	1.24	0.14	0.11	3.02	100.5
S6E9	V2		41.8	1.08	9.0	10.9	0.17	20.9	7.2	0.87	0.26	0.12	5.9	99.3
S7E10	V2		42.7	1.52	11.7	11.3	0.19	13.1	10.6	1.09	0.06	0.16	7.47	101.0
S7E11	V2		41.1	0.99	8.4	10.7	0.17	24.6	6.0	0.6	0.06	0.11	5.96	99.8
S7E4	V2		44.2	1.58	12.4	12.2	0.25	10.8	10.4	2.14	0.12	0.17	4.85	100.4
S7E5	V2		42.1	1.01	7.7	10.4	0.17	26.2	5.8	0.51	0.07	0.12	6.28	101.4
S7E6	V2		44.9	1.51	11.3	11.2	0.19	15.1	9.7	1.4	0.22	0.15	4.36	101.3
S7E7	V2		40.2	1.01	7.4	10.4	0.16	25.1	6.3	0.38	0.07	0.11	7.07	99.3
S7E8	V2		46.4	4.11	12.9	14.8	0.25	4.7	9.9	2.79	1.46	0.59	0.5	100.0
S7E9	V2		45.4	1.26	13.9	10.1	0.15	10.8	11.5	1.58	0.17	0.12	4.46	100.6
S15H4	V2		42.5	0.84	8.5	11.0	0.18	24.7	7.2	1.01	0.13	0.11	3.32	100.7
S17H1	V2		49.1	2.18	15.5	12.4	0.21	4.8	10.9	2.7	0.15	0.23	1.39	100.9
S17H2	V2		48.2	2.16	15.1	12.3	0.2	4.6	10.7	2.59	0.22	0.23	1.83	99.4
S2014	V2		44.8	1.77	13.1	10.7	0.22	8.7	11.1	2.16	0.24	0.17	3.66	97.7
S20E10	V2?		48.5	2.2	13.6	13.0	0.22	5.8	11.3	2.67	0.29	0.22	0.52	99.8
S20E15	V2		45.4	1.43	10.8	11.3	0.18	16.5	9.2	1.68	0.28	0.16	2.06	100.2
S20E17	V2		43.0	1.02	8.4	12.1	0.18	24.1	6.5	1.06	0.13	0.12	3.87	101.8
S20E7	V2		45.4	1.61	13.9	10.6	0.18	8.8	11.6	2	0.21	0.18	3.64	99.2
S22H3	V2		47.2	2.47	13.1	13.3	0.23	5.9	10.9	2.46	0.35	0.27	0.63	98.2
S27E10	V2		46.7	2.53	14.8	11.3	0.19	6.2	10.7	2.69	0.9	0.35	0.82	98.3
S27E12	V2		43.4	1.1	8.5	11.7	0.18	23.3	7.0	1.12	0.09	0.1	1.5	99.4
S27E13	V2		46.7	1.72	12.9	11.2	0.17	12.6	10.5	2.01	0.12	0.16	1.61	100.9
S27E15	V2		46.7	1.85	13.8	11.0	0.18	7.6	11.6	2.37	0.16	0.2	1.77	98.4
S27E17	V2		47.2	3.35	13.7	14.1	0.23	4.5	9.0	3.44	1.17	0.4	1.07	99.7
S27E18	V2		45.8	1.45	13.3	10.5	0.15	9.8	10.5	2	0.16	0.13	3.13	98.1
S27E20	V2		47.6	2.62	13.5	12.2	0.2	7.4	10.7	2.41	0.6	0.31	0.98	99.9
S37E1	V2		38.4	0.59	5.0	9.3	0.15	32.4	3.1	0.1	0.04	0.07	10.07	100.3
S38E10	V2		44.3	1.37	12.5	11.0	0.19	12.2	10.3	1.68	0.21	0.13	2.67	97.7
S38E6	V2		48.6	1.18	14.5	9.0	0.15	7.8	11.1	1.88	0.19	0.13	5.06	100.6
S39E1	V2		49.5	1.35	14.1	9.1	0.15	6.9	9.4	3.28	0.65	0.16	4	99.6
S41E1	V2		45.5	1.09	12.0	9.9	0.17	13.5	9.0	1.57	0.24	0.11	4.08	98.3
S41E3	V2		49.9	1.32	14.1	9.2	0.16	7.3	10.1	2.1	0.41	0.15	2.64	98.4
S42E1	V2		46.8	1.24	12.8	10.9	0.18	12.3	9.9	1.74	0.22	0.13	3.33	100.7
S42E2	V2		50.4	1.36	14.3	9.5	0.17	7.7	10.6	2.4	0.25	0.15	2.32	100.2
S42E4	V2		47.8	1.21	14.1	9.6	0.19	9.1	10.0	1.28	0.42	0.13	3.1	98.0
S42E5	V2		50.6	1.38	14.4	9.7	0.17	7.8	10.3	2.67	0.42	0.16	1.89	100.5
S43E1	V2		43.2	1.24	11.7	11.3	0.18	13.9	9.5	1.67	0.23	0.13	6.72	101.0
S43E2	V2		42.2	1.2	11.3	11.0	0.16	12.9	8.9	1.43	0.12	0.12	7.91	98.4
S43E4	V2		42.5	1.6	12.5	11.3	0.2	10.7	10.6	1.94	0.08	0.16	7.61	100.6
S43E5	V2		42.8	1.3	12.7	9.9	0.2	11.5	10.5	1.81	0.13	0.13	7.01	99.0
S43E6	V2		44.3	1.53	14.1	11.2	0.2	9.0	11.3	1.98	0.49	0.14	5.46	100.9
S44E10	V2		43.7	1.11	9.1	11.3	0.18	22.3	7.4	1.39	0.11	0.15	3.2	101.1
S44E2	V2		43.6	1.38	9.5	11.3	0.17	17.0	7.6	1.7	0.22	0.15	5.05	99.0
S44E4	V2		43.1	1.94	12.3	11.9	0.2	8.4	10.8	2.45	0.16	0.22	5.63	98.5
S44E7	V2		44.2	1.7	12.8	11.3	0.19	9.4	10.7	2.54	0.07	0.2	6	100.3
S44E8	V2		44.3	1.12	10.1	10.8	0.16	20.3	8.1	1.46	0.09	0.14	2.74	100.6
S44E9	V2		43.1	1.12	9.1	11.3	0.18	21.4	7.3	1.43	0.14	0.15	2.1	98.5
S45E10	V2		44.2	1.74	12.3	12.0	0.18	9.9	10.0	2.09	0.3	0.19	5.97	100.2
S45E4	V2		43.0	0.96	9.7	10.8	0.18	22.2	7.8	1.22	0.08	0.09	2.69	100.0
S45E9	V2		45.1	1.69	12.0	11.4	0.18	11.0	10.1	2.11	0.27	0.18	4.39	99.8
S2E2	V3		43.3	1.54	11.4	10.8	0.17	13.1	9.0	2.13	0.52	0.15	5.82	99.0
S2E3	V3		45.7	2.28	13.5	10.8	0.19	7.0	10.7	3.31	0.25	0.24	2.83	98.0
S2E5	V3		46.2	1.92	13.2	11.1	0.18	9.4	10.7	2.4	0.57	0.2	2.11	99.3
S2E7	V3		47.9	3.97	12.7	14.6	0.23	5.0	9.4	2.63	1.02	0.52	0.34	99.9
S2E8	V3		48.7	3.09	13.7	12.9	0.21	4.9	9.9	3.05	0.91	0.4	0.98	100.2
S2E9	V3		46.4	2.7	13.6	12.3	0.22	6.7	10.3	2.87	0.28	0.25	2.17	99.1
S8E10	V3		44.9	1.36	13.0	11.0	0.18	10.8	10.4	2.1	0.13	0.13	4.3	99.6
S8E13	V3		48.0	1.9	13.5	12.0	0.2	6.7	11.7	2.35	0.24	0.18	0.6	98.7
S8E6	V3		46.2	1.68	14.5	11.4	0.19	7.7	11.8	2.03	0.22	0.18	3.88	101.0
S8E9	V3		43.3	3.72	12.7	14.4	0.21	4.8	8.9	2.39	1.04	0.47	4.71	98.3
S9E1	V3		48.1	2.27	14.0	12.8	0.22	5.6	11.1	2.56	0.33	0.23	0.8	99.4
S11E10	V3		48.4	1.79	13.9	10.0	0.18	6.2	11.6	2.46	0.19	0.17	1.83	97.9
S11E12	V3		47.5	1.83	14.2	10.7	0.17	6.9	12.0	2.26	0.19	0.17	2.4	99.5
S11E7	V3		48.7	1.72	14.0	11.6	0.19	6.6	11.9	2.64	0.16	0.16	2.61	101.7
S26H1	V3		48.8	2.13	14.3	12.5	0.21	6.0	11.5	2.49	0.3	0.22	0.21	99.8
S26H3	V3		47.9	2.58	13.2	12.5	0.22	5.8	10.9	2.41	0.32	0.28	3.09	100.5
S33E1	V3		44.5	1.23	11.7	10.4	0.17	14.3	9.2	2.12	0.79	0.12	5.25	100.8
S33E12	V3		44.3	1.31	13.5	10.7	0.17	10.7	11.0	1.92	0.18	0.12	5.02	100.1
S33E4	V3		41.7	0.85	8.3	11.5	0.18	22.6	6.9	1.49	0.3	0.1	4.69	99.9
S33E7	V3		44.7	1.23	11.2	11.3	0.19	16.4	9.1	2.08	0.45	0.14	2.26	100.1
S33E8	V3		46.5	1.62	14.3	10.6	0.18	8.2	11.7	2.52	0.27	0.15	3.49	100.6
S34E2	V3		45.1	1.18	11.5	10.3	0.17	16.6	9.6	1.62	0.17	0.12	2.44	100.0
S34E5	V3		46.8	1.82	13.7	11.4	0.19	7.1	11.7	2.22	0.24	0.17	1.62	98.2
S34E6	V3		46.4	1.8	14.0	10.8	0.18	7.8	13.0	2.06	0.2	0.13	2.37	100.0
S34E7	V3		47.3	2.84	12.6	13.4	0.23	5.5	10.5	2.58	0.31	0.32	0.33	97.4
S35E1	V3		46.4	1.49	15.1	10.3	0.17	7.0	12.1	2.47	0.24	0.14	3.22	99.7
S35E11	V3		47.6	2.25	14.1	11.2	0.19	7.5	11.6	2.74	0.14	0.23	1.93	100.7
S35E12	V3		45.5	1.72	14.2	10.4	0.17	7.6	11.6	2.3	0.27	0.18	2.56	97.7
S35E3	V3		46.3	2.22	13.6	12.3	0.2	6.4	11.3	2.63	0.39	0.22	0.69	97.6
S35E5	V3		47.6	2.47	14.0	12.3	0.2	6.6	11.0	2.78	0.56	0.28	0.67	99.9
S35E7	V3		42.4	0.86	7.2	10.4	0.16	28.5	5.7	1.31	0.25	0.1	2.41	100.4
S35E8	V3		45.8	1.43	13.6	11.0	0.19	10.3	10.7	2	0.09	0.13	3.71	100.2
S36E1	V3		47.8	1.59	14.6	10.7	0.18	7.6	12.0	2.33	0.17	0.16	1.48	99.8
S36E4	V3		43.5	1	7.5	10.3	0.17	28.7	6.0	1.12	0.25	0.11	2.12	101.9
S36E5	V3		47.7	1.95	14.3	11.4	0.18	7.2	12.0	2.36	0.23	0.18	1.26	100.1
S21H1	V4		48.1	3.69	13.8	13.7	0.22	4.4	9.2	3.16	1.21	0.47	1.38	100.8
S21H2	V4		46.6	2.53	13.7	13.3	0.22	6.2	11.6	2.38	0.36	0.22	1.76	100.3
S29E2	V4		63.8	0.83	14.9	5.0	0.15	1.0	1.6	5.76	4.66	0.25	0.84	99.2
S30E1	V4		46.8	3.49	13.1	14.1	0.24	4.8	9.5	2.93	1.05	0.43	1.34	99.4
S30E2	V4		47.4	3.37	14.3	13.4	0.23	4.9	10.2	2.8	0.96	0.44	1.26	100.6
S30E3	V4		47.9	2.84	13.5	12.6	0.21	5.6	10.6	2.69	0.8	0.35	1.63	100.1
S30E4	V4		46.9	3.46	13.3	13.5	0.22	4.6	9.6	2.88	1.05	0.44	1.89	99.4
S11E9	dike		47.1	2.15	14.1	11.0	0.16	6.4	11.1	2.08	0.78	0.26	4.41	100.7
S13H1	dike		48.0	1.94	13.9	12.1	0.2	6.2	11.2	2.42	0.16	0.2	0.63	98.2
S13H5	dike		49.1	3.4	12.5	15.2	0.24	5.2	10.0	2.8	0.3	0.35	0.57	101.4
S14H1a	dike		43.9	1.26	9.3	11.3	0.18	21.2	8.2	1.37	0.24	0.15	0.56	99.0
S14H2	dike		47.6	3.19	12.9	13.2	0.22	4.7	10.0	2.77	1.01	0.39	0.61	98.0
S15H3	dike		45.5	3.02	13.7	13.0	0.22	5.5	10.5	2.73	1.03	0.41	0.42	97.5
S16H1	dike		45.3	2.7	13.6	13.1	0.21	5.5	10.8	2.73	0.96	0.32	1.37	98.0
S16H2	dike		44.1	4.02	13.6	13.7	0.23	5.5	10.5	2.89	0.94	0.9	2.38	100.1
S16H4	dike		46.9	1.58	14.5	10.8	0.18	8.0	12.2	2.11	0.13	0.15	0.59	98.3
S20E18	dike		46.8	3.13	13.8	13.4	0.23	5.5	10.6	2.8	1.14	0.42	0.03	99.4
S22H2	sill		47.4	1.42	15.3	10.6	0.18	7.9	12.6	2.1	0.16	0.12	1.04	100.0
S22H4	dike		46.1	3.05	13.7	13.1	0.22	5.6	10.5	2.73	1.03	0.41	0.37	98.3
S23H1	dike		47.6	2.7	13.4	12.5	0.2	5.7	10.7	2.59	0.79	0.34	0.48	98.3
S23H4	dike V3		46.9	1.61	13.9	10.9	0.18	7.4	12.3	2.25	0.29	0.18	0.78	98.0
S23H5	dike		48.1	1.86	13.5	11.6	0.19	6.8	11.4	2.42	0.42	0.21	0.52	98.3
S24H1	Sill Itsako		49.0	1.72	14.2	12.2	0.21	7.3	11.8	2.43	0.23	0.16	0.06	100.6
S27E4	dike		46.4	2.59	13.2	12.0	0.19	7.4	10.6	2.39	0.61	0.3	0.96	98.0
S27E8	dike		43.3	3.98	13.4	13.6	0.23	5.1	9.9	2.8	1.01	0.7	3.05	98.4
S41E2	dike		48.7	1.3	17.4	9.1	0.17	5.8	10.2	3.44	1.59	0.29	3	101.9

Sample names	Fm.	ppm	Li	Be	Sc	Ti	V	Cr	Co	Ni	Cu	Zn	Ga	Ge	Rb	Sr	Y	Zr	Nb	Cs	Ba	La	Ce	Pr	Nd	Sm	Eu	Tb	Gd	Dy	Ho	Er	Tm	Yb	Lu	Hf	Ta	Tl	Pb	Th	U
S19E1	V1		4.24	0.42	32.4	7296	263	648	61.3	324	114	77.2	13.4	1.6	1.81	282	19.3	75.5	6.21	0.04	57.4	6.27	15.7	2.28	11.3	3.27	1.07	0.62	3.69	3.65	0.72	1.95	0.27	1.84	0.26	2.2	0.41	0.01	1.18	0.6	0.16
S19E2	V1		6.63	0.64	35.7	7513	288	448	42.3	45.1	41.9	87.3	23.4	1.74	2.12	238	21.6	90.8	8.68		163	13.6	30	3.89	17.4	4.16	1.33	0.67	4.09	4.13	0.77	2.19	0.3	2.07	0.28	2.46	0.37	0.08	3.28	1.64	0.25
S38E2	V1		6.49	0.72	34.4	7708	285	401	39.2	33.1	25.7	68.9	20.3	1.59	2.34	238	19.2	85.4	6.59		81.7	9.76	21.6	2.9	13	3.14	1.13	0.55	3.57	3.51	0.68	1.89	0.27	1.73	0.23	2.2	0.33	0.08	2.16	1.41	0.32
S38E8	V1		10.3	0.69	34.2	7682	283	422	39.3	30.9	25.5	76	18.7	1.56	9.38	250	18.9	85	6.61	0.26	146	9.79	21.2	2.7	12.5	3.28	1.11	0.59	3.56	3.42	0.65	1.84	0.24	1.56	0.22	2.21	0.32	0.22	2.8	1.45	0.31
S40E1	V1		5.93	0.8	37	8142	279	292	33.1	16.6	25.1	87.8	20.6	2.03	8.34	410	24.5	114	22.5	0.17	973	51.7	102	11.5	42.6	6.44	2.09	0.91	6.1	5.01	0.96	2.55	0.36	2.29	0.33	3.26	0.41	0.24	8.5	3.18	0.32
S40E2	V1		7.4	0.78	37.4	8142	272	297	33.2	18.5	25.5	87.1	20.4	1.87	4.07	395	24.2	112	21.5	0.04	856	47.6	94.1	10.5	39.4	6.32	1.99	0.86	5.9	4.7	0.9	2.49	0.36	2.18	0.32	3.19	0.42	0.19	7.79	3	0.3
S40E4	V1		6.01	0.82	36.3	8279	276	284	31.7	17.4	25.4	88.4	20.3	1.94	11.5	390	23.9	114	21.5	0.27	905	44.9	94.6	10.4	38.4	6.03	1.89	0.84	5.6	4.61	0.87	2.4	0.33	1.97	0.3	3	0.38	0.2	7.52	2.78	0.28
S40E5	V1		5.13	1.21	29.4	18260	402	98.8	41.4	77.3	234	111	23.4	2.01	19.4	390	31.5	211	25.4	0.23	180	21.3	50.6	6.62	30	6.83	2.31	1.07	7.18	5.81	1.09	2.92	0.4	2.35	0.32	5.16	1.38	0.37	2.07	2.14	0.6
S40E6	V1		9.82	0.79	36.5	7910	276	270	31.5	12.7	22.1	81.3	20.3	1.91	15.3	391	23.7	112	21.1	0.36	1017	48.2	97.5	10.7	39.9	5.88	1.86	0.81	5.52	4.46	0.83	2.31	0.32	1.98	0.3	2.97	0.38	0.18	7.63	2.8	0.29
S1E1	V2				31.81		304.93	811.76	62.86	458.99						210.39	19.53	82.26	4.88		18.92	5.47	14.27		10.93	2.67	1.01		3.7	3.6		2.27		1.69						0.35	
S1E2	V2				23.13		217.59	1226.42	88.54	1119.58						64.69	13.01	50.32	2.16		1.86	2.61	5.5		6.1	1.65	0.62		2.17	2.32		1.58		1.13						0.25	
S1E3	V2		2.97	0.38	28.8	5935	221	1422	86.4	946	84.7	73	13.4	1.11	2.08	105	13.8	48.5	1.91	0.06	6.67	2.2	6.19	1.15	6.23	1.98	0.74	0.42	2.47	2.67	0.53	1.47	0.21	1.26	0.19	1.53	0.13		0.54	0.17	0.05
S1E4	V2				35.78		339.56	699.32	57.71	312.05						205.06	21.58	82.65	4.22		33.56	5.46	12.81		11.07	3.09	1.08		4.08	3.86		2.11		1.86						0.41	
S1E5	V2		2.9	0.48	26.2	11020	272	392	41.1	55	42.5	82.1	18.1	1.58	5.44	320	14.5	85.1	14.7	0.07	176	18.4	36.8	4.52	19.6	3.81	1.53	0.61	3.97	3.31	0.63	1.69	0.23	1.36	0.19	2.33	0.83	0.31	2.05	1.14	0.33
S1E6	V2				36.13		342.99	793.46	59.71	376.77						186.68	21.05	79.51	4.25		19.53	5.07	11.42		10.32	2.95	1.1		3.61	3.8		2.18		1.81						0.3	
S3E1	V2		4.54	1.36	33.6	22770	413.69	36.46	46.17	40.5	241	149	22.9	2.39	25.2	344.47	48.62	298.09	45.43	0.28	331.94			9.38				1.58			1.68		0.63		0.54	7.07	2.58	0.11	2.25		0.92
S4E1	V2		3.75	0.77	42.5	10140	332	506	55.8	191	167	80.9	19	1.26	6.1	255	24	91.5	4.72	0.03	42.9	5.2	14.2	2.34	12.1	3.61	1.28	0.71	4.3	4.33	0.85	2.31	0.33	1.91	0.28	2.59	0.29		0.69	0.33	0.1
S5E11	V2		7.92	1.32	26.9	6066	185	1124	51.3	279	43	67.7	17.2	1.04	24.3	157	17.7	120	7.16	0.57	233	15.7	33.3	4.1	16.6	3.57	1.06	0.57	3.62	3.43	0.67	1.83	0.27	1.64	0.24	3.45	0.41		6.62	3.83	0.89
S5E5	V2		6.29	0.81	40.4	8681	301	884	50.4	66.3	55.2	90.2	18.8	1.7	10.5	214	22.3	113	8.27	0.13	141	11.1	24.4	3.51	15.6	3.82	1.15	0.65	4.06	4.1	0.78	2.24	0.31	2.15	0.3	2.84	0.44	0.14	2.25	1.62	0.42
S5E6	V2		9.55	1.09	43	9918	310	1210	28.4	44.9	53.3	76.9	20.4	1.05	17.1	234	23.7	112	9.75	0.16	229	12.1	27.5	3.85	17.1	4.17	1.38	0.74	4.49	4.37	0.85	2.3	0.33	1.98	0.29	3.04	0.48		2.22	1.69	0.43
S6E10	V2		4.28	0.65	30.1	19390	342	51	44.8	47.8	93.7	81.7	18.4	2.24	10.7	399	22.5	95	22.1	0.03	310	17.3	39.4	5.39	26.7	5.97	2.27	0.9	6.16	4.73	0.88	2.25	0.29	1.63	0.25	2.62	1.29	0.13	1.05	1.45	0.39
S6E11	V2		4.02	0.32	24.9	5458	206	1076	71.5	814	83.6	70.7	10.7	1.57	9.39	139	13.3	60.4	7.95	0.1	303	6.82	15.9	2.44	11.6	3.03	1.05	0.5	3.16	3.03	0.58	1.61	0.23	1.54	0.2	2.02	0.62	0.03	0.74	0.75	0.2
S6E6	V2		2.99	0.24	24	5380	212	1231	78.8	907	88	74.3	12.2	1.57	5	109	14.2	51.2	2.96	0.05	20.3	3.23	8.59	1.49	8.12	2.53	0.85	0.49	3	3.14	0.61	1.7	0.24	1.68	0.23	1.8	0.23	0.02	0.44	0.29	0.08
S6E9	V2		4.42	0.5	30.6	6574	216	1247	84.6	869	105	68.7	13.3	1.1	11.8	147	13.7	67.1	8.32	0.14	47.9	6.56	15.3	2.32	10.7	2.77	0.94	0.49	2.94	2.86	0.57	1.55	0.23	1.3	0.19	2.01	0.57		0.73	0.61	0.19
S7E10	V2		2.18	0.36	25.6	6455	203	711	48.2	312	85.9	36.7	12.2	1.33	0.51	169	15.1	64.9	5.67	0.01	28.1	5.64	14.2	2.24	10.7	2.81	0.97	0.51	3.18	3.03	0.61	1.65	0.24	1.43	0.22	2.02	0.38	0.01	0.56	0.51	0.13
S7E11	V2		3.88	0.36	28.4	5723	204	1922	91.3	1061	67.6	60.4	10.7	1	4.54	85.7	13.3	57.3	4.87	0.09	19.4	4.7	11	1.77	8.66	2.38	0.85	0.46	2.74	2.81	0.56	1.57	0.23	1.39	0.21	1.79	0.31		0.47	0.4	0.1
S7E4	V2		3.62	0.45	34.8	8725	305	983	73.2	454	97.5	90.8	16.1	1.73	0.83	196	20	77.8	5.98		35.9	6.01	14.8	2.35	12	3.73	1.18	0.66	4	3.84	0.72	2.01	0.28	1.86	0.26	2.33	0.39	0.01	0.53	0.47	0.13
S7E5	V2		4.36	0.25	20.6	4957	174	998	76.1	1161	72.2	51.9	7.66	1.39	3.26	72	11.1	51.7	4.47	0.06	18.6	4.51	10.8	1.81	9.15	2.58	0.86	0.45	2.78	2.66	0.51	1.45	0.2	1.31	0.18	1.84	0.34	0.01	0.57	0.45	0.11
S7E6	V2		3.36	0.42	31.5	8064	288	958	63.9	505	108	67.3	14.8	1.73	4.99	202	17.5	76.7	6.52	0.06	55.4	6.55	16.4	2.62	12.9	3.57	1.22	0.63	3.96	3.83	0.76	2.03	0.28	1.86	0.24	2.5	0.46	0.02	0.93	0.57	0.15
S7E7	V2		5.1	0.48	25.4	5939	189	2025	88.9	1123	82.8	61.3	9.29	0.98	4.34	82.8	12.7	58.6	4.74	0.07	14.9	4.75	11.6	1.83	8.77	2.37	0.81	0.44	2.66	2.62	0.51	1.36	0.2	1.17	0.17	1.77	0.3		0.61	0.41	0.12
S7E8	V2		5.13	1.58	29.9	23180	378	51	44.5	44.6	304	152	23.3	2.38	33.5	342	46.2	295	52.8	0.29	377	35.8	76.9	9.49	42.2	9.47	3.04	1.52	9.99	8.67	1.65	4.42	0.62	3.81	0.53	6.67	2.85	0.33	3.17	3.65	1.03
S7E9	V2		5.96	0.73	70.2	12460	480	1095	96.9	529	201	90.3	27.9	2.73	3.68	343	36.8	131	13.5	0.04	152	15.5	34.7	4.88	22.5	5.54	1.97	1.05	6.51	6.7	1.36	3.78	0.52	3.35	0.53	3.99	0.77	0.05	2.06	1.29	0.3
S15H4	V2		2.22	0.19	23.1	4291	186	1501	83.6	1026	80.9	57	11	1.45	2.85	110	12.1	38.6	1.46	0.01	28.7	1.81	5.3	1	5.77	1.97	0.69	0.4	2.38	2.61	0.52	1.49	0.22	1.4	0.19	1.35	0.12	0.03	0.24	0.13	0.04
S17H1	V2		3.33	0.79	37.5	12700	388	42.8	41	46.6	260	90.9	23.1	1.91	2.45	208	35	128	7.93	0.03	50.5	9.02	21.9	3.25	15.1	5.08	1.66	0.97	5.61	6.06	1.2	3.46	0.46	3.07	0.43	3.28	0.42	0.02	1.43	0.89	0.25
S17H2	V2		3.74	0.77	36	12700	410	43.6	40.3	43.7	263	90.6	22.5	2.01	4.2	218	35.9	124	7.89	0.05	53.9	8.77	20.7	3.13	15.1	4.8	1.71	0.96	5.91	5.98	1.25	3.25	0.46	3.02	0.44	3.38	0.42	0.06	1.33	0.85	0.24
S2014	V2		3.22	0.55	36.6	10440	369	564	51.4	306	148	72.1	19.5	1.76	2.12	250	22.7	88.8	5.43		39.4	5.47	15.3	2.54	12.8	3.97	1.3	0.69	4.52	4.22	0.8	2.24	0.31	2.1	0.28	2.63	0.34	0.01	0.8	0.37	0.11
S20E10	V2		1.53	0.55	34.1	12210	340	109	42.9	54	187	98	20.8	1.72	4.55	238	27.9	115	5.81	0.03	44.2	7.05	19.1	3.16	16.2	4.71	1.72	0.9	5.62	5.49	1.07	2.9	0.4	2.5	0.36	3.38	0.37	0.07	0.9	0.53	0.16
S20E15	V2		3.32	0.53	38.1	10640	355	1617	91.2	827	187	108	20.2	2.31	8.68	272	26.1	108	8.09	0.08	83.1	8.71	21.9	3.57	17.4	4.64	1.66	0.9	5.42	5.23	1.08	3.02	0.41	2.46	0.37	3.53	0.56	0.07	1.32	0.91	0.23
S20E17	V2		2.56	0.21	22	5268	189	1424	87.2	939	85.1	68	10.8	1.56	4.75	103	13.5	51.4	3.46	0.08	23.6	3.72	9.65	1.68	8.72	2.46	0.86	0.48	2.96	2.95	0.6	1.69	0.24	1.46	0.21	1.79	0.27	0.03	0.52	0.36	0.09
S20E7	V2		4.6	0.86	47.7	10090	334	555	55.6	206	134	84	18.9	1.2	2.26	245	24.4	95.8	12.1	0.02	128	12.7	27.5	3.55	15.3	3.79	1.31	0.7	4.27	4.17	0.82	2.21	0.32	1.92	0.28	2.53	0.6		1.56	0.98	0.23
S22H3	V2		3.04	0.72	38.1	13130	386	120	42.5	64.6	290	108	20.3	2.16	5.79	198	37.6	145	11	0.03	69.5	9.96	25.6	4	19.3	5.57	1.84	1.13	6.96	7.03	1.44	4.11	0.58	3.53	0.53	4.07	0.69	0.09	1.27	1.02	0.33
S27E10	V2		5.78	1.55	40.7	21170	390	225	58.4	127	224	163	32	3.35	31.1	599	49.4	288	59.6	0.31	369	40.5	88.5	11	48.1	10.2	3.25	1.69	11	9.39	1.76	4.88	0.68	3.87	0.59	7.52	3.75	0.26	2.06	4.6	1.41
S27E12	V2		3.25	0.43	27.4	6762	195	1553	97.3	990	112	74.1	10.7	1.04	1.52	119	12.5	55.9	2.79	0.03	14.9	2.93	7.63	1.33	6.74	2.02	0.74	0.39	2.35	2.38	0.45	1.22	0.17	1.01	0.15	1.6	0.18		0.55	0.2	0.07
S27E13	V2				32.34		331.38	588.95	61.51	388.65						214.47	20.95	90.21	3.9		23.29	5.75	16.25		12.83	3.45	1.2		4.18	4.08		1.98		1.79						0.12	
S27E15	V2		2.17	0.34	22.4	6916	211	392	42.5	260	98.3	61.7	12.8	1.28	0.71	154	15.3	64.6	3.32	0.01	16.3	3.77	10.8	1.86	9.6	2.78	1	0.54	3.27	3.18	0.62	1.68	0.23	1.37	0.2	2	0.23	0.02	0.5	0.29	0.08
S27E17	V2		5.46	1.24	29.5	19740	372	12.9	44.9	27.9	115	132	24.1	2.21	27.5	374	38.8	222	45.5	0.22	332	26.3	58.2	7.32	33.9	7.57	2.55	1.22	7.95	7.05	1.32	3.56	0.49	2.87	0.42	5.19	2.33	0.2	1.84	2.71	0.77
S27E18	V2		6.13	0.52	39.5	10240	362	603	62.8	245	157	97.8	22.3	2.03	1.28	231	24.2	96.4	6.08	0.02	58.4	6.83	17.4	2.83	14.7	4.05	1.48	0.8	4.93	4.6	0.92	2.63	0.35	2.16	0.32	2.92	0.4	0.04	1.12	0.59	0.16
S27E20	V2		3.69	0.79	32.9	15510	295	218	47.7	121	153	106	19.7	1.86	11.7	284	29.8	180	25.3	0.1	163	17.9	39.7	5.45	25.1	6.03	2.08	1.02	6.52	5.81	1.08	2.95	0.41	2.47	0.36	4.41	1.41	0.17	1.25	1.65	0.51
S37E1	V2				18.59		210.04	1473.83	101.26	1618.19						12.02	8.5	44.81	3.96			3.91	9.89		5.95	1.44	0.36		1.58	1.55		1.01		0.74						0.44	
S38E10	V2		3.38	0.46	36.2	7780	302	951	60.3	404	131	72.5	15.8	1.57	3.45	185	20.4	72.1	7.17	0.07	76.9	7.7	17.8	2.54	11.4	3.14	1.14	0.61	3.81	3.95	0.75	2.09	0.29	1.94	0.27	2.07	0.39	0.02	0.96	0.67	0.15
S38E6	V2				31.74		266.92	367.38	37.55	29.28						221.8	18.6	87.82	4.79		67.28	10.03	17.94		12.6	3.13	1.14		3.29	3.25		1.85		1.62						1.24	
S39E1	V2		8.8	0.62	34.7	8557	272	334	37.9	65.9	66.7	83.5	20.3	1.66	15.3	405	21.3	119	10.6	0.09	336	17.3	38.3	4.96	20.9	4.45	1.52	0.75	4.8	4.23	0.83	2.3	0.33	1.98	0.29	3.25	0.47	0.21	5.07	2.82	0.42
S41E1	V2		3.51	0.21	20.6	4165	165	766	38.5	224	58.8	49.4	9.8	1.02	9.01	92.7	12.2	43.2	2.48	0.11	165	3.56	8.43	1.34	6.64	1.85	0.69	0.39	2.37	2.43	0.5	1.43	0.2	1.24	0.19	1.39	0.16	0.02	0.88	0.6	0.14
S41E3	V2		7.22	0.81	34.7	8230	262	383	40.9	68.2	47.2	86	20.2	1.83	4.42	247	24.5	114	9.3	0.01	242	14.8	32.5	4.4	18.9	4.5	1.44	0.78	5.04	4.72	0.96	2.65	0.37	2.23	0.34	3.4	0.49	0.09	4.66	2.59	0.43
S42E1	V2		5.39	0.56	45.6	9226	354	1584	84.5	506	152	105	22.3	2.19	5.54	202	27.8	96.3	5.46	0.27	80.3	7.78	19.1	2.92	14.7	4.08	1.43	0.85	5.1	5.24	1.1	3.07	0.44	2.7	0.41	3.09	0.34	0.1	1.73	1.3	0.3
S42E2	V2		5.29	0.56	24.9	6004	202	282	30.8	52.9	34.9	65.6	14.9	1.34	2.81	178	17.7	82.5	6.63	0.05	144	10	22.4	3.08	14	3.26	1.08	0.6	3.69	3.48	0.7	1.95	0.27	1.7	0.25	2.45	0.36	0.08	3.23	1.75	0.29
S42E4	V2		9.25	0.74	42.7	9441	326	1422	58.8	71.6	81.7	93.9	24.5	2.22	5.65	280	27.3	116	7.93	0.01	312	12.9	29.7	4.13	19	4.75	1.68	0.89	5.37	5.18	1.04	2.96	0.41	2.6	0.4	3.57	0.44	0.11	4.09	2.36	0.44
S42E5	V2		8.62	0.66	35.7	8481	277	374	41.7	68.8	44	81.5	19.8	1.66	5.51	226	23.5	108	8.52	0.02	225	13.3	28.4	3.86	17.4	4.16	1.45	0.75	4.67	4.35	0.88	2.48	0.34	2.12	0.31	3.1	0.43	0.11	3.91	1.96	0.34
S43E1	V2		3.85	0.31	33	7248	261	902	68.8	492	126	74.2	15.2	1.67	2.23	189	20.1	71.2	7.1	0.01	167	6.06	14.7	2.3	11.4	3.21	1.15	0.65	4.03	4.11	0.84	2.36	0.33	2.04	0.3	2.28	0.51	0.04	0.69	0.56	0.15
S43E2	V2		3.8	0.34	33.2	7275	269	1026	71.9	510	132	73	14.8	1.67	1.59	151	18.9	68.8	4.99	0.04	36.8	5.03	12.5	2.09	11	3.14	1.12	0.64	3.83	3.91	0.78	2.23	0.31	1.83	0.28	2.18	0.35	0.01	0.6	0.45	0.11
S43E4	V2		3.63	0.39	35.8	9482	311	646	61.3	355	111	84.7	18.6	1.52	1.09	263	20.7	89.8	7.6	0.01	23.9	7.33	18.7	2.92	14.3	3.78	1.33	0.69	4.29	3.98	0.79	2.17	0.3	1.85	0.27	2.58	0.5	0.03	0.75	0.62	0.16
S43E5	V2		4.05	0.36	38.3	8276	317	610	53.8	293	153	67.3	16.7	1.77	1.35	214	22.8	79	5.05	0.02	54.9	5.06	13.7	2.28	12.1	3.53	1.28	0.72	4.39	4.48	0.93	2.55	0.36	2.19	0.33	2.45	0.32	0.04	0.76	0.48	0.11
S43E6	V2		3.59	0.39	42.6	9174	337	423	56	187	148	80.2	17.3	1.81	6.59	250	25.1	85.7	5.26	0.04	351	5.57	14.7	2.5	13.1	3.87	1.45	0.79	4.79	4.76	0.99	2.81	0.39	2.34	0.36	2.69	0.35	0.08	0.65	0.45	0.11
S44E10	V2				25.64		257.9	1310.39	86.31	1098.91						130.73	14.96	58.86	2.97		22.18	2.96	9.5		7.45	2.21	0.77		3.02	2.94		1.65		1.32						0.08	
S44E2	V2		5.66	0.85	55.5	16910	538	2653	160	1513	238	164	32.8	3.62	7.2	319	39	161	11.1	0.07	81.8	11.5	30.6	5.12	26.2	7.3	2.5	1.35	8.59	8.16	1.59	4.34	0.61	3.57	0.53	5.34	0.81	0.08	1.49	1.01	0.29
S44E4	V2		4.24	0.94	45.1	15390	449	687	77.3	271	189	130	28.5	2.72	1.93	453	30.8	153	11.1	0.06	66.9	10.6	28.8	4.75	23.7	6.19	2.16	1.12	7	6.39	1.26	3.34	0.46	2.63	0.39	4.47	0.73	0.05	1.27	0.89	0.25
S44E7	V2		2.57	0.45	29.2	9985	328	799	60.9	383	120	106	19.6	1.59	0.93	225	16.5	90.6	6.59	0.04	26.8	6.34	16.1	2.71	13.4	3.63	1.29	0.65	4.15	3.87	0.77	2.01	0.27	1.66	0.24	2.54	0.39	0.08	0.94	0.45	0.16
S44E8	V2		1.91	0.23	23.4	6363	211	1271	76	869	98	75	13.3	1.35	1.55	115	12.8	51	2.29	0.02	16.9	2.47	7.07	1.28	7	2.16	0.83	0.45	2.74	2.72	0.55	1.54	0.21	1.31	0.19	1.57	0.16	0.02	0.36	0.15	0.05
S44E9	V2				24.45		251.42	1115.13	86.61	1001.36						117.66	15.7	62.45	2.65		13.06	3.29	10.12		8.16	2.06	0.74		2.91	2.93		1.6		1.37						0.21	
S45E10	V2		4.69	0.51	31.2	10280	297	589	61.6	286	126	92.4	20	1.58	3.49	245	21.2	99.9	7.59	0.03	83.6	9.31	23.2	3.35	16.1	4.08	1.45	0.75	4.76	4.26	0.8	2.25	0.32	1.84	0.26	2.98	0.46	0.04	1.44	0.82	0.22
S45E4	V2		2.09	0.17	28.2	5627	219	1140	81.2	952	97.9	68	12	1.25	2.04	110	15.5	51.3	2.64	0.03	20	2.95	7.86	1.38	7.54	2.34	0.89	0.52	3.03	3.11	0.67	1.9	0.27	1.67	0.24	1.67	0.18	0.04	0.4	0.25	0.07
S45E9	V2		3.92	0.48	31.2	9850	298	568	57.4	255	98.6	89.9	19	1.61	3.39	351	20.8	97.4	7.44	0.03	82.8	9.23	22.2	3.38	16.5	4.15	1.45	0.75	4.73	4.28	0.83	2.27	0.3	1.87	0.27	2.93	0.45	0.08	1.93	0.85	0.23
S2E2	V3				30.28		297.13	748.91	63.37	438.03						374.07	21.15	89.37	6.13		66.53	6.51	15.34		12.57	3.65	1.26		4.05	3.73		2.06		1.78						0.61	
S2E3	V3		4.08	0.72	31.8	12220	315	178	38.9	102	139	83.1	19	1.9	1.39	260	25.8	118	11.8	0.2	76.8	10.7	27.2	3.88	19.1	4.85	1.66	0.88	5.58	5.04	0.98	2.63	0.35	2.1	0.3	3.35	0.74	0.02	1.14	1.04	0.28
S2E5	V3		3.82	0.61	37.5	11090	346	421	50.5	224	169	76.2	17.5	1.95	8.69	217	25.6	98.2	8.05	0.01	79.4	7.29	18.7	2.97	14.3	4.24	1.48	0.76	4.77	4.9	0.95	2.57	0.36	2.3	0.31	2.9	0.51	0.05	0.76	0.69	0.18
S2E7	V3		6	1.27	32.6	22230	332	72.3	42.5	51.5	231	150	22.3	2.35	22.5	316	48.3	297	44.2	0.17	264	29.5	66	8.56	39.5	9.22	2.95	1.49	10.1	8.55	1.6	4.47	0.63	3.69	0.52	7.01	2.42	0.22	1.94	2.98	0.86
S2E8	V3		4.94	1.08	31.7	17690	353	48.5	39.4	46.3	187	125	21.9	2.04	19.3	323	37.5	230	35.1	0.17	235	24.2	54.8	7.27	32.7	7.61	2.43	1.24	7.94	6.89	1.33	3.59	0.51	3	0.43	5.66	1.98	0.24	1.91	2.51	0.72
S2E9	V3		3.48	1.29	32.8	16170	420	191	43.8	113	202	119	24.1	1.55	3.79	337	31.4	151	12.2	0.03	75.7	12.2	29.2	4.6	22.3	6.03	2.09	1.06	6.73	6.34	1.21	3.19	0.44	2.62	0.38	4.19	0.74		1.97	1.01	0.33
S8E10	V3		3.79	0.56	32.3	7999	284	582	59.8	217	82.7	73.4	15.6	1.06	1.43	147	19.4	67.2	4.29	0.09	40.6	5.47	12.8	1.96	9.53	2.86	1.02	0.57	3.4	3.56	0.71	1.91	0.27	1.61	0.23	1.95	0.23		0.65	0.29	0.09
S8E13	V3				43.46		420.94	244.84	45.38	97.49						189.49	31.17	106.18	6.36		50.7	7.55	18.31		15.2	4.17	1.52		5.22	5.75		3.18		2.88						0.81	
S8E6	V3				35.78		352.79	303.83	47.34	122.22						257.57	27.11	104.86	14.64		278.41	32.42	55.32		23.63	5.63	1.4		5.2	4.81		2.76		2.37						1.23	
S8E9	V3		2.44	0.71	14	10890	212	8.91	23.1	15.1	64	53.4	12.5	1.46	8.59	163	19.5	115	25.2	0.03	193	16.5	37.6	4.72	21	4.33	1.43	0.66	4.53	3.9	0.72	1.92	0.26	1.61	0.23	3.06	1.48	0.05	0.94	1.82	0.49
S9E1	V3				40.2		459.15	112.29	43.63	62.75						202.15	36.37	135.84	9.01		57.33	10.06	24.13		19.27	4.58	1.65		6.31	6.49		3.7		3.4						0.96	
S11E10	V3		3.63	0.48	43.1	10770	382	211	40.6	85.9	150	73.8	20.9	1.93	2.55	210	32.2	107	7.62	0.03	62.8	7.83	19.4	3.12	15.3	4.43	1.56	0.93	5.4	5.61	1.19	3.43	0.48	3.04	0.46	3.28	0.51	0.1	1	0.92	0.26
S11E12	V3		4.05	0.9	50.7	11330	401	311	44.5	117	226	87.7	19.8	1.19	3.71	192	31.4	112	7.36	0.02	50.8	7.38	17.4	2.74	13.4	3.98	1.38	0.82	4.77	5.12	1.03	2.93	0.43	2.52	0.38	2.88	0.36		0.94	0.78	0.21
S11E7	V3				46.19		397.42	210.49	46.26	76.03						193.42	31.47	112.37	7.09		52.97	8.13	18.45		14.47	3.65	1.46		5.29	5.66		2.46		2.8						0.93	
S26H1	V3		6.14	1.18	49.8	13100	427	173	45.9	70.2	275	103	20.5	1.3	6.04	192	36.8	134	7.9	0.08	46.5	7.74	19.7	2.96	14.6	4.45	1.51	0.91	5.32	5.7	1.14	3.17	0.46	2.74	0.41	3.18	0.41		0.94	0.61	0.19
S26H3	V3		3.54	0.99	48.1	15870	485	184	43.2	85.2	284	115	22.3	2.23	6.6	204	45.3	159	10.8	0.07	69.1	9.07	22.8	3.63	18.3	5.81	1.66	1.14	6.51	6.87	1.46	4.12	0.55	3.6	0.52	3.95	0.57	0.05	0.94	0.71	0.22
S33E1	V3				32.15		276.11	842.17	64.32	479.81						191.4	18.6	71.69	7.63		100.63	9.43	20.35		12.13	3.66	0.82		3.49	3.38		1.77		1.52						0.71	
S33E12	V3		3.82	0.75	41.3	9045	312	624	66.9	266	141	81.2	19.7	1.17	3.65	290	20.3	77.9	5.01	0.02	30.3	4.82	11.7	1.89	9.3	2.75	0.96	0.55	3.27	3.34	0.65	1.78	0.25	1.51	0.22	1.79	0.26		0.66	0.27	0.08
S33E4	V3				24.84		194.8	1343.19	92.83	934.75						368.63	13	52.85	5.07		33.68	7.1	16.3		8.28	1.63	0.6		2.76	2.32		1.64		1.13						0.35	
S33E7	V3				30.6		272.24	786.77	72.55	583.9						259.41	19.18	70.54	8.16		83.32	10.14	22.02		13.07	2.51	0.9		3.16	3.49		1.82		1.58						0.83	
S33E8	V3				36.72		349.2	352.74	46.38	140.74						218.12	24.44	87.83	4.96		39.62	8.2	17.41		12.53	3.96	1.2		4.38	4.33		2.5		2.06						0.4	
S34E2	V3				33.25		285.41	1043.17	66.99	680.49						190.39	20.06	71.56	6		32.47	5.92	10.8		9.53	3.61	0.88		3.28	3.64		2.01		1.86						0.34	
S34E5	V3		3.66	0.5	32.4	9666	337	207	42.4	94.2	147	60.8	18.4	1.68	3.26	196	23.7	88	6.07	0.04	44.5	6.48	16	2.75	13.6	3.89	1.38	0.75	4.61	4.56	0.91	2.5	0.36	2.12	0.31	2.68	0.37	0.04	0.85	0.49	0.17
S34E6	V3		6.68	1.04	54.4	12390	388	275	55.3	119	119	90.5	20.6	1.24	1.2	341	20.9	90.8	5.15	0.01	39.9	5.39	14.5	2.38	11.7	3.25	1.15	0.6	3.72	3.42	0.64	1.68	0.23	1.36	0.19	2.18	0.26		0.61	0.3	0.08
S34E7	V3		5.83	1.28	48.3	18150	494	116	47.6	70.2	341	141	24.3	2.51	3.15	209	52.5	194	13.8	0.07	93.7	12.3	30.5	4.71	21.5	6.88	2.01	1.34	7.99	8.81	1.74	4.63	0.7	4.32	0.57	5.06	0.79	0.06	1.4	1.27	0.36
S35E1	V3				36.53		313	238.22	44.3	93.13						236.82	21.17	86.56	5.15		51.48	6.24	13.12		11.91	3.12	1.07		4.46	3.88		2.08		1.81						0.47	
S35E11	V3				34.94		389.13	259.89	43.62	134.9						293.48	28.77	122.67	10.19		50.14	10.41	25.26		18.71	4.49	1.71		5.64	5.33		2.88		2.3						0.44	
S35E12	V3		4.02	0.54	38.2	10730	323	281	49.1	120	107	91.8	20.9	1.92	1.65	322	25.2	102	11	0.01	58.9	8.39	20.6	3.26	16.2	4.32	1.52	0.82	5.15	4.94	0.97	2.65	0.38	2.26	0.33	3	0.73	0.02	0.94	0.8	0.27
S35E3	V3		6.43	1.14	53.1	19330	565	209	74.8	110	285	161	32.5	3.13	8.24	445	41.7	183	13.6	0.04	112	12.7	34.2	5.46	27.9	7.41	2.54	1.34	8.48	7.82	1.52	4.11	0.56	3.4	0.48	5.14	0.88	0.08	1.59	1.28	0.35
S35E5	V3		8.31	0.89	32.3	14960	385	176	45.4	102	181	111	23.1	1.92	6.75	334	28.9	153	13.9	0.01	107	12.7	32.4	4.79	23	5.92	2	0.97	6.48	5.71	1.1	2.91	0.41	2.43	0.34	4.11	0.84	0.08	1.45	1.21	0.33
S35E7	V3				20.87		181.25	1294.78	92.55	1471.19						112.88	12.85	53.09	2.94		53.95	6.25	10.14		8.2	2.16	0.47		2.6	2.33		1.54		1.08						0.44	
S35E8	V3				33.47		315.62	490.25	57.49	214.62						166.32	21.39	66.71	3.43		15.25	5.21	12.16		10.38	3.42	1.07		3.8	3.87		2.34		1.85						0.5	
S36E1	V3		5.01	0.38	35.3	9639	327	393	44.4	126	144	90.1	20.9	1.57	2.01	209	21.9	81.7	5.67	0.07	36.3	5.02	13.1	2.19	11.2	3.34	1.28	0.68	4.16	4.18	0.84	2.23	0.32	1.96	0.28	2.28	0.39	0.15	1.17	0.45	0.16
S36E4	V3		2.63	0.22	20.2	5085	163	573	75	1349	87.8	52	8.86	1.36	4.48	89.9	12.6	47.8	3.45	0	28.8	3.92	9.09	1.49	7.61	2.33	0.77	0.45	2.75	2.83	0.55	1.54	0.22	1.44	0.2	1.58	0.22	0.04	0.51	0.41	0.12
S36E5	V3		4.26	0.47	36	11070	351	304	44.7	158	193	80.8	18.9	1.52	3.45	203	27	102	6.48	0.03	47.4	6.72	17.2	2.74	14.2	4.04	1.52	0.81	4.95	4.91	0.96	2.61	0.37	2.22	0.33	2.84	0.36	0.06	0.77	0.51	0.17
S21H1	V4		5.41	1.84	30.3	20700	412	12	48.8	30.5	109	129	24.6	2.57	21	411	38.6	245	54	0.06	338	33	68.6	8.28	35.8	8.29	2.67	1.29	8.36	7.25	1.31	3.45	0.47	3.18	0.42	5.67	2.64	0.83	2.16	3.05	0.85
S21H2	V4		5.28	1.08	47.4	16240	450	55.3	59.9	67	156	112	23.9	2.38	4.32	359	34.6	150	13	0.01	91.3	11.4	28.7	4.38	21.5	5.77	1.86	0.96	6.1	5.83	1.16	3.26	0.43	2.9	0.39	3.88	0.73	0.04	1.24	0.94	0.25
S29E2	V4		7.17	4.28	6.97	5228	21	5.05	3.23	1.9	9.27	91.3	28.6	1.34	49.3	64.8	44.5	331	72.3	0.45	739	40.9	78.6	9.42	36	7.64	2.03	1.19	7.46	7.33	1.36	3.8	0.56	3.48	0.52	6.7	3.3		3.4	3.71	0.67
S30E1	V4		7.2	2.86	42.1	22720	421	32.2	50.8	34.7	145	154	23.9	1.81	20.7	352	43.2	280	43.6	0.1	269	26.4	57.8	7.15	31.7	7.61	2.38	1.19	7.72	6.75	1.26	3.43	0.48	2.76	0.39	5.42	1.88		1.79	2.08	0.6
S30E2	V4		6.14	1.51	34.6	19620	372	60.1	43.8	45.4	172	128	23.8	2.63	8.59	374	40.3	244	40.3	0	279	24.2	57.7	7.77	33.6	8.33	2.36	1.18	7.79	7.6	1.37	3.6	0.5	3.22	0.44	5.4	2.08	0.03	1.72	2.3	0.6
S30E3	V4		5.19	1.39	38.6	17500	350	69.1	46.2	61.1	124	126	21.9	2.48	13	332	34.4	197	34.1	0.1	213	22.2	51.1	6.52	27.7	6.52	2.08	1.02	7.07	6.27	1.21	3.17	0.44	2.75	0.37	4.43	1.74	0.03	1.52	2.14	0.55
S30E4	V4		6.62	2.76	42.9	22840	414	29.7	51.4	41.7	206	153	24.2	1.87	22.8	374	44.5	288	44.3	0.09	283	28	60.7	7.7	33.1	7.8	2.36	1.28	7.92	7.16	1.29	3.43	0.49	2.75	0.4	5.63	2.02		1.87	2.24	0.67
S11E9	dike		3.58	0.66	35.66	12330	317.3	110.7	48.12	110.84	129	92.5	18.2	1.68	8	329.23	25.99	139.92	18.57	0.01	183.15			4.7				0.83			0.92		0.34		0.3	3.58	1.2	0.24	1.21		0.44
S13H1	dike				39.16		402.66	153.69	43.82	71.02						194.12	32.34	115.06	6.86		45.28	8.17	18.51		15.88	4.76	1.49		5.63	5.75		3.57		3.03						0.81	
S13H5	dike		5.63	0.96	35.42	18400	493.4	57.45	46.44	48.9	284	143	22.9	2.13	5.25	251.57	42.89	202.91	12.14	0.12	76.2			4.9				1.31			1.48		0.55		0.47	5.37	0.72	0.12	1.57		0.33
S14H1a	dike				27.75		253.11	1089.8	85.78	887.61						179.45	16.73	79.31	7.13		49.43	7.6	18.01		12.25	2.95	0.93		3.4	3.13		1.82		1.47						0.66	
S14H2	dike		3.87	1.06	30.16	18170	386.4	55.03	44.36	47.53	175	128	22.1	2.19	21.4	353.17	37.33	225.92	33.54	0.21	264.83			7.81				1.29			1.44		0.55		0.47	6.11	2.06	0.31	2		0.82
S15H3	dike				33.12		377.13	58.03	47.17	59.24						349.57	35.89	208.83	33.8		296.33	26.33	57.17		34.1	7.51	2.3		7.61	6.87		3.82		3.12						2.81	
S16H1	dike				29.11		403.39	41.64	51.78	60.75						432.66	27.38	181.97	23.54		180.13	21.64	49.92		29.66	6.56	2.14		6.37	5.52		2.54		2.25						2.16	
S16H2	dike		5.03	0.74	28.78	21940	339.25	34.92	43.42	40.14	72.8	116	20.2	2.12	18.2	468.27	32.23	137.99	31.62	0.17	505.61			7.72				1.16			1.17		0.38		0.32	3.49	1.99	0.12	2.03		0.57
S16H4	dike				37.05		330.2	351.1	48.91	122.42						223.79	22.76	85.42	5.18		23.16	5.57	13.63		12.24	2.92	1.21		4.39	4.38		2.3		1.97						0.8	
S20E18	dike		4.18	1.05	34.54	17540	384.52	58.76	45.89	58.69	201	116	21.1	2.08	21.7	402	38.44	218.24	34.37	0.17	323.64			7.36				1.19			1.28		0.51		0.45	5.56	2.16	0.1	2.15		0.82
S22H2	sill				40.65		342.32	403.66	49.1	164.8						176.9	25.02	79.2	3.62		21.48	4.72	11.93		10.16	3.76	1.17		4.41	4.38		2.53		2.2						0	
S22H4	dike				33.97		384.11	58.66	47.4	60.65						359.96	36.13	205.58	33.69		295.2	26.25	56.26		34.15	7.54	2.44		7.87	6.99		3.79		3.1						2.94	
S23H1	dike				33.33		330.17	86.93	44.92	65.73						351.91	34.09	193.38	29.51		238.48	24.64	51.8		30.46	6.59	2.26		7.36	6.57		3.36		2.88						2.37	
S23H4	dike V3				36.3		349.59	271.55	46.41	105.72						261.42	24.54	96.87	11.12		160.95	15.55	33.57		18.59	4.39	1.4		4.56	4.53		2.51		2.12						0.62	
S23H5	dike				39.03		386.84	239.17	45.55	89.59						227.03	30.15	114.21	11.08		97.82	13.8	28.58		18.44	3.81	1.62		5.43	5.59		3.07		2.74						1.15	
S24H1	Sill Itsako		6.25	0.4	45.6	10290	394	148	47.4	82.3	196	86.6	18.9	1.58	4.48	179	29.9	92.6	5.44	0.07	53.5	6.2	14.9	2.31	11.7	3.42	1.27	0.75	4.55	4.69	0.98	2.78	0.4	2.47	0.37	2.44	0.28	0.06	0.91	0.54	0.18
S27E4	dike				33.01		306.5	251.78	49.48	135.85						286.83	31.47	170.47	23.01		163.12	18.8	41.71		26.28	5.85	2.03		6.61	6.15		3.11		2.71						1.85	
S27E8	dike				26.76		330.38	26.7	41.54	31.99						414.43	32.12	152.44	36.74		458.72	26.2	57.56		36.5	7.5	2.98		8.24	6.41		3.24		2.45						2.32	
S41E2	dike		8.56	1.01	28.19	7869	216.25	35.98	37.17	49.07	55	71.9	18.4	1.75	33	561.88	25.22	128.27	39.61	2.6	817.63			8.92				0.77			0.88		0.37		0.34	2.86	1.62	0.37	5.31		0.85

Sample names	Fm.	$^{208}Pb/^{204}Pb$	$^{207}Pb/^{204}Pb$	$^{206}Pb/^{204}Pb$	$^{176}Hf/^{177}Hf$	2 σ	ε_{Hf}	$^{143}Nd/^{144}Nd$	2 σ	ε_{Nd}	$^{87}Sr/^{86}Sr$
S19E1	V1	37.7907	15.3018	17.7224		0.0000073					
S19E2	V1	37.1751	15.2492	16.9346	0.282636	0.0000048	-4.82				
S38E2	V1	36.9612	15.157	16.6579	0.282607	0.0000042	-5.84				0.70780
S38E8	V1	36.7908	15.1218	16.5386	0.282612	0.0000042	-5.65	0.512302	0.0000063	-6.56	0.70807
S40E1	V1	38.7418	15.4345	18.6374				0.512350	0.0000047	-5.62	0.70636
S40E2	V1	38.7234	15.4236	18.6007				0.511881	0.0000088	-14.76	0.70628
S1E1	V2	37.7479	15.3743	17.9969	0.283198	0.0000041	15.06				0.70338
S1E3	V2	37.8174	15.4329	18.0711	0.283198	0.0000034	15.08				0.70338
S1E4	V2	37.7933	15.3716	18.0389	0.283193	0.000004	14.89				0.70332
S3E1	V2	38.5017	15.489	18.7265							0.70362
S4E1	V2	37.714	15.4216	18.0089	0.283203	0.0000079	15.23				0.70311
S5E11	V2	37.4929	15.1063	16.915		0.0000028		0.512345	0.0000047	-5.71	
S5E5	V2	37.2793	15.0701	16.9389	0.282652	0.0000036	-4.26				0.70679
S5E6	V2	37.3562	15.0888	17.0592	0.282692	0.000003	-2.84	0.512506	0.0000044	-2.57	0.70652
S6E6	V2	37.7648	15.4218	18.037	0.283157	0.0000048	13.61				0.70330
S6E9	V2	38.0612	15.4362	18.2839	0.283138	0.0000049	12.94				0.70628
S7E6	V2	37.9231	15.443	18.098	0.283177	0.0000077	14.31				0.70338
S7E7	V2	37.9827	15.4257	18.1173	0.283173	0.0000036	14.19				0.70349
S7E9	V2	38.0256	15.3296	17.9856	0.283193	0.000005	14.9				0.70363
S15H4	V2	37.5416	15.3724	17.9168	0.283220	0.0000034	15.85				0.70309
S20E15	V2	37.811	15.3603	17.9032	0.283104	0.0000043	11.74				0.70369
S20E7	V2	38.4594	15.3964	18.4259	0.283059	0.0000033	10.16				0.70398
S27E12	V2	37.7582	15.4339	18.099	0.283202	0.0000029	15.21				0.70794
S27E13	V2	37.6621	15.4177	18.0158	0.283211	0.0000044	15.52				0.70315
S27E18	V2	37.8792	15.3751	18.0833	0.283170	0.0000046	14.09				0.70335
S38E10	V2	38.0322	15.3567	18.0635	0.283115	0.0000034	12.12				0.70374
S39E1	V2	37.1137	15.0627	16.4893	0.282501	0.0000046	-9.58	0.512220	0.0000042	-8.15	0.70624
S41E3	V2	36.8255	14.9913	16.1358	0.282531	0.0000048	-8.51				0.70704
S42E2	V2	36.8122	15.0013	16.1661	0.282565	0.0000043	-7.31				0.70665
S42E5	V2	36.8	15.0014	16.1686	0.282574	0.0000027	-7.01	0.512303	0.000006	-6.54	0.70673
S43E1	V2	37.9194	15.3688	18.0556	0.283116	0.0000061	12.15				0.70355
S43E4	V2	37.8974	15.4283	18.0467	0.283139	0.0000104	12.97	0.512992	0.0000052	6.9	0.70357
S43E6	V2	37.7803	15.3919	17.9208	0.283175	0.000005	14.25				0.70337
S44E2	V2	37.7681	15.4128	18.0671	0.283165	0.0000053	13.89				0.70330
S44E7	V2	37.9074	15.4131	18.0767	0.283176	0.0000073	14.29	0.513050	0.0000083	8.05	0.70356
S44E8	V2	37.5621	15.3715	17.9248	0.283204	0.0000053	15.26				0.70328
S45E4	V2	37.9674	15.4621	18.1573	0.283230	0.000005	16.18				0.70326
S45E9	V2	37.8374	15.2977	17.7873	0.283065	0.0000109	10.35	0.512883	0.0000061	4.78	0.70391
S2E2	V3	37.8894	15.4361	18.2036	0.283193	0.0000055	14.88				0.70338
S2E3	V3	38.042	15.4536	18.3113							0.70335
S2E5	V3	37.9368	15.4521	18.202							0.70331
S2E7	V3	38.5979	15.4975	18.94	0.283124	0.0000063	12.46	0.512977	0.0000069	6.62	0.70377
S2E8	V3	38.5267	15.4941	18.808	0.283155	0.0000048	13.56	0.512989	0.000006	6.84	0.70366
S2E9	V3	37.9398	15.4554	18.2417	0.283172	0.0000045	14.14	0.513054	0.0000044	8.12	0.70822
S8E13	V3	37.9907	15.4015	18.2182	0.283174	0.0000046	14.22	0.513033	0.000009	7.67	0.70353
S8E6	V3	39.0141	15.5255	19.112	0.283083	0.0000046	11	0.512719	0.0000065	1.54	0.70392
S9E1	V3	38.1598	15.4592	18.4869	0.283191	0.0000051	14.82				
S11E10	V3	38.0766	15.4443	18.4272	0.283203	0.000004	15.23				0.70348
S26H1	V3	38.2176	15.5662	18.2994	0.283198	0.0000036	15.05				
S26H3	V3	37.9707	15.4411	18.3145	0.283205	0.0000043	15.3	0.513094	0.0000077	8.89	0.70345
S33E12	V3	38.4105	15.4844	18.6862	0.283192	0.0000074	14.86				
S33E7	V3	38.7609	15.4922	19.075	0.283111	0.0000074	11.97				
S35E11	V3				0.283171	0.000005	14.1	0.513027	0.0000122	7.54	0.70354
S35E12	V3	38.0041	15.453	18.392							0.70336
S35E3	V3	37.9532	15.4402	18.2024	0.283188	0.0000049	14.7				
S35E5	V3	38.0145	15.4499	18.2868	0.283182	0.0000048	14.49	0.513055	0.0000098	8.13	0.70363
S35E8	V3	37.9179	15.4556	18.2058							0.70330
S36E5	V3	37.9807	15.4298	18.3146	0.283186	0.0000046	14.64				
S21H1	V4	38.3919	15.4636	18.6247	0.283150	0.0000035	13.36	0.512990	0.0000084	6.87	0.70367
S21H2	V4	38.0081	15.4547	18.2627	0.283223	0.0000039	15.95				
S29E2	V4	38.3614	15.4604	18.4962	0.283182	0.0000045	14.49				
S30E1	V4	38.4071	15.4795	18.6598	0.283145	0.0000023	13.19	0.512992	0.0000053	6.91	0.70806
S30E4	V4	38.4888	15.5065	18.8252	0.283146	0.0000025	13.23	0.512984	0.0000061	6.76	0.70376
S13H5	dike	37.8156	15.3998	18.1175							0.70332
S14H2	dike	38.5245	15.5106	18.765	0.283142	0.0000047	13.09	0.512985	0.000009	6.73	0.70364
S15H3	dike	38.4756	15.4871	18.7332	0.283160	0.0000038	13.74				0.70364
S20E18	dike	38.5508	15.4971	18.7477	0.283154	0.0000057	13.52	0.512984	0.0000051	6.71	0.70379
S22H2	sill	37.8774	15.4337	18.2553	0.283213	0.0000047	15.6	0.513095	0.0000171	8.87	
S22H4	dike	38.5058	15.4949	18.7357	0.283153	0.0000048	13.48	0.512984	0.0000051	6.71	0.70611
S23H4	dike V3	38.9386	15.5336	19.2555	0.283128	0.0000052	12.6	0.512822	0.0000066	3.56	0.70380
S23H5	dike	38.812	15.4818	19.1238	0.283153	0.0000045	13.47	0.512909	0.000007	5.24	0.70370
S24H1	Sill Itsako	37.8957	15.3504	18.0561	0.283164	0.0000037	13.85				
S27E4	dike	38.4799	15.4969	18.8261	0.283130	0.0000043	12.65	0.512994	0.0000071	6.91	0.70375